Mechanistic insights into ribosome recycling and quality control in mRNA translation

Dissertation

zur Erlangung des Doktorgrades

der Naturwissenschaften

vorgelegt beim Fachbereich 14

Biochemie, Chemie und Pharmazie

der Johann Wolfgang Goethe-Universität

in Frankfurt am Main

von

Holger Heinemann

aus Gotha

Frankfurt am Main, 2022

(D30)

Vom Fachbereich 14 Biochemie, Chemie und Pharmazie
der Johann Wolfgang Goethe-Universität als Dissertation angenommen.

Dekan: Prof. Dr. Clemens Glaubitz

1. Gutachter: Prof. Dr. Robert Tampé
2. Gutachterin: Prof. Dr. Michaela Müller-McNicoll

Datum der Disputation: 24.03.2023

“Now this is not the end. It is not even the beginning of the end.
But it is, perhaps, the end of the beginning.”

Winston Churchill

Declaration

Declaration of scientific collaborations

Except where stated otherwise by reference or acknowledgment, the work presented was generated by myself under the supervision of my advisors or by students under my direct supervision during my doctoral studies. All contributions from colleagues are explicitly referenced in the thesis. The material listed below was obtained in the context of collaborative research.

Chapters 2.1.1 - 2.1.8, 6.1, and all included figures. For details and author contributions, see the declaration about previously published parts of the thesis.

Figure 14: Dr. Elina Nürenberg-Goloub (Tampé laboratory, Institute of Biochemistry, Goethe-University Frankfurt) provided recombinant archaeal translation initiation factors and bacterial MetRS. I performed methionylation of initiator tRNA, provided recombinant ABCE1^{IIEA}, and pre-assembled sub-complexes. SEC experiments were performed by Dr. Elina Nürenberg-Goloub and myself. I analyzed the data and designed the figures.

Figure 15: Dr. Elina Nürenberg-Goloub (Tampé laboratory, Institute of Biochemistry, Goethe-University Frankfurt) provided recombinant archaeal translation initiation factors and bacterial MetRS. I performed all experiments, analyzed the data, and designed figures.

Figure 16: Cryo-EM was performed in collaboration with Hanna Kratzat and Dr. Thomas Becker (Beckmann laboratory, Department of Biochemistry, Ludwig-Maximilians-University in Munich). Dr. Elina Nürenberg-Goloub (Tampé laboratory, Institute of Biochemistry, Goethe-University Frankfurt) provided recombinant archaeal translation initiation factors and bacterial MetRS. Complex assembly and cryo-EM sample preparation were performed by Dr. Elina Nürenberg-Goloub and myself in the Beckmann laboratory. SDG centrifugation was performed by Dr. Elina Nürenberg-Goloub, Hanna Kratzat, and myself. I performed SDS-PAGE analysis. Hanna Kratzat performed all cryo-EM data processing with help of Dr. Thomas Becker. Hanna Kratzat fitted protein structures into EM densities. Data were analyzed by Dr. Elina Nürenberg-Goloub, Hanna Kratzat, Dr. Thomas Becker, and myself. I designed all figures.

Figure 17: Same contributions as for Figure 16.

Figure 19: Dr. Elina Nürenberg-Goloub (Tampé laboratory, Institute of Biochemistry, Goethe-University Frankfurt) and I established the pull-down of recombinant ABCE1 from *Saccharolobus solfataricus* cell lysate. I adapted the protocol for pull-down of recombinant ABCE1 from *Sulfolobus acidocaldarius* (*S. acidocaldarius*). I performed all experiments, analyzed the data, and designed the figures.

Figure 20: Expression of native ABCE1 in *S. acidocaldarius* was established in collaboration with Dr. Alejandra Recalde (Albers laboratory, Institute of Biology II, Albert-Ludwigs-University in Freiburg). Prof. Dr. Sonja-Verena Albers and Dr. Alejandra Recalde provided cells, plasmids, and method protocols for the *S. acidocaldarius* genetic toolbox. Dr. Alejandra Recalde transformed *S. acidocaldarius*. I performed expression of native ABCE1 in *S. acidocaldarius*, established and performed native pull-downs, analyzed the data, and designed the figures.

Figure 22: Federico Cerullo (Joazeiro laboratory, center for molecular biology of the university Heidelberg (ZMBH), Ruprecht-Karls-University in Heidelberg) provided *Bacillus subtilis* (*B. subtilis*) MutS2^{WT} and E416A DNA sequences, and *B. subtilis* ΔMutS2 cell pellets. I performed all experiments, analyzed the data, and designed the figures.

Figure S5: Contributions in cryo-EM collaboration and sample preparation as for Figure 16 and Figure 17. Hanna Kratzat (Beckmann laboratory, Department of Biochemistry, Ludwig-Maximilians-University in Munich) prepared the density depictions by local resolution for each initiation complex. I compiled the three depictions in one figure.

Figure S8: Federico Cerullo (Joazeiro laboratory, ZMBH, Ruprecht-Karls-University in Heidelberg) provided *B. subtilis* MutS2^{WT} and E416A DNA sequences. I performed all experiments, analyzed the data, and designed the figures.

Figure S9: Federico Cerullo (Joazeiro laboratory, ZMBH, Ruprecht-Karls-University in Heidelberg) provided *B. subtilis* MutS2^{WT} and E416A DNA sequences, and *B. subtilis* ΔMutS2 cell pellets. I performed all experiments, analyzed the data, and designed the figures.

Table S1: Hanna Kratzat (Beckmann laboratory, Department of Biochemistry, Ludwig-Maximilians-University in Munich) performed all cryo-EM data processing. I compiled the data in table format.

Table S2: I performed co-IP experiments. Dr. Haifei Xu (Joazeiro laboratory, Scripps Biomedical Research Institute, University of Florida) performed protease digestion and mass spectrometry analysis. I compiled a selection of identified proteins.

Declaration of previously published parts of this thesis

Whenever a figure, table, or text is identical to a previous publication, copyright permission and/or co-author agreement has been obtained and is stated explicitly below.

The following parts of the thesis have been previously published:

Chapters 2.1.1 - 2.1.8 and 6.1: Structural and functional characterization of the archaeal ABCE1-30S ribosomal subunit post-splitting complex

Figure 4, Figure 5, Figure 6, Figure 7, Figure 8, Figure 9, Figure 10, Figure 11, Figure 12, Figure 13, Figure S1, Figure S2, Figure S3, and Figure S4

in *The EMBO Journal* 39: e103788 (2020) as "Molecular analysis of the ribosome recycling factor ABCE1 bound to the 30S post-splitting complex" by Elina Nürenberg-Goloub‡ (EN-G), Hanna Kratzat‡ (HK), Holger Heinemann‡ (HH), André Heuer (AH), Peter Kötter (PK), Otto Berninghausen (OB), Thomas Becker (TB), Robert Tampé (RT)* and Roland Beckmann (RB)*.

‡ equal contributions; *corresponding authors

Author contributions as detailed in the publication:

"EN-G, HK, HH, TB, RB, and RT designed the study. EN-G and HH developed the preparation of the post-splitting complex. EN-G, HK, HH, and AH optimized the sample preparation for cryo-EM. EN-G, HK, HH, and AH prepared the EM samples. HK and OB collected and HK processed the cryo-EM data. HK built and refined the model. HK, TB, EN-G, HH, RT, and RB analyzed and interpreted the structures. HH and EN-G performed all functional assays. EN-G and PK conducted the genetic analysis in yeast. EN-G, HK, TB, HH, RB, and RT wrote the manuscript with contributions from all authors. RT initiated the project."

Zusammenfassung

Die Proteinbiosynthese ist ein grundlegender und essentieller Prozess in allen Domänen des Lebens. Polypeptide werden hergestellt, indem die genetische Information der Boten-RNA (mRNA) in Aminosäureketten übersetzt wird. Dieser komplexe und aufwändige Vorgang gliedert sich in die vier Phasen der mRNA-Translation: Initiation, Elongation, Termination und Ribosomen-Recycling. Sie werden durch eine Vielzahl von Translationsfaktoren gesteuert und reguliert.

Während der Initiationsphase wird das Ribosom auf der mRNA zusammengesetzt. Initiationsfaktoren (IFs) binden an die kleine ribosomale Untereinheit (SSU) und helfen bei der Rekrutierung der mRNA und der Initiator-Transfer-RNA, die die erste Aminosäure Methionin liefert ($^{Met}tRNA_i^{Met}$). Eukaryoten (e) und Archaeen (a) verwenden homologe IFs, die einen gemeinsamen strukturellen Kern für den Aufbau des Initiationskomplexes (IC) bilden. So begünstigen a/eIF1 und a/eIF1A die Bindung der mRNA als auch des heterotrimeren Faktors a/eIF2 zur SSU. In Eukaryoten bindet eIF2 zunächst $^{Met}tRNA_i^{Met}$ bevor er zum Ribosom rekrutiert wird. In Archaeen hingegen bindet aIF2 zunächst die SSU bevor $^{Met}tRNA_i^{Met}$ rekrutiert wird. Nach der Positionierung des Start-Codons fördert a/eIF5B den Zusammenschluss mit der großen ribosomalen Untereinheit (LSU), um das translationsbereite Ribosom zu bilden. Abgesehen von diesen gemeinsamen Kerninitiationsfaktoren, verwenden Eukaryoten zusätzlich den multimeren eIF4, welcher die 5‘-Kappe und das 3‘-Poly-Adenosin bindet und durch seine Helikase-Funktion die mRNA für das Ribosom zugänglich macht. Zusätzlich werden die Prozesse am Ribosom während der Initiation sowie zum Teil auch in anderen Translationsphasen durch den Multidomänenfaktor eIF3 unterstützt. Obwohl es den Anschein macht, als würde der Initiationsprozess in Archaeen einer vereinfachten eukaryotischen Variante entsprechen, gibt es nur wenig funktionelle Daten, die den präzisen Ablauf der archaealen Initiation beschreiben. Tatsächlich wird trotz struktureller Parallelen zu Eukaryoten von einem bakteriellen funktionellen Ablauf der Initiation bei Archaeen ausgegangen.

In der Elongationsphase liefern Elongationsfaktoren (EFs) die aminoacylierten tRNAs (aa-tRNAs) an das translatierende Ribosom und unterstützen die GTP-abhängige kinetische Korrektur der Codon-Anticodon-Bindung. Nach dem Transfer des Polypeptids auf die korrekte aa-tRNA durch das katalytische Zentrum des Ribosoms, assistieren die EFs die Translokation der ribosomalen Untereinheiten entlang der mRNA. Dieser Prozess setzt sich fort bis ein Stopp-Codon dekodiert wird. Die Translation wird durch Klasse-1 Freisetzungsfaktoren (RFs) mittels Hydrolyse der Peptidyl-tRNA beendet und das gebildete Protein wird freigesetzt. In Eukaryoten und Archaeen wird anschließend das

Ribosom durch den essentiellen Recycling-Faktor ABCE1 in seine Untereinheiten gespalten.

ABCE1 bindet den terminierten Ribosomenkomplex. Der Einschluss von zwei ATP-Molekülen führt zu drastischen strukturellen Veränderungen von ABCE1. Die Bewegung der ABCE1-Domänen schiebt den RF zwischen die ribosomalen Untereinheiten und bewirkt auf diese Weise die Dissoziation von LSU und SSU. Energetisch betrachtet, ist das ATP-abhängige Ribosomen-Recycling eine Besonderheit, da alle anderen Translationsprozesse GTP-getrieben sind. Nach der Spaltung bleibt ABCE1 stabil an die SSU gebunden und bildet so den Post-Spaltungs-Komplex (Post-SC). Der Prozess der mRNA-Translation schließt sich zu einem Zyklus durch die Rekrutierung von IFs an den Post-SC und dem Beginn einer neuen Translationsrunde. Interessanterweise wurde ABCE1 ursprünglich eine katalytische Funktion während der Initiation zugesprochen, basierend auf Co-Immunpräzipitationen mit IFs in verschiedenen Eukaryoten. Folglich erscheint ABCE1 als zentraler Faktor zwischen Termination und Initiation in der mRNA-Translation. Der Post-SC stellt somit einen zentralen ribosomalen Komplex dar, der als Plattform für die Initiation der Translation fungiert.

Nachdem die Funktion von ABCE1 beim Ribosomen-Recycling in den letzten Jahren ausführlich untersucht wurde, blieb die Rolle von ABCE1 während der anschließenden IC-Assemblierung ungeklärt. Daher bestand das Hauptziel dieser Dissertation darin, den molekularen Mechanismus von ABCE1 während der Bildung des Post-SC und des Aufbaus des Initiationskomplexes zu entschlüsseln. Verfügbare schwach- oder intermediär-aufgelöste Strukturen des Post-SCs (in Archaeen und Eukaryoten) konnten bisher die Interaktionsschnittstelle von ABCE1 mit der SSU nicht final aufklären. Entsprechend lag der Fokus auf der strukturellen und funktionellen Analyse des Post-SC. In Zusammenarbeit wurde der native archaealen Weg der Ribosomenspaltung durch ABCE1 und die nachfolgende Dekoration des Post-SCs mit aIFs *in vitro* rekonstituiert. Mittels kryogener Elektronenmikroskopie (Kryo-EM) wurde die hochauflösende Struktur des archaealen Post-SCs aufgeklärt. Es war das erste vollständige Modell einer archaealen SSU bei atomarer Auflösung und enthüllte ein bisher unbeschriebenes ribosomales Protein, das wir eS21 nannten. Neben den bekannten Interaktionsdomänen Helix-Loop-Helix Motiv und Eisenschwefelcluster-Domäne von ABCE1 mit der SSU, wurden zusätzlich die strukturell bisher unbekannten Hinge-Regionen als wichtige Interaktionspunkte identifiziert. Dabei diente Hinge 2 als zentraler Ankerpunkt für ABCE1 an der SSU. Durch detaillierte biochemische Charakterisierung von Mutationen einzelner bedeutender Aminosäurereste in der Hinge 2-Region wurden Wechselwirkungen mit dem ribosomalen RNA-Rückgrat der SSU aufgedeckt. Die Bindung von ABCE1 an ribosomale

Komplexe wird allosterisch an die Nukleotidbindungsstellen (NBS) kommuniziert und in den ATPase-Zyklus integriert. Für diesen Prozess wurden die konservierten C-terminalen aromatischen Aminosäuren als zentrale Übertragungspunkte identifiziert. So beeinflusste ihr Austausch erwartungsgemäß nicht die Bindung an die SSU, beeinträchtigte jedoch signifikant die NBS-abhängige Spaltfunktion. Somit konnte eine allosterische Kommunikation von den essenziellen Bindungsresten der Hinge 2 über den konservierten aromatischen *Patch* und weitere Domänen hin zu den NBS nachgewiesen werden. Mittels dieser Ergebnisse konnte der Spaltungs- und ATPase-Zyklus von ABCE1 aufgeklärt werden. Darüberhinaus lieferten diese Ergebnisse Hinweise über die molekulare Funktionsweise von ATP-Bindungs-Kassetten (ABC) Proteinen.

Die zuvor etablierte Rekonstitution des archaealen Translationsapparats ermöglichte die Untersuchung des schrittweisen IC-Aufbaus in Gegenwart von ABCE1 *in vitro*. Umfangreiche biochemische Analysen identifizierten die stabile Bildung verschiedener ICs. Kryo-EM Strukturanalyse von IF-dekorierten Post-SCs bestätigte die biochemischen Daten. So konnten Post-SCs mit aIF1 und aIF1A, zusätzlich mit aIF2, mRNA und $^{Met}tRNA_i^{Met}$, sowie der gleiche Komplex ohne aIF1A, strukturell aufgeklärt werden. Insgesamt stehen die Ergebnisse im Einklang mit den jüngsten strukturellen Erkenntnissen über die Translationsinitiation in Archaeen und der Rolle von ABCE1 bei der eukaryotischen Initiation.

Die physiologische Relevanz der *in vitro* assemblierten Komplexe konnte mittels Co-Immunpräzipitationen bestätigt werden. Zunächst wurden Zelllysate des Crenarchaeons *Saccharolobus solfataricus* mit definierten Mengen an bereits charakterisierten, heterolog exprimierten und gereinigten ABCE1 versetzt. Massenspektrometrische Analyse der erhaltenen ABCE1-Ribosomenkomplexe bestätigte die Assoziation zahlreicher Translationsfaktoren, unter Anderem aIFs, und metabolischer Proteine. Diese semi-native Herangehensweise indizierte die physiologische Relevanz der Ergebnisse. Das Hauptziel dieses Teils der Dissertation lag daher darin die genetische Toolbox des acido-thermophilen Crenarchaeons *Sulfolobus acidocaldarius* für die homologe Expression von nativem ABCE1 mit Affinitäts-Tag zu etablieren. Die Co-Immunpräzipitation von nativem ABCE1 aus *S. acidocaldarius* ergab bei biochemischer Analyse vergleichbare ribosomale Komplexe wie die bereits massenspektrometrisch charakterisierten Komplexe mit rekombinantem ABCE1 aus *S. solfataricus* Zelllysat. Diese ersten nativen ABCE1-Ribosomenkomplexe wurden für die Strukturanalyse mittels Kryo-EM präpariert. Dadurch wird es in Zukunft erstmals möglich sein, die native IC-Assemblierung am Post-SC in Archaeen strukturell aufzuklären.

Obwohl inzwischen bekannt ist, dass ABCE1 während der Translationsinitiation an der SSU gebunden bleibt und so Teil von Früh- und Spätphasen-ICs ist, fehlten nach wie vor Hinweise über die Funktion von ABCE1 während der IC-Assemblierung. Um den wechselseitigen Einfluss von ABCE1 auf die Bindung von aIFs an die SSU zu untersuchen, wurden verschiedene aIFs seitenspezifisch *via* Einzel-Cysteinreste mit Fluorophoren zur Bestimmung der Bindungsaffinität zur SSU oder dem Post-SC mittels Fluoreszenzpolarisation (FP) markiert. Der Fokus lag dabei auf aIF1, da es bereits FP-Daten der aIF1-Bindung an die SSU gab, die als Vergleich zur Etablierung der Methode dienten. Eine Cystein-Variante von *S. solfataricus* aIF1 wurde generiert und erfolgreich mit verschiedenen Fluorophoren, in zwei unterschiedlichen methodischen Ansätzen, markiert. Die Bindung von fluoreszenzmarkiertem aIF1 an die SSU und den Post-SC wurde mit verschiedenen biochemischen Methoden nachgewiesen. Dennoch schwankten die FP-Daten drastisch und erlaubten dadurch lediglich eine Bestimmung der Gleichgewichtsdissoziationskonstante zur SSU, welche im Einklang mit der Literatur war. In Gegenwart von ABCE1 konnten keine thermodynamischen Parameter bestimmt werden. Ein möglicher Einfluss von ABCE1 auf die IF-Rekrutierung an die SSU oder ein möglicher Auslöser für die ATP-Hydrolyse von ABCE1 und seine Freisetzung von der SSU blieben somit ungeklärt. In Zukunft sind andere biochemische und biophysikalische Methoden nötig, um die letzte ungelöste Fragestellung der Rolle von ABCE1 in der mRNA-Translation aufzudecken.

Die umfangreichen Prozesse und involvierten Faktoren während der verschiedenen Phasen der mRNA-Translation verdeutlichen, dass dieser komplexe Mechanismus hochgradig reguliert sein muss, um die Lebensfähigkeit von Zellen zu gewährleisten. Daher haben sich Wege der mRNA-Überwachung und der Ribosomen-assoziierten Qualitätskontrolle (RQC) entwickelt, welche in Eukaryoten biochemisch und strukturell in ihren Grundzügen bereits charakterisiert sind. Spezielle RFs erkennen blockierte Ribosomen unabhängig von einem Stopp-Codon. Sie hydrolysieren nicht die Peptidyl-tRNA, sondern ermöglichen nur die Dissoziation des Ribosoms durch ABCE1. Faktoren der mRNA-Überwachung extrahieren die fehlerhafte mRNA aus dem Ribosomenkomplex. Anschließend wird die mRNA direkt abgebaut, um weitere Translationsfehler auf ihrer Grundlage zu verhindern. Zurück bleibt die LSU, die durch Peptidyl-tRNA blockiert ist und mit Hilfe der RQC recycelt wird. Die E3-Ubiquitin-Ligase Ltn1/Listerin (in Hefe/Säugetieren) assoziiert am Ribosomen-Ausgangstunnel und ubiquitiniert die anomale Polypeptidkette an Lysin-Seitenketten für die Degradierung durch das Proteasom. Rqc2/NEMF bindet die blockierte LSU und verlängert das Polypeptid C-terminal mit Alanin und Threonin (CAT-Verlängerung in *Saccharomyces cerevisiae*)

bzw. ausschließlich Alanin (Ala-Verlängerung in Säugetieren), um Lysine für die Degradation über das Ubiquitin-Proteasom System freizulegen. Sollten diese Mechanismen nicht rechtzeitig blockierte Ribosomen erkennen und auflösen, können nachfolgende translatierende Ribosomen auflaufen und so zu einer Ribosomen-Kollision führen. Es bildet sich eine definierte Interaktionsfläche der kollidierten Di- oder Polysomen, die durch spezialisierte RQC-Faktoren erkannt wird. So werden kollidierte Ribosomen durch Hel2/ZNF598 an spezifischen ribosomalen Proteinen ubiquitiniert und dadurch weitere Prozesse der Protein- und mRNA-Qualitätskontrolle gesteuert.

Vor Kurzem wurden in Bakterien der RQC Faktor MutS2 identifiziert, der speziell auf kollidierte Poly- und Disomen abzielt. Für das ABC-Protein MutS2 wurde aufgrund seiner Positionierung auf dem kollidierten Disomen-Komplex eine Funktion ähnlich der Ribosomenspaltung durch ABCE1 vorgeschlagen. Allerdings gab es bisher keine funktionalen Daten zur Ribosomdissoziation und dem molekularen Mechanismus von MutS2. Um erste Einblicke in diesen zu erhalten, war mein Ziel die ATP-Bindung von MutS2 zu charakterisieren und einen *in vitro* Assay mit kollidierten Disomen zur Analyse der MutS2-Aktivität zu etablieren. MutS2 konnte ATP und das nicht-hydrolysierbare Analog AMP-PNP binden, nicht jedoch ADP oder AMP. Nach erfolgreicher Isolation von Disomen aus *Bacillus subtilis*, ergab die Zugabe von MutS2 keine Veränderung des Ribosomenprofils. Auch Nukleotid Zugabe und Entfernung des Affinitäts-Tags erzielten keine Veränderung der Disomenpopulation. Es konnte somit kein Einfluss von MutS2 auf die Disomenstabilität bestätigt werden. Diese initialen Ergebnisse liefern wichtige Ansatzpunkte für zukünftige Studien von RQC-Faktoren.

Zusammengefasst konnten in dieser Doktorarbeit wesentliche Mechanismen der Assemblierung und Dissoziation verschiedener ribosomaler Komplexe in der mRNA-Translation aufgeklärt werden. Die besondere Rolle von ABCE1 über das Ribosomen-Recycling hinaus in der Translationsinitiation wurde zum ersten Mal ausführlich strukturell und funktionell für Archaeen gezeigt. Es wurde verdeutlicht, dass die Rolle von ABCE1 in der mRNA-Translation weiterhin nicht vollständig aufgeklärt ist und in Zukunft weitere Analysen nötig sind, um den gesamten Translationsprozess präzise in allen Lebensdomänen zu verstehen. Darüber hinaus verdeutlichen die initialen mechanistischen Studien zu MutS2, dass zukünftig komplexe Prozesse der Qualitätskontrolle in den Fokus der mRNA-Translationsforschung rücken müssen, um umfassend diesen fundamentalen zellulären Prozess in physiologischem Kontext verstehen zu können.

Abstract

Protein biosynthesis is a fundamental process across all domains of life. Polypeptides are produced by translating the genetic information of the messenger RNA (mRNA) into amino acids. This elaborate procedure is divided into the four distinct phases: initiation, elongation, termination, and ribosome recycling. The phases are controlled and regulated by a multitude of translation factors. During initiation, the ribosome assembles on the mRNA. Initiation factors (IFs) bind to the small ribosomal subunit (SSU) and assist the recruitment of mRNA and initiator transfer RNA, which delivers the first amino acid methionine ($^{Met}tRNA_i^{Met}$). After positioning the SSU at the start codon of the mRNA, additional IFs support the joining of the large ribosomal subunit (LSU). Next, elongation factors (EFs) deliver amino-acylated tRNAs (aa-tRNAs) to the translating ribosome and assist kinetic proofreading and ribosome subunit translocation after the catalytic transfer of the polypeptide onto the aa-tRNA. When a stop codon is reached, translation is terminated by release factors (RFs) that hydrolyze the peptidyl-tRNA to release the nascent protein chain. Afterwards, the ribosome is recycled in Eukaryotes and Archaea by the conserved and essential factor ABCE1, which splits the ribosome into the LSU and SSU. ABCE1 remains bound to the SSU forming the post-splitting complex (post-SC). mRNA translation closes into a cycle by recruitment of IFs to the post-SC and the start of a new round of initiation. The post-SC presents the platform for translation initiation. However, the role of ABCE1 in initiation remains elusive. Therefore, the main goal of my thesis was to unravel the molecular mechanism of ABCE1 on the post-SC and during initiation complex (IC) assembly.

Using a reconstituted system, the high-resolution structure of the archaeal post-SC was solved by cryogenic electron microscopy (cryo-EM) following the native splitting route. It was the first complete model of an archaeal SSU at atomic resolution and revealed a previously undescribed ribosomal protein, which we termed eS21. The hinge 2 region of ABCE1 was identified to be the major interaction interface that anchors to the SSU. Functional characterization of single residue mutations in hinge 2 unraveled essential interactions with the ribosomal RNA backbone of the SSU. Sensing of SSU-binding was found to be allosterically transmitted to the nucleotide-binding sites (NBSs) for integration into the ATPase cycle of ABCE1.

Reconstitution of the archaeal translation apparatus allowed for dissection of IC assembly in the presence of ABCE1. Three different ICs were resolved by cryo-EM. The results were in accordance with recent structural findings of eukaryotic translation initiation and highlighted that the involvement of ABCE1 is conserved.

In a semi-native approach, recombinant ABCE1 was pulled-down from crenarchaeal cell lysates. Mass spectrometric analysis of co-immunoprecipitated ribosomal complexes identified the association of numerous translation factors to the post-SC in a cellular context. The establishment of the genetic toolbox of the acidothermophilic *Sulfolobus acidocaldarius* allowed the homologous expression of ABCE1. Pull-down of native ABCE1 revealed similar ribosomal complexes as the semi-native and reconstituted approaches. Together, my results gave first physiological relevance of ABCE1 involvement in mRNA translation initiation in Archaea. Native archaeal ABCE1-ICs were vitrified for structural analysis by cryo-EM. Thereby, future structural analysis will allow to analyze the interactions of ABCE1 on native ICs and identify its role in IC assembly.

To address the molecular process of IC assembly, the binding affinity of aIF1 to the SSU was determined by fluorescence polarization. Similar studies will allow for a detailed functional analysis on IF recruitment to the SSU in presence of ABCE1.

mRNA surveillance and ribosome-associated quality control (RQC) mechanisms evolved to ensure cell viability. The pathways overcome ribosome stalling and defective translation components. Stalled ribosomes are terminated by special RFs, which do not hydrolyze the peptidyl-tRNA, but allow dissociation of the ribosome by ABCE1. Faulty messages are degraded *via* mRNA decay pathways and the LSU is rescued by RQC factors. Recently, the bacterial RQC factor MutS2 was identified to specifically target collided di- and polysomes but its molecular mechanism remains unknown. In this thesis, initial functional analyses showed tri-phosphate specific nucleotide binding of MutS2. While the dissociation of collided disomes by MutS2 could not be observed, the results pave the way for future *in vitro* studies of bacterial RQC factors acting on specific ribosome populations.

In the future, mRNA translation research must focus on complex quality control processes to comprehensively understand this fundamental cellular process in a holistic context.

Table of contents

1 Introduction

1.1 From a universal genetic code to an intricate mRNA translation and quality control machinery

The universal code of life was discovered many decades ago. Today, it is basic knowledge that genetic information is encoded in deoxyribonucleic acid (DNA) with specific base pairing forming a double helix (Watson & Crick, 1953), which is condensed by histones and organized in chromosomes. However, the essence of life is the fundamental process of transcribing the genetic (DNA) information into messenger ribonucleic acid (mRNA) which in turn is translated by the triplet code (codons) into amino acids forming polypeptide chains with highly selective and specific cellular functions (Woese, 1968; Crick, 1970). In the three domains of life (Bacteria, Archaea, and Eukaryotes), protein biosynthesis varies in spatial organization and functionality. In Prokaryotes, transcription of DNA into mRNA and translation of the mRNA into proteins is directly coupled and occurs simultaneously, while in Eukaryotes, transcription and translation are spatially separated. The DNA is transcribed in the nucleus and the mRNA is exported into the cytoplasm, where it is translated by ribosomes. While the basics of protein biosynthesis were set in the 20th century, the main dogma of biology was a DNA-driven world. However, with the emergence and evolvement of structural techniques focusing on the ribosome, a new understanding of RNA as a central regulatory determinant of physiological processes was established at the beginning of the 21st century (Woese, 2001). It pathed the way for today's knowledge on mRNA translation and the importance of controlled ribosome function. A small (30S/40S for Bacteria and Archaea/Eukaryotes, respectively) and a large (50S/60S) subunit embrace each other at an interface forming the 70S/80S ribosome (Lake, 1976). The ribosomal subunits are built-up by core ribosomal RNAs (rRNA) and many proteins (rps), with some being universally conserved and others being specific for the domain of life, organism, or organelle (Ban *et al*, 2014). The small ribosomal subunit (SSU) primarily functions in mRNA binding, while the large subunit (LSU) positions the anti-codon holding aminoacyl transfer RNAs (tRNAs) and catalyzes the peptide bond formation. Numerous additional factors can be spatially or temporally associated with the ribosome depending on the organism, organelle, and cellular status (Steitz, 2008; Klinge *et al*, 2012; Voorhees & Ramakrishnan, 2013; Greber & Ban, 2016; Bieri *et al*, 2018). Heterogeneous ribosome populations have been a focus of study in the last decade and the role and function of specialized ribosomes are still discussed (Xue & Barna, 2012; Guo, 2018; Ferretti & Karbstein, 2019; Gay *et al*, 2022). In the perspective of the essential and

intricate function of the ribosome, associated quality control mechanisms have evolved to consistently maintain the translation functionality (Joazeiro, 2019; Nürenberg-Goloub & Tampé, 2019; Filbeck *et al*, 2022). Accordingly, defects in the sophisticated system of mRNA translation an quality control are connected to numerous diseases, e.g. cancer, neurodegeneration, and other ribosomopathies (Mills & Green, 2017; Tahmasebi *et al*, 2018; Aspesi & Ellis, 2019; Boussaid & Fontenay, 2022). Although the overall process of mRNA translation is highly conserved across all domains of life, each phase and the involved components harbor features specific for Bacteria, Eukaryotes, and Archaea. While Bacteria and Eukaryotes have each developed their own adapted mechanisms and features, Archaea combine prokaryotic and eukaryotic features into a unique mode of translation (Kisselev & Buckingham, 2000; Voorhees & Ramakrishnan, 2013; la Teana *et al*, 2013; Londei, 2015; Petrov *et al*, 2015; Weixlbaumer *et al*, 2021; Xu *et al*, 2022).

1.2 The mRNA translation cycle

Translation of mRNA into polypeptides by the ribosome is divided into the four phases of initiation, elongation, termination, and ribosome recycling. All steps are facilitated by specialized translation factors. The translation-competent ribosome is assembled during initiation. First, initiation factors (IFs) are recruited, which catalyze mRNA and initiator tRNA ($tRNA_i^{fMet}$) binding, before being released for joining of the large ribosomal subunit. Next, the ribosome translocates across the mRNA and elongates the nascent peptide chain. With the help of elongation factors (EFs), aminoacylated tRNAs (aa-tRNAs) are delivered. When a stop codon is reached, the nascent polypeptide chain is released with the help of release factors (RFs) during the termination phase. The formed post-termination complex (post-TC) is recognized by ABCE1, which splits the ribosome apart into its small and large subunits in the phase of ribosome recycling. Finally, ABCE1 remains bound to the SSU forming the post-splitting complex (post-SC), which functions as a platform for initiation factor recruitment and a new round of translation initiation (Figure 1) (Nürenberg & Tampé, 2013; Hellen, 2018; Shirokikh & Preiss, 2018).

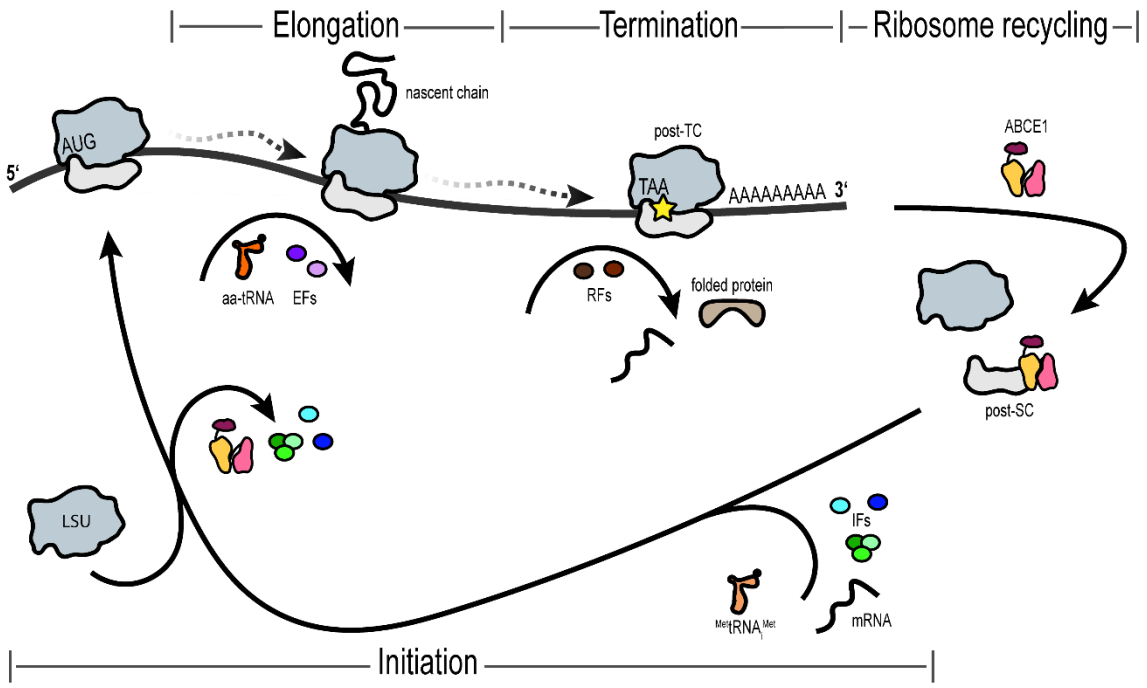

Figure 1: Illustration of the mRNA translation cycle. mRNA translation begins with the formation of a translation competent ribosome on the target mRNA. During initiation, multiple initiation factors (IFs) bind to the small ribosomal subunit and recruit mRNA as well as initiator tRNA, which recognizes the start codon. After mRNA and tRNA are correctly positioned, most IFs are released and the large ribosomal subunit joins, forming the translation-ready ribosome. During elongation, the ribosome moves along the mRNA. With the help of elongation factors (EFs) respective amino-acylated tRNAs (aa-tRNAs) are recruited and peptide bond formation is catalyzed for nascent chain elongation. When the ribosome reaches a stop codon (yellow star), release factors (RFs) bind at the peptidyl transferase center (PTC) and hydrolyze the ester bond of the peptidyl tRNA, thereby releasing the nascent polypeptide. The resulting post-termination complex (post-TC) is recognized by the ribosome recycling factor ABCE1 in Eukaryotes and Archaea (RRF in Bacteria). In concert with the RF, ABCE1 splits the ribosome into large and small subunits. ABCE1 stays stably bound to the small ribosomal subunit, forming the post-splitting complex (post-SC), which is the platform for initiation factor recruitment for a new round of mRNA translation initiation.

1.2.1 Initiation

During the initiation phase, a translation competent ribosome is formed on a target mRNA to decode the genetic information. In Bacteria, initiation is kinetically controlled and referred to as the rate-limiting step of mRNA translation (Milón & Rodnina, 2012; Gualerzi & Pon, 2015). Apart from the ribosomal subunits, only the three initiation factors IF1, IF2, and IF3, formyl-methionyl initiator tRNA ($^{fMet}tRNA_i^{fMet}$), and mRNA are needed for successful initiation in Bacteria. Most mRNAs contain a Shine-Dalgarno leader sequence upstream of the AUG start codon in the 5'-untranslated region (5'-UTR). The purine-rich sequence AGGAGGU serves as ribosome binding site by anchoring the mRNA to the

complement anti-Shine-Dalgarno sequence ACCUCCU at the 3'-end of the 16S rRNA of the 30S subunit (Shine & Dalgarno, 1974, 1975). IF1 binds to the universally conserved SSU protein uS12 at the 3'-end of the essential rRNA helix 44 (h44) in the A site of the small ribosomal subunit (Carter *et al*, 2001). aIF1 assists IF2 and IF3 binding and coordinates the selection of $tRNA_i^{fMet}$ and mRNA. IF2 recruits $^{fMet}tRNA_i^{fMet}$ to the 30S ribosomal subunit. As a multi-domain factor, aIF2 consists of an N-terminal, GTP-binding (G), and C-terminal domain. Part of the G-domain is conserved in translational GTPases, like elongation factors EF-Tu and EF-G. While the C-domain binds $^{fMet}tRNA_i^{fMet}$ (Guenneugues *et al*, 2000), the N-domain anchors IF2 to the 30S subunit (Julián *et al*, 2011). IF3 influences translation initiation on multiple levels by being crucial for initiation fidelity, preventing premature subunit joining, distinguishing unsuitable mRNAs, and modulating tRNA association and dissociation rates from the 30S subunit P site (Milón & Rodnina, 2012). During 30S initiation complex (IC) assembly, first IF2 and IF3 bind to the 30S subunit followed by IF1, which stabilizes the forming IC. After mRNA binding and $^{fMet}tRNA_i^{fMet}$ recruitment, IF1 and IF3 are released and the 50S subunit joins. Finally, after mRNA-tRNA codon-anti-codon base pairing, IF2 leaves the ribosome, which is then translation competent (Milón *et al*, 2012; Goyal *et al*, 2015; Rodnina, 2018).

In Eukaryotes, the process of mRNA translation initiation is much more complex compared to Bacteria. Translation in the cytoplasm is spatially separated from transcription in the nucleus. The mRNA is processed and requires the multi-protein initiation factor platform eIF4F for translation access. It circularizes the mRNA by binding both, the 7-methyl-guanosine (m^7G) 5'-cap (eIF4E) and poly-adenosine (poly-A) 3'-tail (poly-A binding protein (PABP) *via* eIF4G). The RNA helicase eIF4A unwinds and eIF4G bridges the mRNA with the ribosome (Gingras *et al*, 1999). First, a 43S pre-initiation complex (pre-IC) is formed. The small factors eIF1 and eIF1A bind to the small 40S ribosomal subunit in a cooperative fashion (Maag & Lorsch, 2003) and accelerate the binding of the ternary complex of the eIF2αβγ heterotrimer, initiator tRNA, and GTP (eIF2-$^{Met}tRNA_i^{Met}$-GTP) (Passmore *et al*, 2007). The multimeric factor eIF3 and eIF5 complete the 43S pre-IC, which in complex with eIF4F and the mRNA, scans for the AUG start codon in 5' to 3' direction. aIF1 and aIF1A promote an open conformation of the 40S mRNA channel to allow efficient scanning (Passmore *et al*, 2007). Upon AUG recognition by the ternary complex, initiator tRNA is accommodated at the mRNA by codon-anti-codon base pairing. The 48S pre-IC is formed by eIF1 release. eIF5B is recruited by eIF1A (Maag *et al*, 2006; Mitchell & Lorsch, 2008), which promotes GTP hydrolysis in eIF2, leading to its release. Furthermore, eIF5B promotes dissociation of eIF1A and the joining of the 60S large ribosomal subunit completing the 80S translation competent ribosome (Jackson *et al*, 2010).

Archaea, as Prokaryotes, do not possess a nucleus allowing spatially and temporally coupled mRNA transcription and translation (French *et al*, 2007; Schramm *et al*, 2021; Weixlbaumer *et al*, 2021). In the well-studied Crenarchaeon *Saccharolobus solfataricus* a minor portion of mRNA are polycistronic and leadered, with and without Shine-Dalgarno sequence. Shine-Dalgarno sequence-containing mRNAs are able to bind the 30S subunit with correct AUG positioning without the help of initiation factors (Tolstrup *et al*, 2000; Benelli *et al*, 2003). However, most mRNAs identified in *S. solfataricus* are leaderless and monocistronic, thereby relying on initiator tRNA for correct incorporation into the 30S ribosomal subunit and AUG recognition during initiation (Benelli *et al*, 2003; Wurtzel *et al*, 2010; la Teana *et al*, 2013). A similar preference for leaderless mRNAs in the Euryarchaeon *Haloferax volcanii* (Brenneis *et al*, 2007) suggests an overall trend for Archaea (Wurtzel *et al*, 2010). Archaea and Eukaryotes share a common structural core of initiation factors at the SSU during initiation (Schmitt *et al*, 2019). Accordingly, the archaeal initiation factors aIF1, aIF1A, the heterotrimer aIF2αβγ, and aIF5B are all orthologs of their eukaryotic counterparts. aIF1 binds near the P site at the 3'-end of h44 of the 30S subunit and ensures fidelity of start codon recognition. aIF1 and aIF1A synergistically stimulate aIF2 binding to the 30S subunit (Hasenöhrl *et al*, 2006, 2009; Monestier *et al*, 2018). In contrast to eIF2, aIF2 first binds to the 30S subunit, where it recruits initiator tRNA acting like the bacterial IF2 (Hasenöhrl *et al*, 2009; Milón *et al*, 2010). The ternary complex with GTP forms directly on the SSU but can also assemble *in vitro* in the absence of the 30S subunit (Pedullà *et al*, 2005; Stolboushkina *et al*, 2008; Schmitt *et al*, 2012; Stolboushkina *et al*, 2013; Dubiez *et al*, 2015). As for Eukaryotes, the 43S initiation complex in Archaea consists of the small ribosomal subunit, aIF1, aIF1A, the ternary complex, and mRNA (Coureux *et al*, 2016; Schmitt *et al*, 2019). After accommodation of initiator tRNA in the P site and start codon base pairing, aIF1 is released forming a 48S IC (Coureux *et al*, 2020; Schmitt *et al*, 2020). Like its eukaryotic ortholog, the GTPase aIF5B is the LSU-joining factor. Together with aIF1A, it facilitates joining of the 50S subunit, forming the 70S ribosome. Interestingly, in an isolated system, aIF5B rescues translation in the absence of aIF2 by stimulating binding of initiator tRNA to the 30S ribosomal subunit, thereby serving the same function as its bacterial ortholog IF2 (Maone *et al*, 2007). A similar mode is also observed for eIF5B (Terenin *et al*, 2008). Afterwards, the ribosome is translation component and elongation of the nascent polypeptide chain can begin.

1.2.2 Elongation

Elongation is the most conserved phase of mRNA translation. Extension of the nascent polypeptide chain is a continuous process of decoding the mRNA template at the ribosomal A site, recruitment and accomodation of aa-tRNAs, peptide bond formation at the PTC, ribosome translocation, and release of empty tRNAs from the E site until a stop codon is reached. Multiple elongation factors with functional orthologs in all three domains of life are involved in the elongation process (Dever *et al*, 2018; Rodnina, 2018). EF-Tu (Bacteria) and its orthologs (eEF1A and aEF1α) are translational GTPases that bind aa-tRNAs and GTP with nanomolar affinity (LaRiviere *et al*, 2001; Gromadski *et al*, 2007), forming ternary complexes (EF-Tu/aa-tRNA/GTP). In the ribosome-decoding center, GTP-hydrolysis is activated by interaction of EF-Tu with the sarcin-ricin loop (SRL) of the LSU 23S rRNA (28S rRNA in Eukaryotes) (Schmeing *et al*, 2009; Voorhees *et al*, 2010). The aa-tRNA is free for base pairing and the delivery factor in its GDP-bound state is released from the ribosome. The cognate aa-tRNA is accommodated very fast compared to a non-cognate aa-tRNA, allowing time for aa-tRNA exchange in a proofreading mechanism (Rodnina *et al*, 2017). Next, the peptide bond between peptidyl tRNA in the P site and accommodated aa-tRNA in the A site is formed by entropic catalysis (Sievers *et al*, 2004). In Bacteria, EF-P assists in peptide bond formation of polyproline regions on which the ribosome stalls (Doerfel *et al*, 2013; Ude *et al*, 2013; Huter *et al*, 2017). The eukaryotic ortholog eIF5A not only promotes peptide bond formation of polyproline regions by inducing a favorable positioning of the substrates (Saini *et al*, 2009; Gutierrez *et al*, 2013; Melnikov *et al*, 2016; Schmidt *et al*, 2016), but rather works in a general fashion by globally assisting peptide bond formation (Schuller *et al*, 2017). Like eIF5A, aIF5A is post-translationally modified with hypusine, which is essential for its function (Cooper *et al*, 1983; Prunetti *et al*, 2016; Bassani *et al*, 2018). With peptide bond formation, the extended peptidyl-tRNA is positioned in the A site. For subsequent translocation of the ribosome, the subunits move relative to each other in a rotation-like motion. EF-G (Bacteria) or a/eEF2 promote the translocation of the tRNAs by GTP-hydrolysis. The deacylated tRNA moves from the P to the E site and the newly extended peptidyl-tRNA from the A to the P site. EF-G/GDP or eIF5A/GDP are afterwards released from the post-translocated ribosome and the A site becomes available again for delivery of the next aa-tRNA (Belardinelli *et al*, 2016; Dever *et al*, 2018; Rodnina, 2018).

1.2.3 Termination

Translation is terminated when a stop codon is reached in the ribosomal A site. Release factors read out the stop codons and hydrolyze the peptidyl-tRNA ester bond. In contrast to the elongation phase, termination functions differently in Bacteria than in Eukaryotes and Archaea. Bacterial class I release factors RF1 and RF2 recognize the stop codons UAG/UAA (RF1) and UGA/UAA (RF2) with their conserved recognition motifs PVT and SPF, respectively (Laurberg *et al*, 2008; Weixlbaumer *et al*, 2008; Korostelev *et al*, 2010). After the accommodation of RF1/RF2, the peptidyl-tRNA is hydrolyzed at the PTC *via* the conserved GGQ motif in RF1/RF2. The glutamine residue of the GGQ motif controls the specificity for water as a nucleophile of the catalysis reaction (Shaw & Green, 2007), which proceeds *via* a tetrahedral intermediate and results in deacylated tRNA and the free nascent polypeptide (Jin *et al*, 2010; Rodnina, 2013). Afterwards, the class II release factor RF3 is recruited. After the release of the nascent polypeptide, a stable RF3•GTP-ribosome complex is formed, which promotes the dissociation of RF1/RF2. Finally, RF3 hydrolyzes GTP and RF3•GDP is released from the ribosome (Peske *et al*, 2014; Rodnina, 2018).

In Eukaryotes and Archaea, class I release factors a/eRF1 and class II factors eRF3/aEF1α control mRNA translation termination (Zhouravleva *et al*, 1995; Alkalaeva *et al*, 2006; Saito *et al*, 2010; Kobayashi *et al*, 2012). eRF1 and eRF3 form a ternary eRF1-eRF3•GTP complex, which binds to the ribosome (Mitkevich *et al*, 2006; Taylor *et al*, 2012; des Georges *et al*, 2014). The three-domain structure of eRF1 mimics tRNA (Song *et al*, 2000). GTP-hydrolysis by eRF3 is triggered by interaction with eRF1 and the ribosomal SRL, resulting in accommodation of eRF1 at the stop codon (Frolova *et al*, 1996; Dever & Green, 2012; Hellen, 2018). eRF1 decodes all three stop codons *via* the conserved NIKS motif and discriminates against sense codons with help of the GTS and YxCxxxF motifs (Song *et al*, 2000; Chavatte *et al*, 2002; Frolova *et al*, 2002; Kolosov *et al*, 2005; Brown *et al*, 2015). Movements in eRF1, which are allowed after GTP hydrolysis by eRF3, lead to hydrolysis of the peptidyl-tRNA ester bond *via* the GGQ motif of eRF1 as described for Bacteria (Frolova *et al*, 1999). Lastly, eRF3•GDP must dissociate to form the post-TC and allow ribosome recycling (Shoemaker & Green, 2011; Shao *et al*, 2016).

1.2.4 Ribosome recycling

Bacteria and Eukaryotes/Archaea diverged evolutionarily in how to terminate mRNA translation. Accordingly, they also evolved different proteins for dissolving post-TCs to recycle the ribosomal subunits. In Bacteria, ribosomes are split into subunits by EF-G and the ribosome recycling factor (RRF), which binds to the A site. GTP-hydrolysis by EF-G pushes RRF into the intersubunit space, thereby splitting the ribosomal subunits apart (Gao *et al*, 2005; Peske *et al*, 2005; Fu *et al*, 2016). It is suggested that after splitting, mRNA is spontaneously released and tRNA dissociation is promoted by IF3 (Borg *et al*, 2016; Fu *et al*, 2016; Rodnina, 2018). In Eukaryotes and Archaea, the essential and conserved ATP-binding cassette (ABC) protein ABCE1 (RNase L inhibitor 1, Rli1, in yeast; pixie in *Drosophila*) is the universal ribosome recycling factor (Pisarev *et al*, 2010; Barthelme *et al*, 2011; Shoemaker & Green, 2011). ABCE1 binds the post-TC near the ribosomal GTPase activating center and directly contacts a/eRF1 forming the pre-splitting complex (pre-SC) (Becker *et al*, 2012; Preis *et al*, 2014; Shao *et al*, 2016). ABCE1 undergoes multiple domain rearrangements during the different phases of ribosome recycling, which is highlighted by X-ray and cryo-EM structures as well as Förster resonance energy transfer (FRET) studies (Figure 2B, section 1.3.2) (Karcher *et al*, 2008; Becker *et al*, 2012; Heuer *et al*, 2017; Gouridis *et al*, 2019; Kratzat *et al*, 2021). Importantly, ribosome recycling by ABCE1 is dependent on class I release factors. After splitting, mRNA and deacylated tRNA can be removed from the 40S subunit *via* redundant mechanisms by initiation factors eIF1, eIF1A, eIF3, and eIF3j (Pisarev *et al*, 2007), by Ligatin (eIF2D), or by the MCT-1/DENR heterodimer, which has orthologous domains to eIF2D (Skabkin *et al*, 2010; Lomakin *et al*, 2017; Young *et al*, 2018, 2021). Translation can re-initiate on the same mRNA from recycled 40S subunits *in vitro* in the presence of eIF2, eIF1, eIF1A, and $^{Met}tRNA_i^{Met}$. Furthermore, eIF4F facilitates 3'-directionality of re-initiation (Skabkin *et al*, 2013). Notably, ABCE1 stays associated with the SSU in the closed, ATP-occluded state, forming the post-splitting complex (post-SC) (Figure 2B) (Kiosze-Becker *et al*, 2016; Heuer *et al*, 2017; Nürenberg-Goloub *et al*, 2018). While a trigger for ATP hydrolysis by ABCE1 and its subsequent release from the SSU remains elusive, structural evidence exists that the post-SC functions as a platform for initiation factor recruitment, including ABCE1 in 43S early- and 48S late-stage ICs (Heuer *et al*, 2017; Mancera-Martínez *et al*, 2017; Kratzat *et al*, 2021). Thus, ribosome recycling bridges termination with a new round of initiation *via* the post-SC, thereby closing the mRNA translation cycle (Figure 1).

1.3 The ribosome recycling factor ABCE1 is a unique ATP-binding protein

1.3.1 Mechanistic overview of ATP-binding cassette proteins

ATP-binding cassette (ABC) proteins facilitate a multitude of cellular functions, which are mostly but not exclusively related to the transport of various substrates (e.g. vitamins, lipids, and ions) across membranes (Thomas & Tampé, 2020). ATP-binding and hydrolysis events in the conserved nucleotide-binding domains (NBDs) power conformational rearrangements directly connected to the protein function. The ABC protein superfamily was first grouped by bacterial sequence alignment of the nucleotide-binding domains (NBDs) into exporters, (mostly) importers, and non-transporters (Saurin *et al*, 1999; Dassa & Bouige, 2001). In the mammalian ABC protein superfamily, however, proteins were grouped into the seven subfamilies ABCA-G not only based on the NBD but also on the transmembrane domain (TMD) sequence homology and domain organization (Klein *et al*, 1999; Dean *et al*, 2001). Importantly, members of the subfamilies E and F do not contain TMDs, but only exist as non-membrane bound twin-NBDs with accessory domains that function *inter alia* in mRNA translation (Gerovac & Tampé, 2019) or DNA repair (Lamers *et al*, 2000; Obmolova *et al*, 2000). In recent years, a new classification of ABC transporter subfamilies based on the TMD fold has been proposed for more precise grouping of mechanistically similar ABC proteins (Thomas *et al*, 2020). While the TMD structure is important only for ABC transporters, all ABC proteins rely on the conserved ATP-binding motifs of the NBDs for energy-coupled function. Two head-to-tail oriented NBDs form composite nucleotide-binding sites (NBSs), which are allosterically coupled. Two ATP molecules bind in the NBD interface resulting in closure of the interface and NBD dimerization (Smith *et al*, 2002). The NBDs can only open again after ATP hydrolysis and the subsequent release of inorganic phosphate (P_i) and ADP. Thus, the NBDs perform a tweezer-like motion, which is transferred to accessory domains (TMDs in transporters) catalyzing the respective protein function (Hopfner, 2016). As the energy-coupling via the NBSs is crucial for ABC proteins, the NBDs contain several conserved motifs. Notably, ABC proteins are rather promiscuous and accept various nucleotides *in vitro*. The A-loop stacks the adenine of the nucleotide *via* an aromatic residue. Walker A/P-loop binds the α- and β-phosphates. Walker B provides the catalytic glutamate. The H-loop (His-switch) coordinates the γ-phosphate *via* a water molecule. The signature LSGGQ binds the γ-phosphate in the opposite NBD. The D-loop functions in allosteric crosstalk between the two NBDs. The Q-loop contacts the accessory or TMD domain and therefore is likely to be involved in energy transfer and inter domain signaling (Rees *et al*, 2009; Locher, 2016). In

many ABC proteins, one NBS has degenerated motifs, contributing to the overall structural and mechanistic multitude of ABC proteins (Thomas & Tampé, 2020).

1.3.2 Structural organization and functional features of ABCE1

The ribosome recycling factor ABCE1 is the only member of the ABC protein subfamily E. ABCE1 is not found in Bacteria; however, it is essential and conserved in Eukaryotes and Archaea. The two NBDs of ABCE1 are oriented from head-to-tail and are connected *via* a short hinge region (hinge 1). The NBDs form two composite NBSs with a degenerated Walker A in NBS II. All other motifs are symmetric but differ marginally from the classic ABC transporter motifs, *e.g*. signature LSGGGLQ (NBS I) and LSGGELQ (NBS II) instead of consensus LSGGQ. The C-terminal residues form a second hinge region (hinge 2) (Figure 2A). Additionally, ABCE1 harbors a unique N-terminal iron-sulfur cluster (FeS) domain (FeSD) consisting of two essential diamagnetic $[4Fe\text{-}4S]^{2+}$ clusters (Barthelme *et al*, 2007). ABCE1 was first identified as an inhibitor of the interferon-induced RNA nuclease RNase L (Rli 1) (Bisbal *et al*, 1995) and later as host protein 68 (HP68) in HIV capsid assembly (Zimmerman *et al*, 2002), thereby being associated with immune response and viral infection. The mechanistic function of ABCE1 in these processes still remains largely elusive. Its involvement in mRNA translation was first reported to be an initiation factor since it interacts with other IFs and promotes their recruitment to the SSU in yeast, human, and fruit fly (Dong *et al*, 2004; Chen *et al*, 2006; Andersen & Leevers, 2007). Later, the main function of ABCE1 was found to be the essential ribosome recycling factor that splits ribosomes apart into the large and small subunits during canonical mRNA translation termination, in mRNA surveillance, and ribosome-associated quality control pathways, as a quality checkpoint in ribosome biogenesis, and after hibernation (Pisarev *et al*, 2010; Barthelme *et al*, 2011; Shoemaker & Green, 2011; Strunk *et al*, 2012; van den Elzen *et al*, 2014). After ABCE1 binds to target ribosomes, the pre-SC forms, in which ABCE1 is in an intermediate, semi-closed state with a rotated nucleotide-binding domain 2 (NBD2) compared to free ABCE1 (Figure 2B). ATP-dependent rearrangements of the NBDs and the FeSD destabilize the ribosome. ATP occlusion and tight closure of both NBSs are accompanied by a large rotation of the FeSD between the ribosomal subunits, which leads to a collision with the class I release factor pushing it into the intersubunit space and ultimately dissociating the subunits (Figure 2B) (Barthelme *et al*, 2011; Kiosze-Becker *et al*, 2016; Heuer *et al*, 2017; Nürenberg-Goloub *et al*, 2018). Therein, the NBSs of ABCE1 function asymmetrically in allosterically coupled ATP-binding and hydrolysis. The low ATP-turnover NBS II controls binding to the ribosome by ATP-occlusion. It facilitates ATP-

binding in the high-turnover NBS I, which powers the structural rearrangements necessary for ribosome splitting (Nürenberg-Goloub *et al*, 2018). Despite the functional insights and structural data on the ABC system of ABCE1 during ribosome splitting, it remains elusive how the ribosome is sensed, and the information of ribosome-binding is transmitted and integrated into the ATPase cycle. Furthermore, the early findings of ABCE1 involvement in translation initiation come full circle with recent structural findings of ABCE1 being part of initiation complexes. However, the role of ABCE1 during IC assembly and the potential interplay with factors on the small ribosomal subunit, as well as the ultimate trigger for ABCE1 release from the SSU are enigmatic.

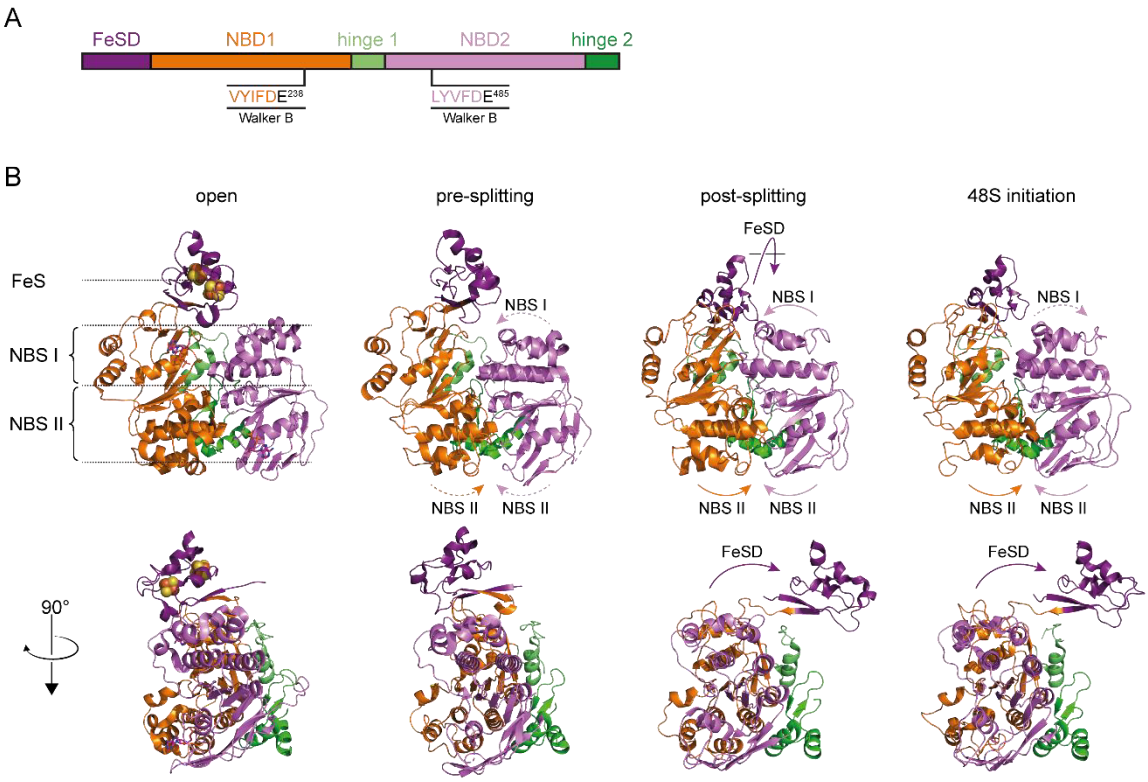

Figure 2: Domain architecture of ABCE1 and structural rearrangements during ribosome recycling. A) ABCE1 domain architecture with catalytic glutamate-containing Walker B motifs (adapted from Figure 4B and (Nürenberg-Goloub *et al*, 2020)). *S. solfataricus* numbering. **B)** Structural snapshots of ABCE1 during ribosome recycling and subsequent translation initiation. In the open, ADP-bound state (PDB 3BK7), the nucleotide-binding sites (NBSs) allow nucleotide exchange. In the pre-splitting state (PDB 5LZV), the NBSs are in a semi-open/intermediate (dotted arrows) conformation due to movement of the nucleotide-binding domains (NBDs). In the post-splitting complex (PDB 5LL6), AMP-PNP is occluded in both NBSs in a closed conformation (solid arrows). The iron-sulfur cluster domain (FeSD) rotates by approximately 150°. During initiation complex assembly, ABCE1 remains present on the small ribosomal subunit in late stage 48S ICs (PDB 6ZU9). NBS I partially opens to the intermediate state (dotted arrow), but NBS II remains closed with occluded ATP (solid arrows) as the last checkpoint for ABCE1 release.

1.4 Quality control pathways in mRNA translation

The intricate mechanism of mRNA translation is highly controlled. The basis for all quality control pathways is the surveillance of the ribosome translation rate. Among other reasons, ribosomes slow down on rare codons, challenging mRNA structures, and demanding amino acid sequences like poly-proline regions because the respective aa-tRNAs are less abundant, translocation is physically blocked, or the molecular geometry of the polypeptide in the PTC and peptide exit tunnel is altered, respectively. In the context of cellular proteostasis, ribosome stalling allows folding of the nascent chain, translational frameshifting, recruitment of auxiliary factors for co-translational modification or translocation, and for signaling to other processes (Pavlov *et al*, 2009; Zhang & Ignatova, 2011; Woolstenhulme *et al*, 2013; Caliskan *et al*, 2015; Kim *et al*, 2015; Buskirk & Green, 2017). The slowdown of the translation rate is deliberate for these processes and specific factors have evolved for assistence (*e.g*. EF-P and a/eIF5A promote peptide-bond formation in poly-proline regions, see section 1.2.2). However, prolonged pausing of the ribosome leads to potentially toxic nascent polypeptides and is recognized as a translation error. Therefore, quick and efficient degradation of the aberrant mRNA and polypeptide are crucial for cell survival. In Bacteria, transfer-messenger RNA (tmRNA), a hybrid structure with features of tRNA and a coding mRNA sequence, is the main system for rescue of stalled ribosomes (*e.g*. truncated RNAs without a stop codon) and functions in a process termed *trans*-translation. The tRNA part allows for accommodation in the A site and the mRNA part contains an open reading frame (ORF) encoding the peptide AANDENYALAA, which targets the nascent chain for degradation. The ORF ends on a stop codon, thereby allowing conventional translation termination and rescue of the ribosomal subunits (Keiler *et al*, 1996; Karzai *et al*, 1999; Moore & Sauer, 2007; Keiler, 2008; Buskirk & Green, 2017).

In Eukaryotes, stalled ribosomes trigger the no-go decay (NGD), the nonsense-mediated decay (NMD), or no-stop decay (NSD) quality control and mRNA surveillance pathways at structured mRNAs, premature or missing stop codons, respectively (Frischmeyer *et al*, 2002; van Hoof *et al*, 2002; Doma & Parker, 2006; Nürenberg-Goloub & Tampé, 2019). NMD functions *via* translation termination by eRF1-eRF3 and PABP and leads to subsequent degradation of the faulty mRNA. Additionally, NMD controls cellular mRNA levels globally, by degrading not only faulty but also functional mRNAs (Karousis & Mühlemann, 2019; Kurosaki *et al*, 2019; Yi *et al*, 2021). NGD and NSD pathways utilize the stop codon-independent class I release factor ePelota (Dom34 in yeast), which is delivered to stalled ribosomes by the class II RF Hbs1 (Chen *et al*, 2010; Becker *et al*, 2011; Tsuboi *et al*, 2012). Importantly, Archaea also rescue stalled ribosomes *via* aPelota,

which is delivered by aEF1α (Kobayashi *et al*, 2010). The superkiller (SKI) complex is recruited by Hbs1 and extracts the mRNA from the stalled ribosome for degradation by the exosome (van Hoof *et al*, 2002; Saito *et al*, 2013; Zinoviev *et al*, 2020; Kögel *et al*, 2022). After GTP hydrolysis, Hbs1 is released from the ribosome. The resulting post-TC still contains peptidyl-tRNA and is a substrate for ABCE1/Pelota-mediated ribosome splitting (Shoemaker *et al*, 2010; Pisareva *et al*, 2011; Becker *et al*, 2012). The SSU is thereby recycled and can be repurposed. However, the LSU remains blocked by peptidyl-tRNA. The ribosome-associated quality control (RQC) pathway targets blocked LSUs. The RING domain E3 ubiquitin ligase Listerin (Ltn1 in yeast) and nuclear export mediator factor (NEMF, Rqc2 in yeast) are the core elements of the RQC machinery (Brandman *et al*, 2012; Doamekpor *et al*, 2016; Joazeiro, 2019). NEMF/Rqc2 senses the blocked LSU and recruits Listerin/Ltn1, which ubiquitylates the nascent chain for proteasomal degradation (Bengtson & Joazeiro, 2010; Defenouillère *et al*, 2013; Shao *et al*, 2015). However, yeast Rqc2 in parallel specifically recruits alanyl and threonyl-tRNAs and catalyzes the C-terminal elongation of the nascent chain (C-terminal Ala-Thr elongation, CAT tailing). Mammalian NEMF likewise synthesizes a poly-alanine tail (Ala-tail), allowing for ubiquitylation of the extended nascent chain by Listerin/Ltn1 (Shen *et al*, 2015; Kostova *et al*, 2017) or induce Listerin/Ltn1-independent degradation of the polypeptide by the ubiquitin-proteasome system mediated by other cytosolic E3 ligases (Sitron & Brandman, 2019; Thrun *et al*, 2021). CAT tails were further shown to induce aggregation of the nascent chains and subsequent stress response (Choe *et al*, 2016; Yonashiro *et al*, 2016). In Bacteria, the Rqc2 homolog RqcH functions redundant to the tmRNA mechanism. RqcH elongates the peptidyl-tRNA specifically by C-terminal poly-alanine tails that act as direct degrons for the protease ClpXP (Lytvynenko *et al*, 2019). In Archaea, there is poor knowledge about similar quality control and surveillance mechanisms. However, an archaeal Rqc2 homolog (aRqcH or aRqc2) was identified. Interestingly, the aRqcH/aRqc2 gene is located in direct neighborhood of ABCE1 and aPelota in the genome of many Archaea, indicating a function coupled with splitting of ribosomal complexes (Lytvynenko *et al*, 2019).

For high translation efficiency, multiple ribosomes simultaneously translate the same mRNA, depending on its length and features determining translation initiation and elongation rate. Consequently, if a leading ribosome slows down or stalls, the tailing ribosome may collide with it. A conserved dimerization interface on the SSUs forms a specific di-ribosome (disome) structure (Ikeuchi *et al*, 2019). The E3 ubiquitin ligase Hel2/ZNF598 (yeast/mammals) recognizes disomes and collided ribosomes of higher order, and ubiquitylates the ribosomal proteins uS3, uS10, and eS10. In concert with

ribosome splitting by ABCE1 and ePelota, NGD and RQC responses lead to degradation of the mRNA and nascent polypeptide (NGD^{RQC+}) (Simms *et al*, 2017; Sundaramoorthy *et al*, 2017; Juszkiewicz *et al*, 2018; Ikeuchi *et al*, 2019). Ubiquitylation of the collided disome by E3 ligase Not4 at ribosomal protein eS7 activates NGD for mRNA degradation without RQC (NGD^{RQC-}), leaving the nascent polypeptide intact (Ikeuchi *et al*, 2019). Notably, Not4 also ubiquitylates ABCE1 in the context of translational quality control of mitochondrial outer membrane complexes and mitophagy (Wu *et al*, 2018). Different pathways indicate how the cell may utilize an intricate network and interplay of quality control mechanisms for numerous physiological functions (Nürenberg-Goloub & Tampé, 2019; De & Mühlemann, 2022).

1.4.1 Novel quality control factors acting on ribosome collisions in Bacteria

In Eukaryotes, stalled and collided ribosomes are subject to RQC and mRNA surveillance, wherein endonucleases are recruited to ubiquitylated ribosomes for cleavage of the mRNA and subsequent degradation *via* the exosome (Matsuo *et al*, 2017; Simms *et al*, 2017; D'Orazio *et al*, 2019; Glover *et al*, 2020). In Bacteria, the rescue of stalled ribosomes mainly functions *via* the A site-binding tmRNA. However, if ribosomes stall on intact messages, supposedly mRNA first is degraded to produce a tmRNA target (Hayes & Sauer, 2003; Ivanova *et al*, 2004; Müller *et al*, 2021). Recently, two novel factors involved in RQC and mRNA surveillance at collided ribosomes were identified in *B. subtilis* (MutS2) and *E. coli* (SmrB) (Cerullo *et al*, 2022; Saito *et al*, 2022). Ribosome collisions promote the binding and activity of SmrB in *E. coli*, which cleaves the mRNA upstream of the collision. It is suggested that the tailing ribosome translates until it reaches the end of the truncated mRNA, resulting in tmRNA-mediated rescue. Furthermore, collided ribosomes could be rescued *via* 3' exonuclease cleavage of the remaining mRNA for subsequent recruitment of tmRNA (Saito *et al*, 2022). MutS2 is a paralog of the DNA mismatch repair protein MutS. While featuring the typical MutS III/IV DNA-binding/clamp and MutS V nucleotide-binding domains, MutS2 does not contain the MutS I/II DNA mismatch repair domains but instead harbors additional C-terminal coiled-coil and small MutS-related (Smr) endonuclease domains (Figure 3A) (Burby & Simmons, 2017; Cerullo *et al*, 2022). MutS2 senses collided ribosomes and specifically binds to the leading ribosome *via* its MutS III/IV DNA-binding/clamp domain. Based on conformational rearrangements of MutS in DNA mismatch repair (Groothuizen & Sixma, 2016) and the specific positioning of MutS2 at the stalled ribosome, it is proposed that MutS2 functions as a ribosome splitting factor *via*

ATP-driven conformational rearrangements like the ribosome recycling factor ABCE1 (Cerullo *et al*, 2022). However, no functional data exists to support the proposed MutS2 ribosome splitting function. A potential mRNA cleavage function of MutS2 at collided ribosomes remains elusive.

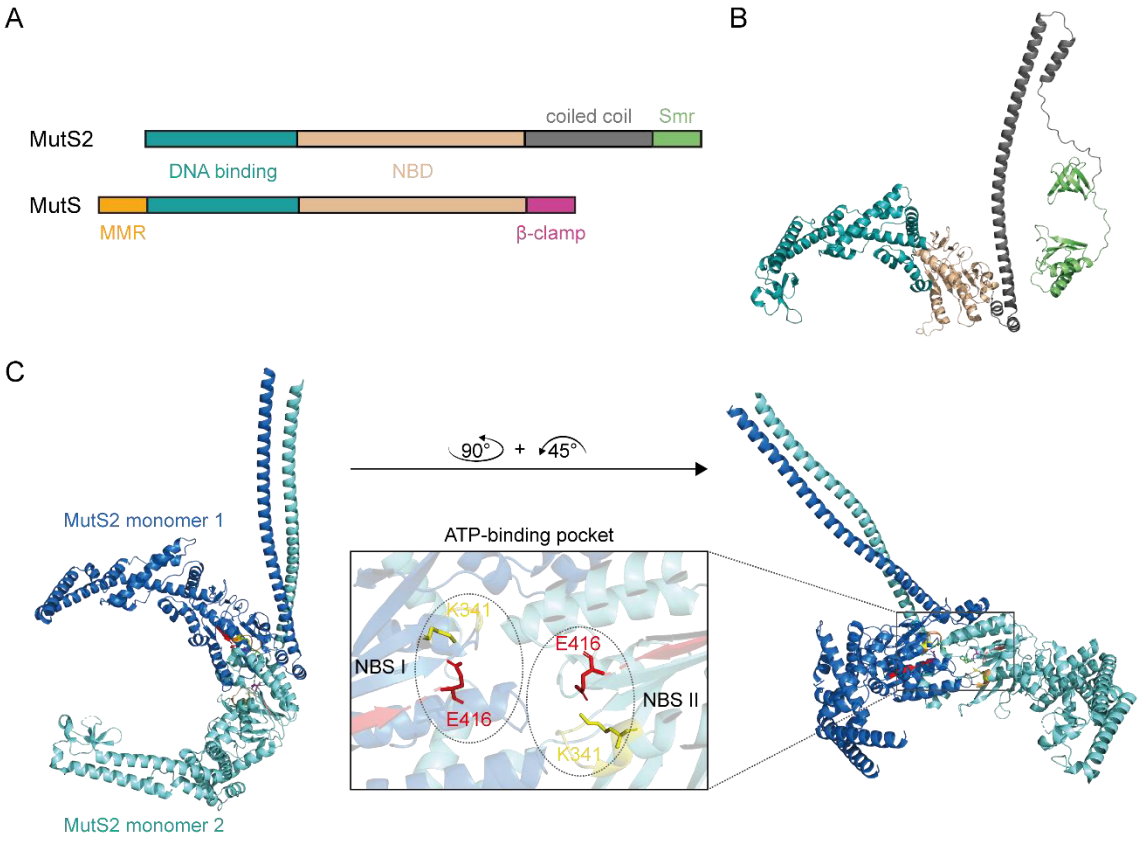

Figure 3: Domain architecture and structural features of MutS2. A) MutS2 and MutS domain architecture. MutS2 consists of an N-terminal DNA-binding/clamp domain (MutS III/IV) (teal), a nucleotide-binding domain (MutS V) (wheat), a coiled-coil region (gray), and a C-terminal small MutS-related (Smr) endonuclease domain (lime). MutS DNA and nucleotide-binding domains are similar to MutS2, but MutS does not feature a coiled-coil region or a Smr domain. Instead, MutS has an N-terminal DNA mismatch repair (MMR) domain (MutS I/II) (orange) and a C-terminal β-clamp domain (magenta). **B)** Predicted structure of a *B. subtilis* MutS2 monomer (AlphaFoldDB and Uniprot P94545) colored according to domain architecture in A. **C)** Cryo-EM structure of the *B. subtilis* MutS2 homodimer (PDB 7QV3). Part of the MutS2 monomer 1, N-terminus, and Smr endonuclease domains of both monomers are not resolved. Zoom into the ATP-binding pocket with identical nucleotide-binding sites (NBS I and NBS II). Walker A and B motifs are colored yellow and red, respectively. Walker A coordinating K341 and Walker B catalytic E416 residues, which are important for ATP-binding and hydrolysis, are shown as sticks.

1.5 Scope and aims of this work

This doctoral thesis covers the mRNA translation phases of ribosome recycling and initiation, and how they relate to each other to close the mRNA translation cycle. I focused on understanding the mode of function of the essential ribosome recycling factor ABCE1. Previously, it was described how ABCE1 binds to target ribosomes, how the dissociation process leads to conformational domain rearrangements of ABCE1, and how the ribosome-splitting mechanism is coupled to ATP-binding. Cryo-EM structures of ABCE1 bound to the small ribosomal subunit gave the first insights into how recycling is connected to a new round of translation initiation based on the post-splitting complex (Barthelme *et al*, 2011; Becker *et al*, 2012; Kiosze-Becker *et al*, 2016; Heuer *et al*, 2017; Mancera-Martínez *et al*, 2017).

I aim to unite the knowledge of ABCE1 function in ribosome recycling with a detailed structural understanding of the post-SC as a translation initiation platform. Thus, the main goal of this thesis is to image the archaeal post-splitting complex at high resolution by cryo-EM. I continue the preceding work of *in vitro* reconstitution of archaeal ribosome recycling by ABCE1 (Nürenberg-Goloub, 2018).

Further, I aim to decipher the mode of initiation factor recruitment to the post-SC. A key question of my thesis is whether ABCE1 influences the process of initiation complex assembly, or if any initiation factor can trigger ABCE1 release from the small ribosomal subunit. Therefore, biochemical assays should be established for readout of thermodynamic properties of factors during initiation complex assembly. To structurally characterize archaeal translation cycle intermediates, the co-immunoprecipitation of recombinant ABCE1-ribosome complexes from archaeal cell lysates should be established. In addition, I intend to set up the expression of ABCE1 in the acidothermophilic Archaeon *S. acidocaldarius* to gain insight into the native assembly of ABCE1-initiation complexes in Archaea.

In the context of ribosome recycling and mRNA surveillance, two new bacterial ribosome quality control factors (MutS2 in *B. subtilis* and SmrB in *E. coli*) were shown to rescue stalled, collided di-ribosomes. While functional data is scarce, it was proposed that MutS2 might rescue collided disomes by dissociation of the subunits, based on its ATPase and clamp domains (Saito *et al*, 2022; Cerullo *et al*, 2022). Therefore, I aim at biochemical characterization of MutS2 with focus on nucleotide-binding and an *in vitro* disome-splitting assay to address a potential MutS2 function.

2 Results and discussion

2.1 Structural and functional characterization of the archaeal ABCE1-30S ribosomal subunit post-splitting complex

The ribosome recycling factor ABCE1 is essential in Eukaryotes and Archaea. ABCE1 recognizes terminated or stalled ribosomes and dissociates them into subunits in concert with the A site-bound class I release factors a/eRF1 or a/ePelota, respectively (Pisarev *et al*, 2010; Barthelme *et al*, 2011; Shoemaker & Green, 2011). ABCE1 binds the ribosome near the GTPase control center (Shao *et al*, 2016; Kiosze-Becker *et al*, 2016). Nucleotide-binding leads to closure of the NBDs, which transmits steric movement to the ribosome, resulting in subunit dissociation (Barthelme *et al*, 2011; Becker *et al*, 2012). Accompanied, the FeSD undergoes a large conformational relocation to rRNA helix h44 of the small ribosomal subunit in the post-splitting complex (Kiosze-Becker *et al*, 2016; Heuer *et al*, 2017). Finally, ABCE1 remains bound to the 30S subunit in a closed conformation with ATP occluded in both NBSs (Nürenberg-Goloub *et al*, 2018). Although the general positioning of ABCE1 and molecular interactions of the FeSD and NBS I with the 30S subunit were analyzed by cryo-EM structures of the post-SC, especially NBS II remained poorly resolved (Kiosze-Becker *et al*, 2016; Heuer *et al*, 2017). To understand the mode of function of ABCE1 in its entirety, the biochemical findings of asymmetry and dynamic movement in both NBSs (Gouridis *et al*, 2019) need to be connected to high-resolution structures that resolve both nucleotide-binding sites. Therefore, I aimed at reconstitution of the archaeal ribosome-splitting route by ABCE1 *in vitro* to prepare the archaeal post-SC in a precise and controlled manor with high sample quality for structural analysis by cryo-EM in collaboration with Hanna Kratzat, Dr. Thomas Becker, and Dr. André Heuer of the Beckmann laboratory (Ludwig-Maximilians-University, Munich).

2.1.1 *In vitro* assembly of the archaeal post-splitting complex *via* the native mRNA translation route

To obtain archaeal post-SCs, we actively split isolated native *T. celer* 70S ribosomes using recombinant ABCE1, aRF1, and aPelota from the related archaeon *S. solfataricus*. Thus, we ensured to resemble the cellular recycling route for all ribosomes present in the native mixture: ribosomes with the A site occupied by a stop codon (aRF1), a sense codon (e.g., in stalled ribosomes) or vacant ribosomes (aPelota). Thereby, we circumvented a low-Mg^{2+} and high K^{+} treatment necessary for facilitated ribosome splitting as previously performed in yeast (Heuer *et al*, 2017). To stabilize the post-SC, a well-characterized, hydrolysis-deficient ABCE1 mutant was used. The mutant, with both catalytic glutamates being substituted by alanine (E238/485A, short IIEA), efficiently split 70S ribosomes and remained quantitatively bound to 30S subunits (Nürenberg-Goloub *et al*, 2018) (Figure 4A). Notably, 70S ribosomes from *S. solfataricus* are intrinsically instable (Barthelme *et al*, 2011) and thus unsuitable for our *in vitro* splitting approach. The purified 30S-$ABCE1^{IIEA}$ post-SC was subjected to single-particle cryo-EM analysis. 3D classification revealed that the vast majority (97%) of 30S particles were associated with $ABCE1^{IIEA}$. After refinement, the average resolution was 2.8 Å (Figure 4B). Local resolution assessment showed that the body of the 30S formed a very rigid structure whereas the 30S head and ABCE1 showed flexibility and lower resolution (4–6 Å) (Figure 5). However, using focused refinement, the local resolution was improved to 3.0 Å for ABCE1 and to 2.8 Å for the 30S head. Thereby, building of a complete molecular model of the *T. celer* SSU associated with ABCE1was possible (Figure 4C, Figure 5).

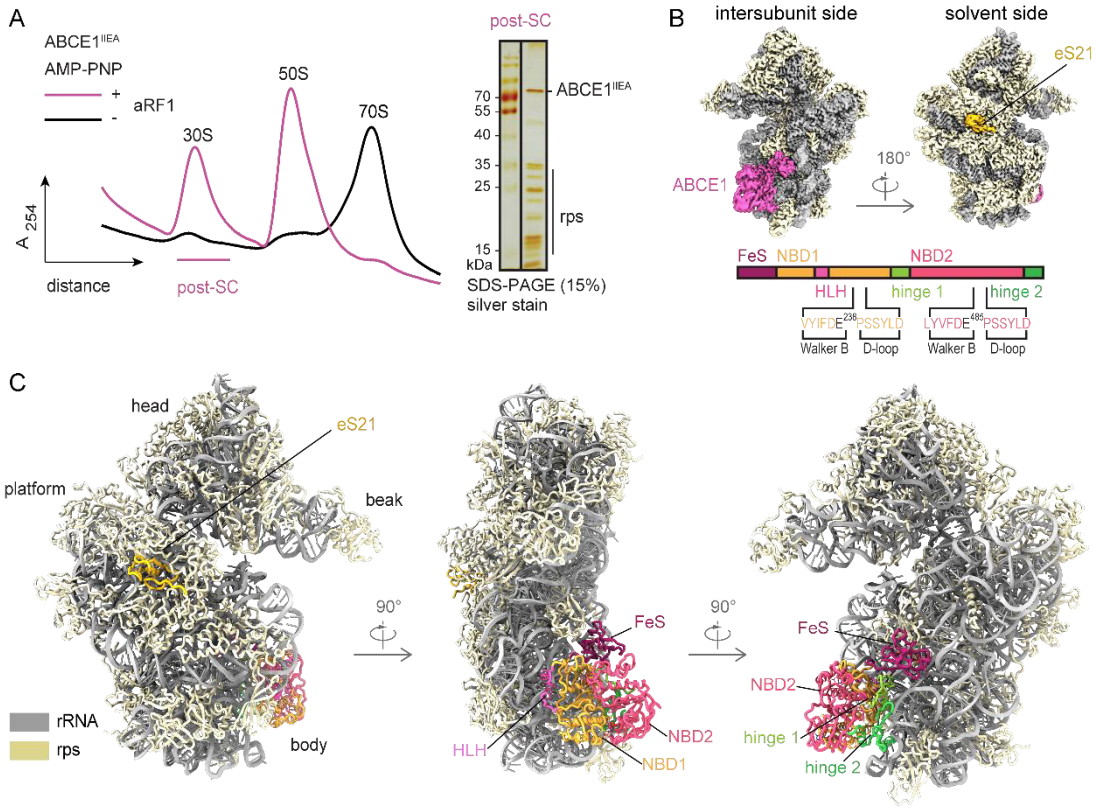

Figure 4: ***In vitro*** **assembly and cryo-EM structure of the archaeal post-splitting complex** (Nürenberg-Goloub *et al*, 2020)**. A)** ABCE1^{IIEA} efficiently splits 70S ribosomes in the presence of AMP-PNP and aRF1/aPelota. The 30S population contains a stoichiometric ratio of ABCE1 and ribosomal proteins, forming the post-splitting complex. rps, ribosomal proteins. **B)** Cryo-EM density of the post-SC highlights the archaeal ribosomal protein eS21 and ABCE1. Domain architecture of ABCE1 including the mutation sites is shown below. **C)** Molecular model of the archaeal post-SC, domain colors as in (B).

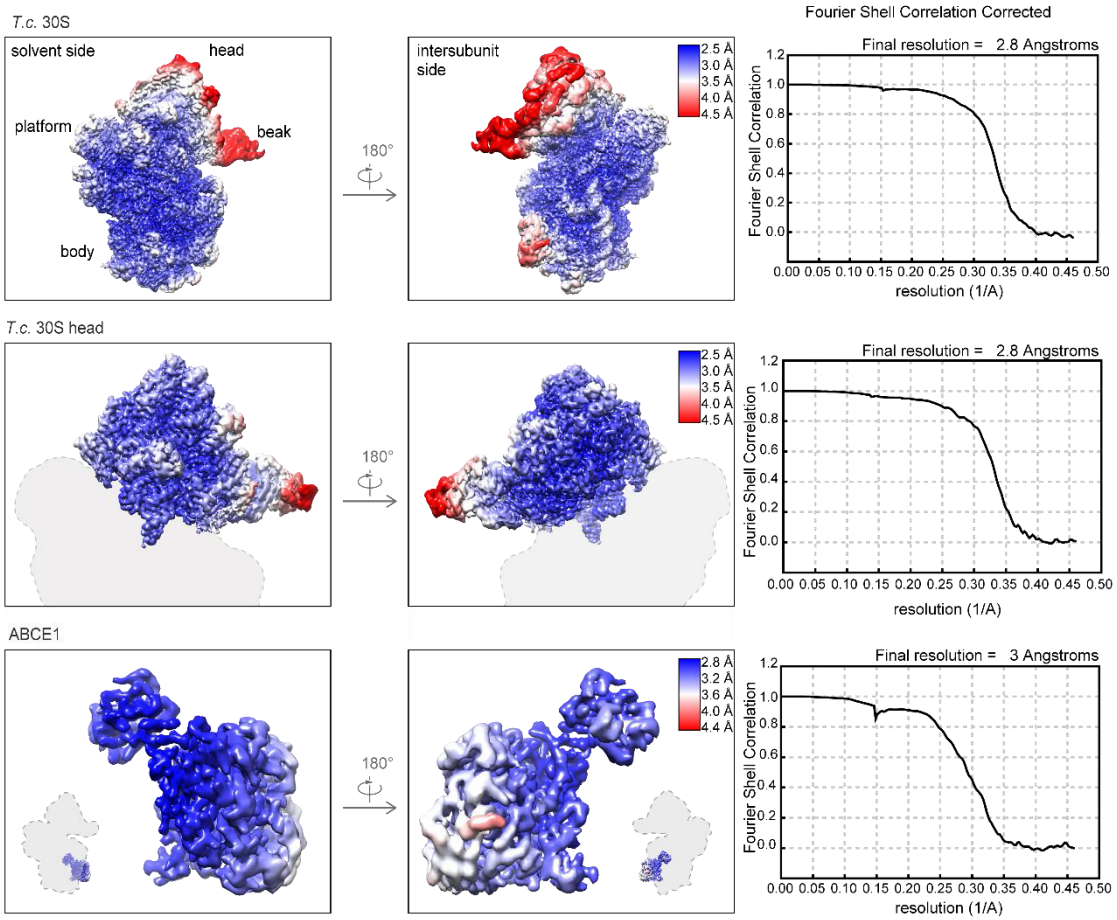

Figure 5: Local resolution of the post-SC (Nürenberg-Goloub *et al*, 2020)**.** Cryo-EM maps of the overall 30S-ABCE1 post-SC (top), locally refined 30S head (middle), and ABCE1 (bottom) moieties. Maps are colored and filtered according to local resolution, and corresponding gold standard FSC curves are shown. Using focused refinement, local resolution of the 30S head and ABCE1 was improved from approximately 4–6 Å to 2.8 Å and 3.0 Å, respectively.

This section was reprinted with permission from Nürenberg-Goloub *et al* 2020 with minor changes.

2.1.2 Molecular model of the *Thermococcus celer* small ribosomal subunit

The *T. celer* 30S ribosome structure comprises 1,485 nucleic acid residues of 16S ribosomal RNA (rRNA) (Figure S2) and 28 ribosomal proteins (Figure 6A). As an initial template, we used the structure of the closely related *Pyrococcus furiosus* ribosome at 6.6 Å resolution (Armache *et al*, 2013), to which *T. celer* rRNA has 96% and ribosomal proteins 78–95% sequence identity, respectively. All residues were manually exchanged to the correct *T. celer* sequence and fitted into the cryo-EM map. Several protein N- and C-termini, as well as loop regions, were built *de novo*. This was possible for the entire 30S

subunit except for rRNA and proteins forming the beak (eL8, eS31, and parts of h33), which is known to be the most flexible moiety of the SSU (Figure 5).

Interestingly, we discovered a previously unobserved density for a ribosomal protein on the 30S platform, which was identified as a so far uncharacterized protein, and its structure was built *de novo* (Figure 4B, Figure 6). The 59 amino acid (aa) long protein (6.6 kDa) is in a cleft between uS2, uS5, and uS8, close to helix (h) 36 and h26/h26a of 16S rRNA. There, it occupies the same position as eS21 in the *Saccharomyces cerevisiae* (Sc) 40S ribosome, whereas, in the 30S ribosome from *Escherichia coli*, the equivalent position is not covered (Figure 6B). The sequence matches UniProtKB: A0A218P055 (A0A218P055_THECE) and contains a zinc-binding zinc ribbon domain, for which we could assign density for two bound zinc ions. It is conserved in other archaeal species, yet sequence identity with eS21 is rather low (Figure 6C) with 7% for the full-length protein, but 27% for residues 10–24 representing the zinc ribbon. In accordance with the universal nomenclature for ribosomal proteins (Ban *et al*, 2014), we refer to the identified protein as eS21.

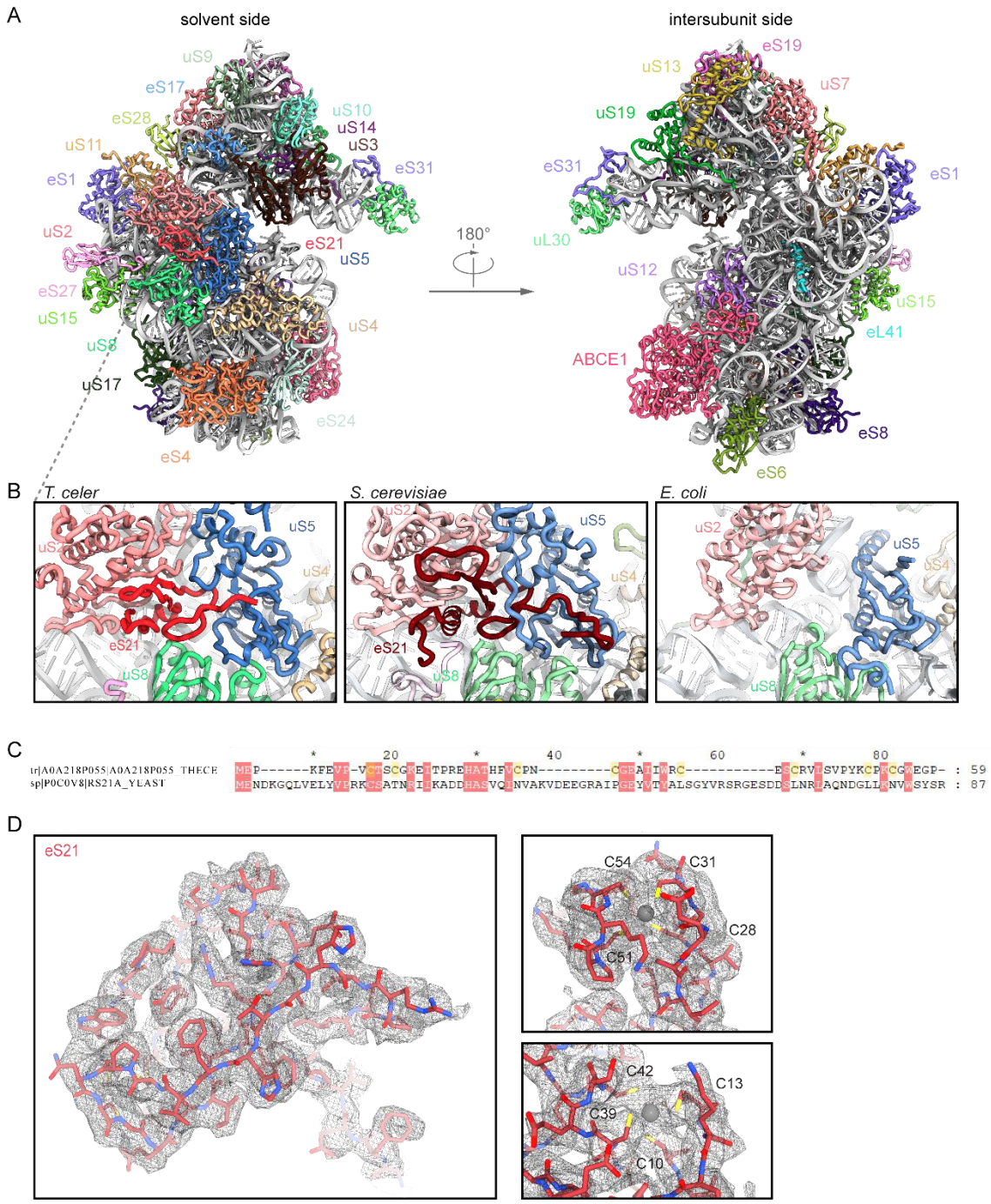

Figure 6: Molecular model of the *T. celer* 30S ribosomal subunit and location of eS21 (Nürenberg-Goloub *et al*, 2020)**. A)** *T. celer* 30S ribosomal subunit contains 28 ribosomal proteins, including the large subunit protein eL41. **B)** Close-up view of eS21 located at the solvent side between uS2, uS5, and uS8. Comparison with other species reveals that the respective position at the ribosome is not occupied in *E. coli*, but by eS21 in *S. cerevisiae*. **C)** Sequence alignment of *T. celer* eS21 and *S. cerevisiae* eS21a shows low homology, indicating that the two proteins are only weakly related. **D)** Cryo-EM density for eS21 and fit of the *de novo* model. The protein forms two zinc-binding pockets, each coordinated by four cysteines.

This section was reprinted with permission from Nürenberg-Goloub *et al* 2020 with minor changes.

2.1.3 The architecture of the post-splitting complex is conserved between Eukarya and Archaea

Binding to 70S/80S ribosomes in pre-splitting and to 30S/40S ribosomes in post-splitting complexes is known to be mainly mediated by the ABCE1-specific HLH motif and hinge region contacting the body of the SSU. Upon transition from the pre- to the post-splitting state, the NBSs move from a semi-open to a fully closed, nucleotide-occluded state. Concomitantly, the FeSD rotates around a cantilever toward the decoding site of the SSU close to rRNA helix h44 (Heuer *et al*, 2017).

The overall architecture of the archaeal post-SC is similar to the yeast 40S-ABCE1 complex (Heuer *et al*, 2017) showing the same hallmarks. The FeSD occupies a position close to rRNA h44, hinge region and HLH motif anchor the NBDs to the 30S body, and the two NBSs are in a closed conformation. Yet, the resolution of the archaeal post-SC (2.8 Å overall) is significantly higher than the one of the yeast post-SC (3.9 Å overall), especially in NBS II and the hinge region, thus allowing to describe interactions between ABCE1 and the SSU as well as interactions between the two NBSs on a molecular level. These molecular insights allowed us to draw conclusions and make predictions about the allosteric crosstalk between the two NBSs of ABCE1 as well as ABCE1 and the ribosome. Moreover, these insights guided the corresponding functional studies.

This section was reprinted with permission from Nürenberg-Goloub *et al* 2020 with minor changes.

2.1.4 The iron-sulfur cluster domain establishes inter- and intramolecular interactions specific for the post-SC

Based on the high-resolution data, we can delineate crucial interactions between the FeSD domain, NBD1, hinge 1, and the 30S ribosomal subunit. The FeSD is embedded in a pocket between rRNA h44, the h5-h15 junction, and the universally conserved ribosomal protein uS12 (Figure 7A). The majority of FeSD interactions with the ribosome are conserved, while the loop regions of the FeSD opposite of the ribosome (e.g., L36-K43) are variable in sequence and structure, underlining the significance of the interaction of the FeSD with the ribosome (Figure 8A,Figure S1). Most interactions are formed by salt bridges and hydrogen bonds established between conserved residues in ABCE1 (R2, K15, N17, E19, K59) and the phosphate backbone as well as 2'OH groups of rRNA (Figure 7A). Similarly, also the interaction sites between ABCE1 and uS12 are conserved (P25, R28, and S29 of ABCE1 to Q76 and H100 of uS12) (Figure 7A). Interestingly, we observed a

few cases where the ribosome and ABCE1 co-evolved to maintain the interaction pattern. For example, the interaction between S29 of ABCE1 and H100 of uS12 is substituted by the contact of K36 (ABCE1) with N99 (uS12) in yeast (Figure 8B), underlining the importance of an interaction at this position for re-orientation of the FeSD after ribosome splitting.

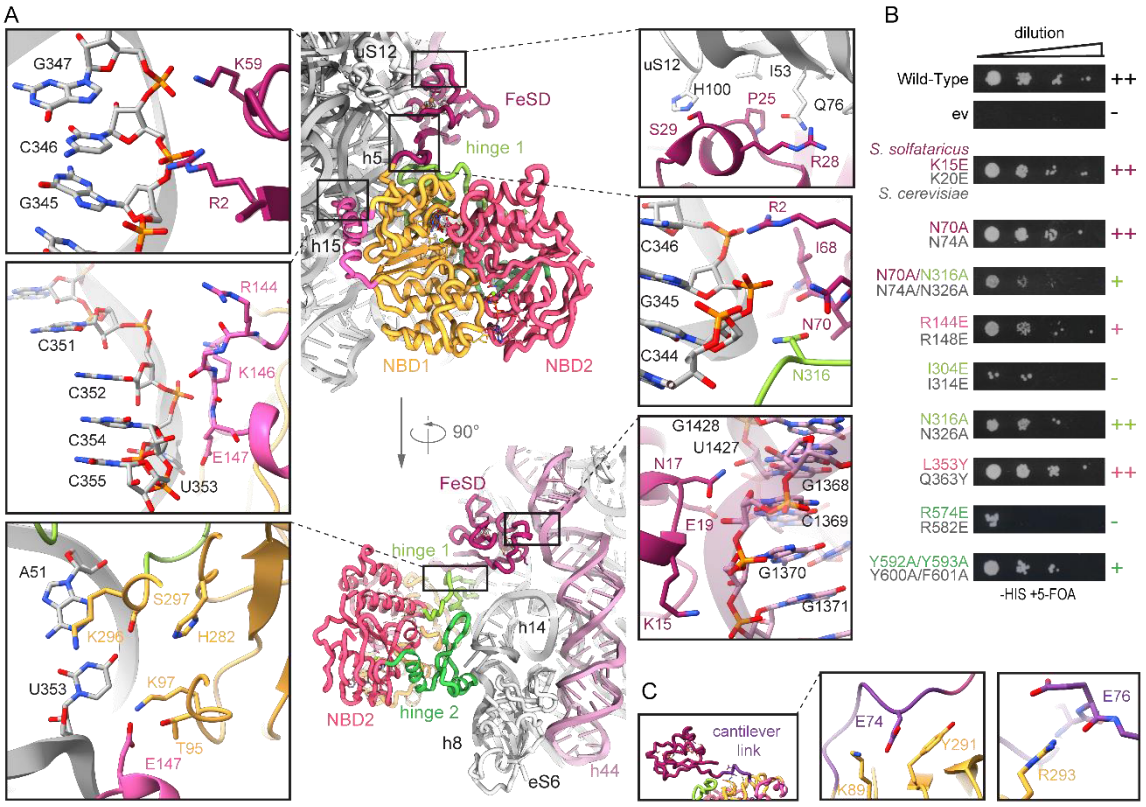

Figure 7: The conserved ABCE1-30S interface is formed by essential interactions (Nürenberg-Goloub *et al*, 2020)**. A)** Zoom-ins into ABCE1-30S connections. Most interactions are salt bridges or H-bonds between ABCE1 residues and the rRNA phosphate backbone. The FeSD contacts rRNA h5 *via* R2 and K59, interacts with uS12 *via* S29 and R28, and contacts h44 by N17 and K15. The helix-loop-helix motif connects to rRNA h15 *via* R144 and E147. The positioning of the cantilever is stabilized by an interaction network of R2, I68, and N70 with N316 of hinge 1 and rRNA h5. **B)** Yeast survival of ABCE1 variants (*S. solfataricus* colored, *S. cerevisiae* in gray). Most residues connecting to 30S in the post-SC show a growth defect when exchanged for a small one (alanine) or a negative charge (glutamate). ++ no effect, + growth defect, − lethal. **C)** The cantilever link forms salt bridges of E74 and E76 with NBD1 residues K89 and R293, respectively.

The FeSD is linked to the main twin-ATPase body via a flexible linker connecting the cantilever β-sheet β4 with NBD1 (Figure 7C, Figure S1). This linker (D73-V79 in *S. solfataricus*) forms an α-helix in free ABCE1 and the pre-SC (Karcher *et al*, 2008; Brown *et al*, 2015), but unfolds into a loop in the post-SC. As in the yeast post-SC (Heuer *et al*, 2017), this cantilever helix is also unfolded in *S. solfataricus*. At high resolution, we deciphered a chain of inter- and intramolecular interactions that are a consequence of

FeSD repositioning after splitting. We observed a similar stabilization of the cantilever loop by an interaction of Y291 in NBD1 (Y301 in Sc) with the backbone of E74 (N78 in Sc) (Figure 7C, Figure S1). In our high-resolution structure, we identified additional stabilizing contacts for the cantilever loop. E74 also interacts with the side chain of K89 (NBD1) and the carbonyl group of E76 binds the guanidino group of R293 (NBD1) (Figure 7C). Moreover, an interaction network is formed between R2 (R7 in Sc) at the N-terminus, I68 and N70 (N74 in Sc) of the cantilever β-sheet β4, and N316 (N326 in Sc) in hinge 1, as well as the phosphate groups of G345 and G346 in rRNA h5 (Figure 7A). In yeast, the mutations Y301A and R7A impair the anti-association activity of ABCE1 *in vitro* and are synthetically lethal *in vivo* (Heuer *et al*, 2017). Additionally, we confirm the synthetic lethality of N74A with N326A (Figure 7B, Figure 8C).

Taken together, the closure of the NBSs displaces the FeSD, which leads to new interactions of the cantilever β-sheet and the cantilever loop with the ribosome, NBD1 and hinge 1, allowing for an allosteric communication of post-SC formation to the NBSs.

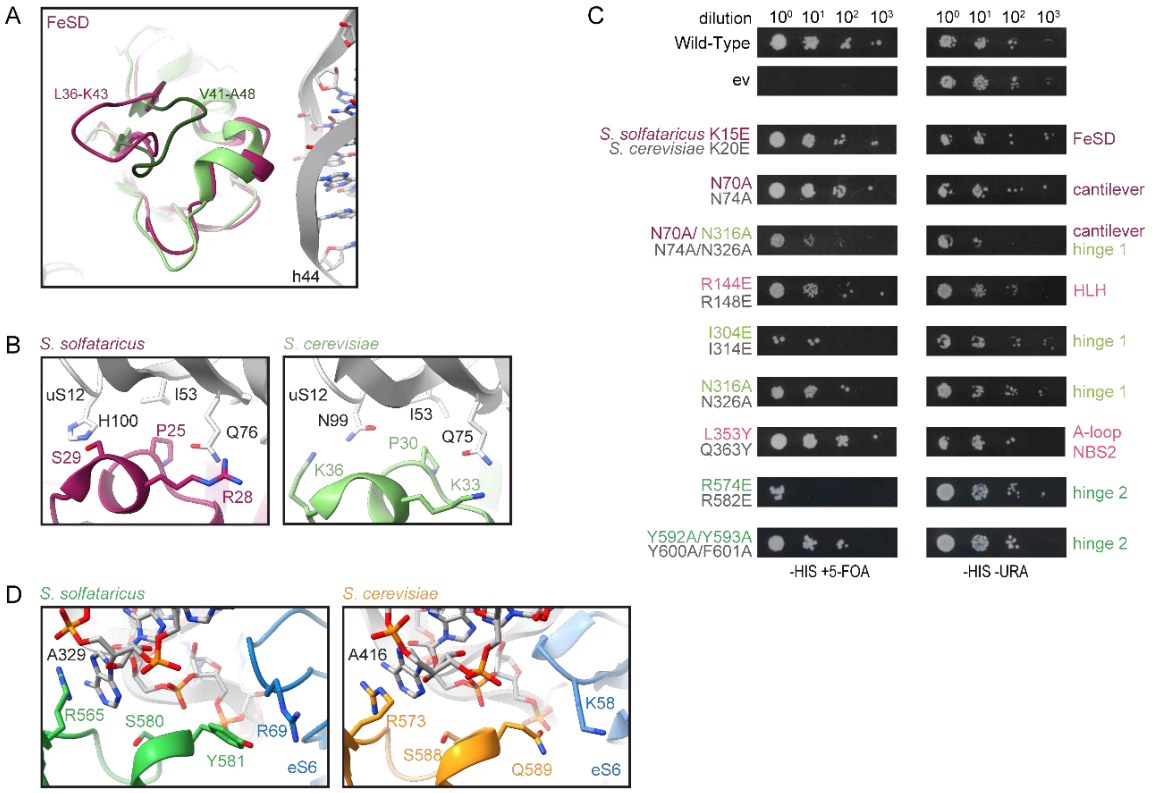

Figure 8: Conserved interactions of ABCE1 with the 30S subunit are essential for ABCE1 function (Nürenberg-Goloub *et al*, 2020)**. A)** FeSD interactions are conserved between *S. solfataricus* and *S. cerevisiae*, except for the loops L36–K43 (Ss) and V41-A48 (Sc), which face away from the ribosome and vary in sequence and structure. **B)** The interaction between S29 and H100 (uS12) is substituted by K36 and N99 (uS6) in yeast, indicating co-evolution of ABCE1 and the ribosome. **C)** Yeast plasmid shuffling assay illustrates cell viability and growth either dependent or independent on the plasmid with mutant ABCE1 in the presence or absence of 5-FOA, respectively. **D)** Stacking of Y581 with R69 (eS6) occurs in yeast as Q589 with K58 (eS6), giving another hint for ABCE1-ribosome co-evolution to maintain essential interactions.

This section was reprinted with permission from Nürenberg-Goloub *et al* 2020 with minor changes.

2.1.5 Hinge 2 serves as a linchpin during ribosome splitting

The NBDs of ABCE1 are located at the body of the 30S subunit with main anchor points contributed by the HLH motif (to h15) and the dipartite hinge region (to junction of h8 and h14) (Figure 7A). In stark contrast to the pre-splitting complex, the HLH is displaced from its contact point at h5 by 16 Å toward h15. In the post-SC, h15 is in contact with the loop containing two basic residues (R144-G145-K146-E147) between helices α6 and α7 (Figure 7A). A charge reversion of the respective arginine in yeast (R148E) leads to a substantial growth defect, confirming importance of the position (Figure 7B, Figure 8C). The other residues in the HLH loop rather stabilize an interaction formed by NBD1 with

U353, which flips out of h15 and forms a Watson-Crick base pair with A51 in h5, establishing the h5-h15 junction. Multiple residues (T95, K97, E147, H282, K296, and S297) are facing this base pair, suggesting that this specific tertiary structure is precisely monitored by NBD1 and the HLH motif of ABCE1 (Figure 7A). In contrast to yeast, no contacts are observed between ABCE1 and eS24, which is also present but significantly shorter at its C-terminus in *T. celer*.

The ABCE1-specific hinge region is subdivided into hinge 1 (*S. solfataricus* 298–325) and hinge 2 (*S. solfataricus* 547–594, Figure S1). Interactions with the ribosome are mainly established by hinge 2. Hinge 1 connects NBD1 and NBD2 *via* a flexible linker (*S. solfataricus* 326–338), which is—as in other structures—only partially visible. Similar to the HLH/NBD1 region, hinge 2 also recognizes a special tertiary structure of the rRNA. It binds at the junction between rRNA helices h8 and h14, where A329 flips out of h14 and stacks upon the ribose of A138 in h8. The geometry is read out by the conserved R565 forming a cation-π-stack with A138 (Figure 9A, D, and Figure S1). Notably, this interaction is maintained during ribosome splitting (Figure 10), and the exchange of the corresponding residue (R573E) leads to loss of function in yeast (Karcher *et al*, 2008). Hence, the *S. solfataricus* ABCE1^{R565E} variant (Figure S3) was unable to bind 30S ribosomes (Figure 9E, Figure 12A) and failed to split 70S ribosomes (Figure 9F, Figure 12B), whereas the ATPase activity was similar to wild-type ABCE1 (Figure 9G).

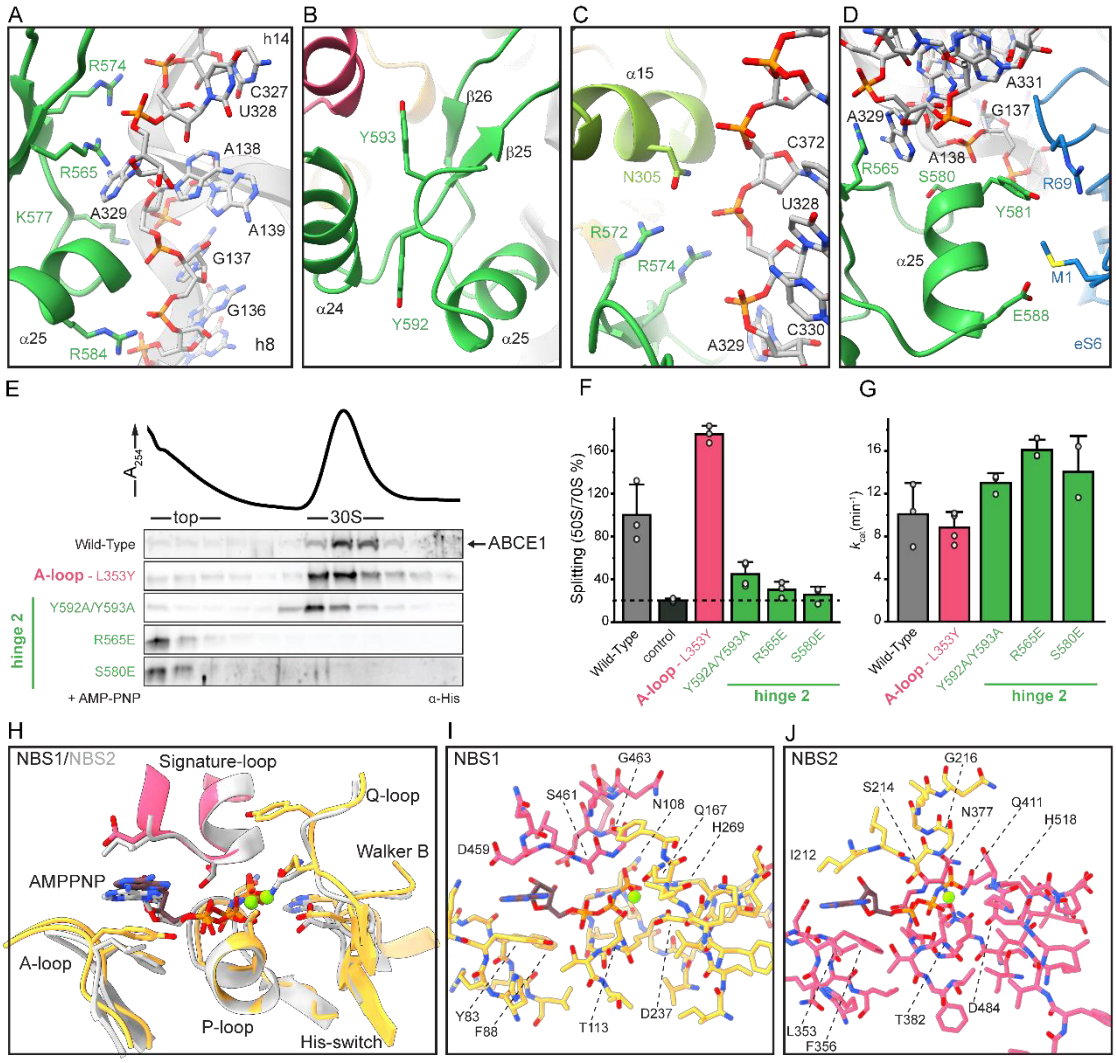

Figure 9: Structural and functional analysis of ABCE1 hinge regions and NBSs in the post-SC (Nürenberg-Goloub *et al*, 2020)**. A-D)** Hinge 2 (emerald) residues interacting with the ribosome. R565E forms a conserved cation-π-stacking with A329 of h8; R574 forms a salt bridge with the phosphate backbone of U328 in h14. Aromatic C-terminal residues Y592 and Y593 adopt a parallel coordination. R572 of hinge 2 and N305 of hinge 1 (lime) form an interaction that might be important for sensing. Essential S580 does not contact the ribosome, whereas Y581 and E588 form H-bonds to R69 and M1 of eS6 (blue), respectively. **E)** Mutations in the α-helices of hinge 2 prevent 30S binding while the Y592A/Y593A (C terminus) and L353Y (A-loop in NBS II) exchanges do not influence ribosome binding. **F)** 70S ribosome splitting efficiency normalized to wild type. Hinge 2 mutations Y592A/Y593A, R565E, and S580E display strongly impaired splitting activity. Unspecific ribosome dissociation level as determined in control experiments in the absence of ABCE1 is marked by the dotted line. Data shown are the mean ± SD of three (or two) independent experiments. **G)** ATP turnover per ABCE1 is not affected in all tested mutants. Data shown are the mean ± SD of three (or two) independent experiments. **H-J)** Overview of ATP coordination in both NBSs and overlay of the two NBSs reveal only slight differences, which cannot elucidate the functional asymmetry. Residues of NBD1 and NBD2 involved in coordination are shown in gold and punch, respectively.

The second main contact to the h8-h14 junction is formed by a salt bridge between R574 and the phosphate of U328 (Figure 9A, C). Moreover, R572 and N305 in hinge 1 stabilize the interaction network around this junction on the side of h14 (Figure 9C), while K577, S580, and R584 are in close contact with h8 (to G137 and A139) (Figure 9A, D). Further, hinge 2 forms an additional interaction site with eS6 by stacking Y581 against R69 (eS6) (Figure 9D). This interaction also occurs in yeast between Q589 and K58 (eS6), indicating a co-evolution of ABCE1-ribosome interactions as previously described for FeSD and uS12 (Figure 8D).

While the hinge 2 region serves as a constant linchpin to the ribosome, the interaction pattern of hinge 1 is substantially altered compared to the pre-SC. In hinge 2, only R574 switches from U329 in the pre-SC to the adjacent U328 in the post-SC, while all other residues remain with their respective interaction partners (Figure 10A). In contrast, the entire hinge 1 region opens up relative to hinge 2, which results in a 5 Å shift of the hinge 2 β-sheets β25 and β26 (Figure 10A, Figure S1) and a 10 Å movement of hinge 1 helix α15. Together with the movement of the HLH (Figure 10B) and the FeSD, this conformational rearrangement, which we term “hinge opening”, leads to the formation of new ribosomal contacts specific for the post-SC. Thus, α15 of hinge 1 binds U328 and the conserved N316 binds to A314 as well as the phosphates of G343 and G345 close to the h5-h15 junction (Figure 7A). As mentioned above, U328 also contacts R574 in hinge 2 (Figure 9C) while N316 is connected to the rearranged cantilever loop of the FeSD. Consequently, the FeSD, hinge 1, and hinge 2 form a post-SC state-specific intricate interaction network.

Functional analyses and lethality screens confirm the essential role of the hinge 2 region for ABCE1 function. As mentioned before, ABCE1^{S580E} (Figure S3) exhibits wild-type ATPase activity (Figure 9G) but neither binds to 30S ribosomes (Figure 9E, Figure 12A) nor splits 70S ribosomes (Figure 9F, Figure 12B). Additionally, the corresponding mutant is lethal in yeast (Sc S588E) (Karcher *et al*, 2008). Interestingly, S580 is the N-terminal residue of helix α25 and does not directly interact with the ribosome but points toward α25 (Figure 9D). Thus, the mutation to glutamate at this position inhibits ribosome binding *via* destabilization of helix α25 rather than by direct repulsion. The importance of R574 for ribosome recognition is confirmed by plasmid-rescue analysis in yeast, demonstrating that the respective R582E mutation is lethal (Figure 7B, Figure 8C).

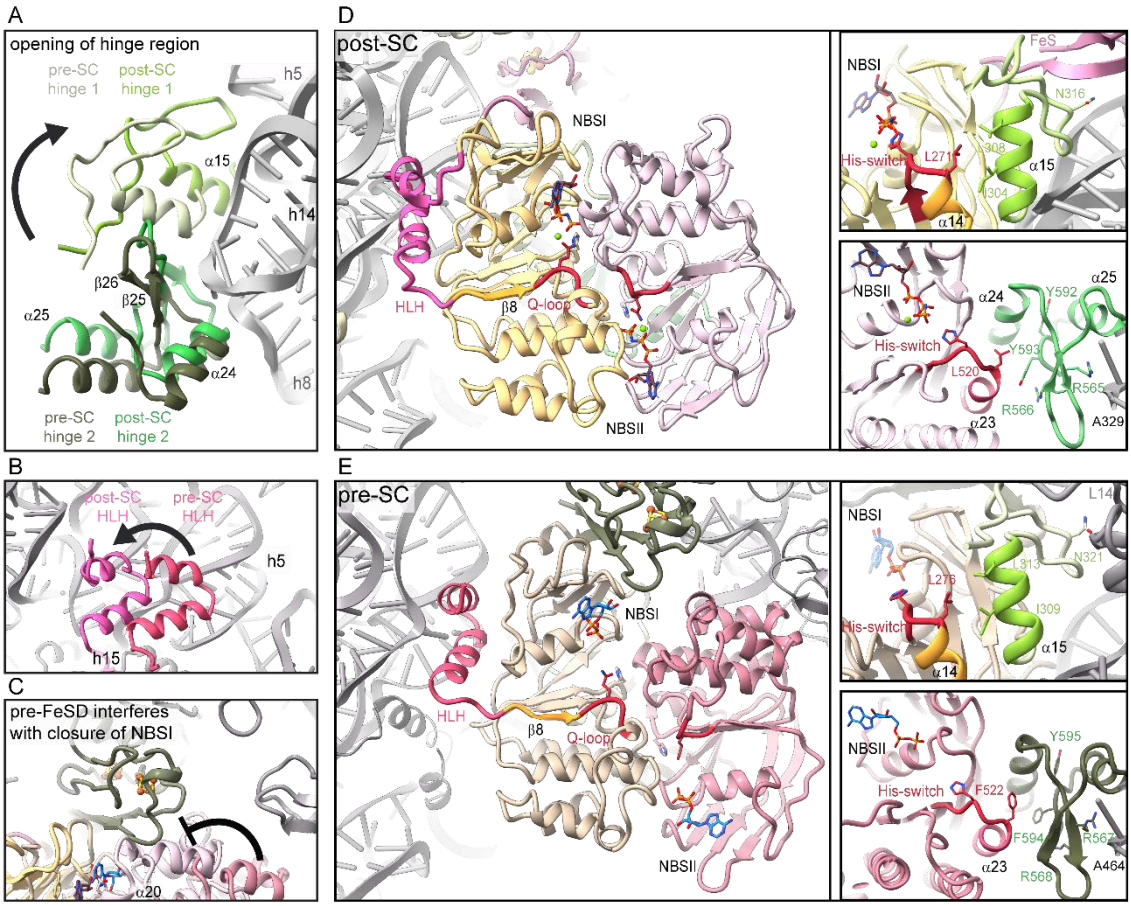

Figure 10: Hinge regions and HLH sense the ribosome splitting event and allosterically communicate with the NBSs (Nürenberg-Goloub *et al*, 2020)**. A)** Hinge 1 moves away from hinge 2 during transition from pre-SC (cotton) to post-SC (lime), thereby forming new interactions with the ribosome. In contrast, hinge 2 movement from pre- (moss) to post-SC (emerald) does not change the interaction with the ribosome. **B)** The HLH motif is displaced from h5 in the pre- (watermelon) to h15 in the post-SC (pink). **C)** Positioning of the FeSD (sage) interferes with the closure of NBD2 (blush) in the pre-SC (rose). **D)** Possible communication pathways from ribosome binding sites to the NBSs in the post-SC. HLH is connected to the Q-loop of NBS I *via* β8. I304 of hinge 1 connects to α14, which is adjacent to the His-switch in NBS I. Analogously; hinge 2 binding to the SSU might be communicated *via* Y593 and R566 to α23 next to the His-switch of NBS II. **E)** Interaction pattern of the communication pathways between HLH and hinge 1 to NBS I as well as hinge 2 to NBS II is different in the pre-SC compared to the post-SC.

This section was reprinted with permission from Nürenberg-Goloub *et al* 2020 with minor changes.

2.1.6 Structural asymmetry of the nucleotide-binding sites

Apparently, ABCE1 can act as a timer for ribosome recycling (Heuer *et al*, 2017; Nürenberg-Goloub *et al*, 2018). During this process, the NBSs receive and integrate signals about the state of the ribosome, e.g., discriminate between pre-splitting and post-

splitting complexes. In the post-SC, both NBSs have mainly been observed in the closed state (Gouridis *et al*, 2019), coinciding with a movement of the FeSD (Kiosze-Becker *et al*, 2016; Heuer *et al*, 2017) as initially suggested (Becker *et al*, 2012). Yet, in all obtained cryo-EM structures of pre- and post-SCs, the identity of the bound nucleotides, especially in NBS II, remained unclear. Based on our high-resolution data, we can resolve both catalytic pockets and unambiguously identify the non-hydrolysable ATP-analogue AMP-PNP complexed with an Mg^{2+} ion in each NBS (Figure 9H–J, Figure 11). In agreement with the yeast post-SC and the structures of symmetric ABC-type NBD dimers (Lammens *et al*, 2011; Korkhov *et al*, 2012), AMP-PNP is sandwiched between the typical conserved motifs of ABC-type ATPases. In NBS I, the A-loop residue Y83 stacks on the purine base, which is contacted by the aliphatic part of D459 adjacent to the signature motif of the opposite NBD2. In addition, the ribose is stabilized by stacking with F88 (Figure 9I). The γ-phosphate is directly contacted by N108 (Walker A), H269 (His-switch), S461-G463 (signature motif), and Q167 (Q-loop), while T113 (Walker A) and D237 (Walker B) coordinate the Mg^{2+} ion. Analogous residues are superimposable in NBS II, i.e., we find that N377 (Walker A), S214, G216 (signature motif), and H518 (His-switch) coordinate the γ-phosphate while Q411 (Q-loop), T382 (Walker A), and D484 (Walker B) contact the Mg^{2+} ion (Figure 9J). Notably, the characteristic A-loop is degenerated in NBS II of most (but not all) organisms, featuring aliphatic or even polar (Gerovac & Tampé, 2019). Despite the degenerated A-loop (L353 instead of the aromatic residue), the accommodation of the purine base is similar to the one observed in NBS I (Figure 9H). The base is sandwiched between L353 and I212 adjacent to the signature motif of NBD1. Yet, we hypothesized that higher flexibility of the nucleotide in NBS II due to the degenerated A-loop might explain (i) the reduced intrinsic ATPase activity in NBS II (Nürenberg-Goloub *et al*, 2018) and (ii) the lower resolution of this site in cryo-EM studies (Heuer *et al*, 2017). To test this hypothesis, we substituted L353 with a tyrosine, thereby generating a consensus A-loop in NBS II. However, 30S binding, 70S splitting efficiency, and ATPase activity of $ABCE1^{L353Y}$ (Figure S3) were comparable to wild-type (Figure 9E-G, Figure 12). Consequently, the respective yeast mutation Q363Y had no effect on growth and survival (Figure 7B, Figure 8C). Thus, the functional asymmetry of ABCE1 may originate from the connection of each NBS to an allosteric regulatory element on the ABCE1 surface, i.e., the FeSD, HLH motif, and hinge regions, rather than from single residues within the ATP-binding pockets.

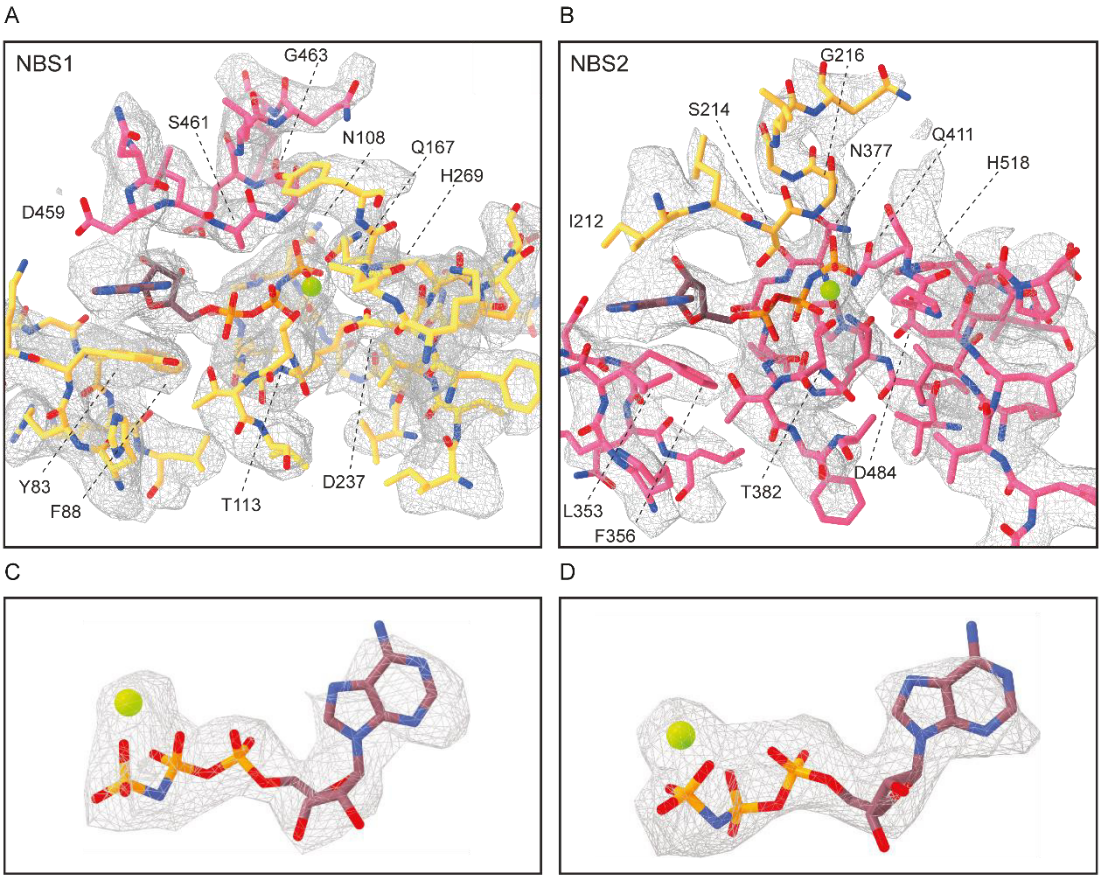

Figure 11: Fitting of NBS I and NBS II in the cryo-EM density (Nürenberg-Goloub *et al*, 2020)**. A)** Zoomed view on the model for NBS I fit into the electron density map shown in the same view as in **Figure 9I**. Residues of NBD1 and NBD2 are shown in gold and punch, respectively, and residues contributing to Mg^{2+}-AMP-PNP binding are labeled. **B)** Same as in (A) but for NBS II, corresponding to Figure 9J. **C, D)** Electron density and fit model for isolated Mg^{2+}-AMP-PNP from both NBS I (C) and NBS II (D). Density for the Mg^{2+}-ion coordinated by the γ- and β-phosphates of the trinucleotide in both NBSs is clearly observed.

This section was reprinted with permission from Nürenberg-Goloub *et al* 2020 with minor changes.

2.1.7 Ribosome binding is allosterically communicated to conserved motifs in the NBSs of ABCE1

Ribosome splitting completely alters the interaction pattern of ABCE1 with the ribosome at all contact points excluding the hinge 2 region. Based on the high-resolution structure, we elaborated allosteric communication pathways between the ribosome-ABCE1 interface and the NBSs. In the pre-splitting complex, the FeSD does not interfere with the NBS I semi-open state (Brown *et al*, 2015). However, upon closure, the loop K12-P13-D14 of the FeSD would clash into NBD2, in particular into residues preceding the NBS I signature

motif and α20, involving the L453-E454-S455 stretch (Figure 10C). The movement of NBS I is thus coupled with rearrangements of the FeSD and *vice versa*. Moreover, the flexible HLH motif *via* β8 is linked to the Q-loop of NBS I (Figure 10D, E). Mutations in the Q-loops strongly affect the ATPase activity of ABCE1 and compromise its function in yeast (Karcher *et al*, 2008; Barthelme *et al*, 2011). As stated above, we observed clear density for Q167 sensing the presence of the γ-phosphate. Additionally, we envision that the hinge opening is directly transmitted to the H-loops in both NBSs, which are key motifs in controlling ATPase activity of ABCE1 and other ABC proteins (Zaitseva *et al*, 2005; Barthelme *et al*, 2011; Hürlimann *et al*, 2017). In the post-SC, hinge 1 forms a specific contact with the h5-h15 junction where N316 interacts with G345. Compared to the pre-SC, hinge 1 α15 moves closer toward NBS I and forms a contact with α14, directly adjacent to the H-loop of NBS I (Figure 10D, E). The conserved I304 in α15 points toward α14, allowing communication between hinge 1 and NBS I. Consistent with this essential function, the corresponding mutation I314E is lethal in yeast (Figure 7B, Figure 10D and E, Figure 8C). Similarly, a conserved series of residues communicates ribosome binding from hinge 2 to the H-loop of NBS II. Herein, R565 in hinge 2 senses the h8–h14 junction while R566 and Y593 contact helix α23. Analogously to α14 in NBD1, helix α23 occupies the position adjacent to the H-loop in NBS II (Figure 10D, E). We substituted the conserved Y592 and Y593 with alanine and probed for ABCE1 function. Consistent with the role of Y593 in ribosome sensing without direct contact with rRNA or ribosomal proteins, the 70S splitting ability of ABCE1$^{Y592A/Y593A}$ (Figure S3) is substantially inhibited (Figure 9F, Figure 12B) while the 30S binding efficiency and ATPase activity are similar to wild type (Figure 9D and E, Figure 12A). Additionally, the respective double mutant Y600A/F601A exhibits a growth defect in yeast (Figure 7B, Figure 8C). The five-stranded β-sheet harboring the degenerated A-loop in NBS II is near hinge 2. Comparing the pre-SC with the post-SC, we observed a conformational change in this region which contributes to ATP occlusion by allowing the hydrophobic stacking of L353 and the adenine base (Figure 9J).

We finally inspected the Walker B/D-loops, which are known to assure transport directionality in the ABC transporter associated with antigen processing (TAP) (Grossmann *et al*, 2014). Notably, the D-loops are, together with the H-loops, already part of the contact interface between the NBDs in the pre-splitting state. This interface drastically alters upon closure of the NBSs, ribosome splitting, and post-SC formation, allowing a multilayered communication network between both sites in addition to the allosteric regulation by the ribosome (Figure 10D, E).

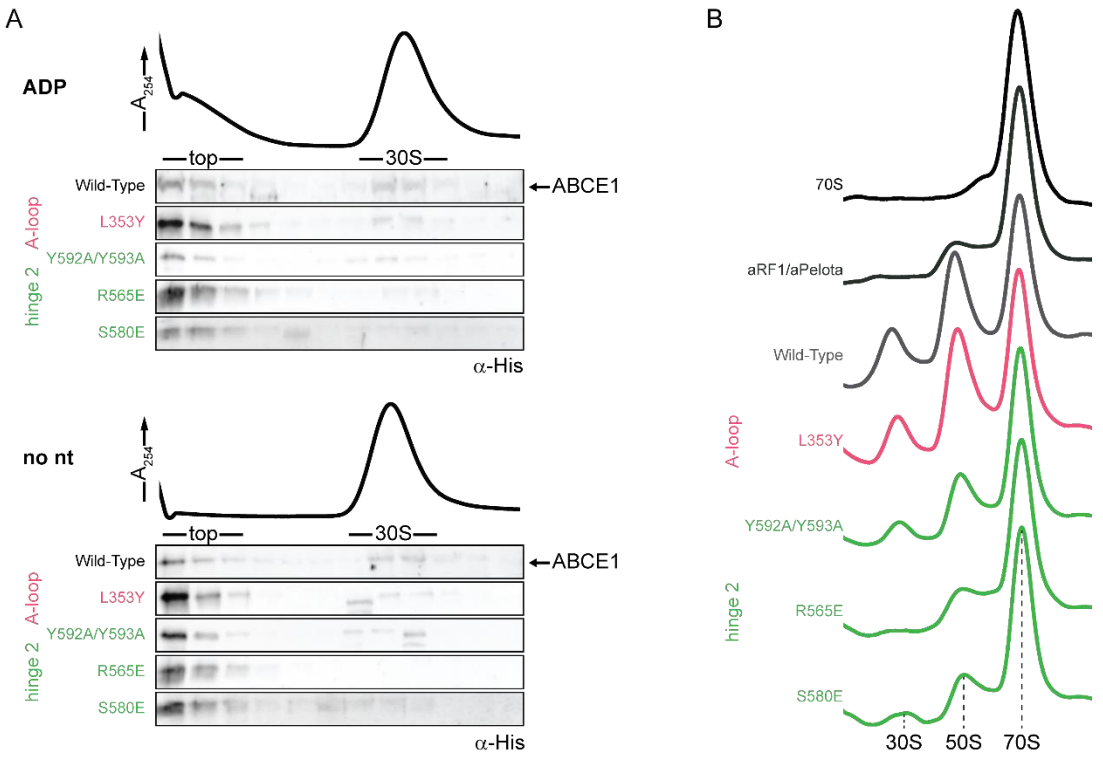

Figure 12: Detailed biochemical characterization of ABCE1 variants (Nürenberg-Goloub *et al*, 2020)**. A)** As wild-type ABCE1, all variants are unable to bind 30S ribosomes in the presence of ADP or in the absence of nucleotide (no nt), thereby excluding that the respective mutation does not lead to unspecific binding to the ribosome. **B)** Examples of sucrose density gradient profiles of 70S ribosome splitting reactions illustrate reduced splitting efficiencies of hinge 2 mutants compared to wild-type ABCE1. SDG profile of the background control (aRF1/aPelota) is similar to R565E, highlighting its essential anchoring function (see Figure 9E, F).

This section was reprinted with permission from Nürenberg-Goloub *et al* 2020 with minor changes.

2.1.8 Learnings from the post-SC and a detailed model of ribosome splitting by ABCE1

By using an ATPase-deficient mutant of ABCE1 in an *in vitro* ribosome recycling assay, we were able to capture the archaeal post-splitting complex comprising the 30S subunit and ABCE1. Our structure reveals this essential, asymmetric ABC-type protein in a fully nucleotide-occluded state at atomic resolution. Furthermore, the cryo-EM structure allows a prediction of the communication pathways within the post-splitting complex, which we functionally and genetically assessed. Ribosome binding is sensed by the HLH motif and hinge region that opens up during ribosome splitting. This “hinge opening” modulates the His-switches in both NBSs by altering the contact interface to adjacent α-helices. We

observed that NBS I is in an active conformation with all residues needed for catalytic activity in place, i.e., activation of a water molecule for nucleophilic attack on the γ-phosphate (Chen *et al*, 2003; Lammens *et al*, 2011; Hofmann *et al*, 2019). The functional and dynamic asymmetry of the two NBSs (Barthelme *et al*, 2011; Nürenberg-Goloub *et al*, 2018; Gouridis *et al*, 2019) does not arise from incomplete ATP alignment due to a non-canonical A-loop in NBS II, as we confirmed by biochemical and yeast viability studies. In the ABC transporter TAP and its functional homolog TmrAB, the position of the non-canonical site cannot be switched without compromising the transport function, indicating that additional signals from outside the binding pocket are integrated into the ATPase cycle (Chen *et al*, 2003; Procko *et al*, 2006; Zutz *et al*, 2011). Consistently, we envision an allosteric regulatory network that extends from the ABCE1-ribosome interface into the NBSs. The spatial separation of hinge 1 from hinge 2 is linked to both NBSs and in addition, might be a prerequisite for the closure of NBS II (Figure 10). In agreement, the introduction of mutations disrupting ribosome binding in hinge 1 (R311A in Sc; R301 in Ss) or hinge 2 (R573E, R582E, and S588E in Sc; R565, R574, and S580, in Ss, respectively) compromise ABCE1 function (Karcher *et al*, 2008) (Figure 7B, Figure 9B–D, Figure 8C, Figure 12). The exchange of G303 in hinge 1 (Figure S1), located at the contact interface to NBD1, leads to a reduced wing size in *Drosophila melanogaster* (G316D in the *pixie* gene), further highlighting the role of the hinge region for ABCE1 function (Coelho *et al*, 2005). Notably, hinge 1 and hinge 2 occupy a position analogous to the regulatory elements of bacterial ABC importers (Newstead *et al*, 2009; Johnson *et al*, 2012; Chen *et al*, 2013) (Figure S4), showing that regulation from this site can be exploited by ABC-type proteins.

Closure of NBS II allosterically activates NBS I, which is consistent with the increased ATPase activity of ABCE1 in the presence of 70S/80S ribosomes and release factors (Pisarev *et al*, 2010; Shoemaker & Green, 2011; Nürenberg-Goloub *et al*, 2018). On a structural level, we assume that NBS II can close prior to NBS I to prime ribosome splitting at the pre-SC (Figure 13). In more detail, the movement of the signature motif toward NBS II is possible when still bound to the 70S/80S ribosomes, since ABCE1 anchors *via* the hinge 2 region and HLH motif, and none of the mobile parts participate in ribosome binding. Furthermore, 70S/80S are split as soon as both NBSs occlude Mg^{2+}-ATP and switch to the closed conformation (Figure 13), as found within the post-SC (Heuer *et al*, 2017; Nürenberg-Goloub *et al*, 2018; Gouridis *et al*, 2019). During the closing movement, the FeSD is pushed away by NBD2 and, concomitantly, interactions between NBD1, the HLH motif, and the ribosome must be temporarily broken, allowing hinge 1 to move away from hinge 2 (Figure 13). Structurally, separation of the two hinge regions occurs

concomitantly with FeSD movement and adoption of the fully closed state of the ABCE1 NBDs. These structural rearrangements may well determine the ribosome splitting rate. Consistently, in the presence of Mg^{2+}-AMP-PNP, ABCE1 transiently associates with 30S ribosomes within 5 s, while the closure of NBS II takes approximately 7 min and stabilizes the post-SC (Gouridis *et al*, 2019).

Remarkably, translation termination is a slow event. Several ribosome profiling studies showed a high enrichment of reads indicating a high occupancy of ribosomes on stop codons (Andreev *et al*, 2017). Moreover, a significant population of ABCE1-containing termination complexes was found in native polysomes, along with translating ribosomes (Behrmann *et al*, 2015). Similarly, the half-life of ribosomes stalled during translation and rescued by the Pelota/Hbs1/ABCE1 system is supposedly long. In light of this, it makes sense that ribosome splitting is regulated and coordinated by the action of the intrinsically slow NBS II. Slow closure of NBS II could ensure correct engagement within the pre-splitting complex, and slow ATP hydrolysis could determine the dwell time of ABCE1 after splitting to prevent premature re-association with large ribosomal subunits or coordinate downstream events such as translation initiation and/or tRNA/mRNA recycling. In this context, the question remains open as to how ATPase activity and thus the 30S/40S dissociation is modulated (Figure 13). Here, external factors, e.g., components of the initiation machinery, might play a direct or indirect role in communicating conformational rearrangements during pre-initiation complex formation into the NBSs of ABCE1 to trigger its release. In particular, and possibly by modulating its ATPase activity, the non-essential eukaryotic eIF3j subunit (Hcr1 in Sc), which was recently shown to contact ABCE1 *via* its N-terminus in 43S initiation complexes in yeast and human (Kratzat *et al*, 2021), assists ABCE1 in ribosome recycling, and thereby may also promote post-SC disassembly (Young & Guydosh, 2019).

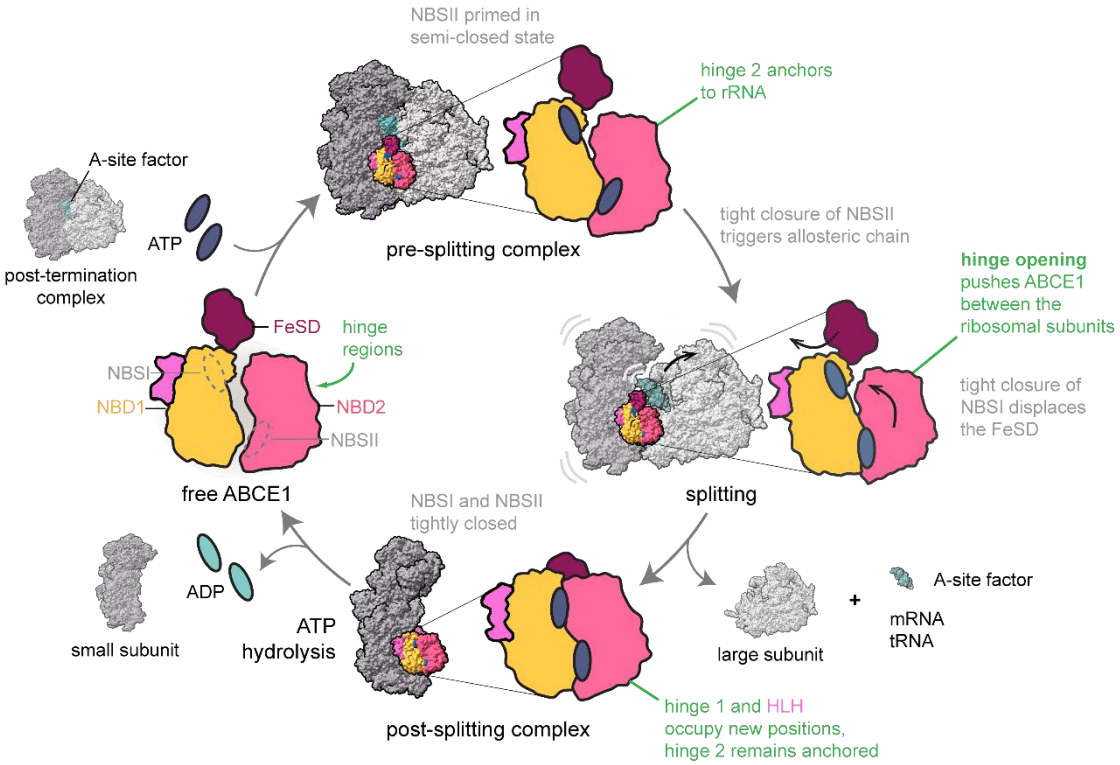

Figure 13: Model for ribosome splitting by ABCE1 (Nürenberg-Goloub *et al*, 2020)**.** ABCE1 binds to 70S/80S ribosomes containing mRNA, tRNA in the P site (not shown), and an A site factor (a/eRF1 after canonical termination; a/e Pelota during stalled ribosome recognition) to form pre-splitting complexes. Here, NBS II is primed in a semi-closed state and anchored to ribosomal RNA *via* hinge 2. ATP occlusion and tight closure of NBS II trigger an allosteric chain within ABCE1 leading to a tight closure of NBS I. Consequently, the FeSD is displaced and the parallel hinge opening rearranges ABCE1 in the ribosomal subunit cleft. Thereby, the subunits are split apart and the FeSD is repositioned at h44. During and/or after the splitting process, the A site factor dissociates and mRNA and tRNA are recycled (not shown). At the post-SC, ABCE1 occludes two ATP molecules in the NBSs. ATP hydrolysis is a prerequisite for NBS opening and dissociation of ABCE1 from the SSU. Black arrows indicate domain movements within ABCE1.

This section was reprinted with permission from Nürenberg-Goloub *et al* 2020 with minor changes.

2.2 The post-splitting complex is the basis for mRNA translation initiation complex formation

In *S. solfataricus,* mRNA binding to the 30S subunit follows bacterial and eukaryotic patterns. The first archaeal translation initiation factors that bind to the SSU are aIF1 and aIF1A, like in Eukarya. Synergistically, they stimulate the binding of aIF2/GTP, which then binds the methionylated initiator tRNA ($^{Met}tRNA_i^{Met}$), forming the ternary complex (aIF2/GTP/$^{Met}tRNA_i^{Met}$) on the SSU as in Bacteria (Hasenöhrl *et al*, 2009). In Eukarya, on the contrary, the ternary complex first assembles before binding to the SSU. *S. solfataricus* leadered mRNA that contains a Shine-Dalgarno sequence can directly bind to the 30S ribosomal subunit. Leaderless mRNA, which lacks a 5'-untranslated region (5'-UTR), is recruited by $tRNA_i$ that is already associated with the SSU (Benelli *et al*, 2003). After start codon recognition, aIF1 is released. The subsequent GTP hydrolysis by aIF2 leads to its release from the SSU (Schmitt *et al*, 2019). Finally, aIF5B is recruited for subunit joining (Maone *et al*, 2007).

The function of ABCE1 in mRNA translation was first described as promoting the formation of pre-initiation complexes and directly interacting with various initiation factors in yeast, human, and fruit fly (Dong *et al*, 2004; Chen *et al*, 2006; Andersen & Leevers, 2007). Later, it was identified that the main function of ABCE1 in translation is to recycle terminated and stalled ribosomes (Pisarev *et al*, 2010; Barthelme *et al*, 2011; Shoemaker & Green, 2011). The formation of the stable post-splitting complex revealed that the ABCE1-bound SSU functions as a platform for initiation factor recruitment (Kiosze-Becker *et al*, 2016; Heuer *et al*, 2017; Mancera-Martínez *et al*, 2017; Nürenberg-Goloub *et al*, 2018). Thereby, the early findings were directly connected to the recycling function. Since ABCE1 stays bound to the SSU in a closed conformation with two occluded ATP molecules (Nürenberg-Goloub *et al*, 2018), its release is directly connected to the opening of the NBSs and thereby ATP hydrolysis.

Inevitably, the questions arise:

- Does ABCE1 affect initiation factor recruitment to the SSU?
- Is there a specific trigger for ABCE1 release?
- Does ABCE1, on the post-SC, simply function as a timer to restrict premature (re-) initiation or LSU (re-) joining?

To address these questions, I followed three different approaches: (i) *In vitro* reconstitution of the archaeal translation initiation apparatus, which was previously established in the laboratory (Nürenberg-Goloub, 2018), and assembly of recombinant initiation complexes with the post-SC as starting point for biochemical and structural characterization (sections 2.2.1, 2.2.2, and 2.2.3). Based on the conserved positioning of initiation factors on the ribosome, I did not address aIF5B in the *in vitro* assembly of ICs, since eIF5B occupies a similar position on the SSU as ABCE1 (Fernández *et al*, 2013), thereby mutually excluding each other on the ribosome. (ii) Establishment of ABCE1 pull-down from archaeal cell lysates for structural and biochemical analysis of (near) native archaeal post-splitting/initiation complexes (section 2.2.4). (iii) Fluorescence-based determination of thermodynamic parameters of aIFs binding to the 30S subunit and post-SC (section 2.2.5).

2.2.1 ABCE1 does not directly interact with initiation factors *in vitro*

Utilizing a previously established *in vitro* reconstitution of the recombinant *S. solfataricus* translation apparatus (Nürenberg-Goloub, 2018), the early findings in Eukaryotes of a direct interaction of ABCE1 with initiation factors were addressed (Dong *et al*, 2004; Andersen & Leevers, 2007). An *in vitro* interactome of ABCE1 and initiation factors was created *via* size-exclusion chromatography (SEC) (Figure 14). The catalytically inactive ABCE1 double-mutant E238/485A (IIEA) (ABCE1^{IIEA}) and non-hydrolysable ATP and GTP-analogs (AMP-PNP and GMP-PNP) were used to stabilize ABCE1 and aIF2 in defined conformations, respectively. Notably, we could not observe the assembly of stable complexes between ABCE1 and various IFs except for the aIF2-^{Met}tRNA$_i^{fMet}$ ternary complex.

Separate symmetric elution peaks in SEC suggested that, neither ABCE1 nor aIF2 form a stable complex with aIF1 (Figure 14E, H) and aIF1A (Figure 14F, I) *in vitro*. For ABCE1-aIF2, the elution overlapped, but represented separate peaks (V_e = 1.58 ml and 1.51 ml for ABCE1 and aIF2, respectively), as confirmed by the ABCE1-specific absorption at 420 nm of the iron-sulfur cluster domain (Barthelme *et al*, 2007). Thereby, a direct stable interaction between the two proteins can be excluded in our setting (Figure 14D). Similar findings were observed for interaction of ABCE1 with initiator tRNA (tRNA$_i^{fMet}$) (Figure 14L). The expected aIF2 specificity for methionylated initiator tRNA (^{Met}tRNA$_i^{fMet}$) was confirmed (Figure 14K, N). A direct interaction of ABCE1 with the ternary complex (aIF2/GMP-PNP/^{Met}tRNA$_i^{Met}$, V_e = 1.48 ml) was not observed (Figure 14O).

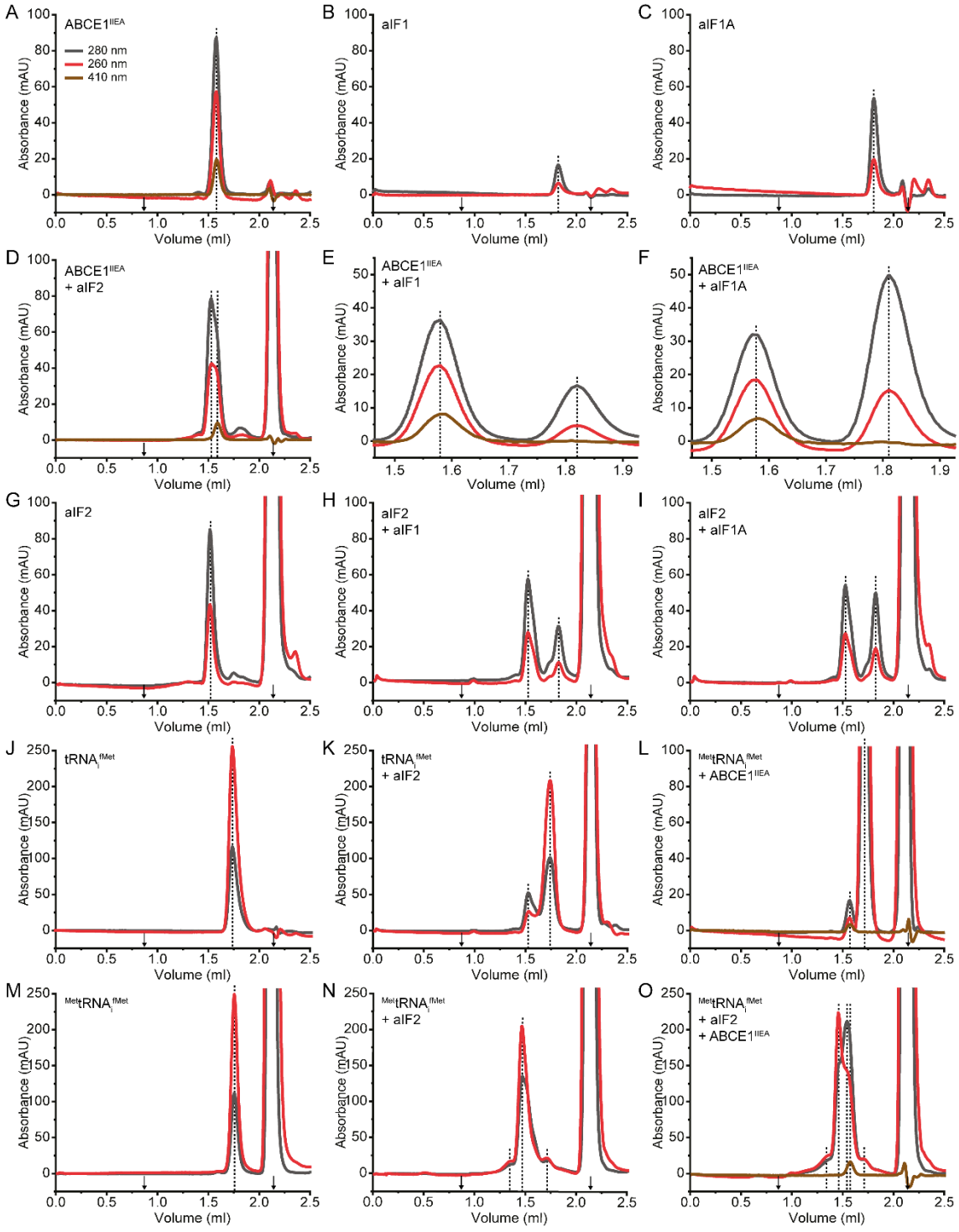

Figure 14: ABCE1 does not assemble stable complexes with initiation factors *in vitro*. Interactions were analyzed by SEC (Superdex® 200 Increase 3.2/300 GL, Cytiva). Column void (V_0 ≈ 0.8 ml) and total volume (V_t ≈ 2.15 ml) are indicated by arrows. Elution volume (V_e) of the respective protein, tRNA, or complex is marked by a dashed line. Each single protein and tRNA eluted in a symmetric peak indicating stable and monodisperse samples. The aIF2αβγ heterotrimer was pre-assembled with excess GMP-PNP, which eluted at V_t with high absorbance (D, G, H, I, K, N, O). ^{Met}tRNA$_i^{Met}$ samples contained ATP/ADP from the methionylation reaction, which eluted at V_t with high absorbance (L-O). V_e ≈ 1.58 ml (ABCE1, A), 1.82 ml (aIF1, B), 1.81 ml (aIF1A, C), 1.51 ml (aIF2, G), 1.74 ml (tRNA$_i^{Met}$, J), 1.76 ml (^{Met}tRNA$_i^{Met}$, M), and 1.48 ml

(aIF2/GMP-PNP/^{Met}tRNA$_i^{Met}$, N). ABCE1 did not directly interact with aIF2, aIF1, aIF1A, ^{Met}tRNA$_i^{Met}$, or the ternary complex in SEC (D, E, F, L, O, respectively). aIF2 bound ^{Met}tRNA$_i^{Met}$ in SEC but neither aIF1, aIF1A, tRNA$_i^{Met}$, nor ABCE1 (N, H, I, D and O, respectively).

Our *in vitro* results showed that ABCE1 does not directly interact with aIF1, aIF1A, and aIF2. In contrast, eIF3, eIF5, and eIF2 co-immunoprecipitated with genetically tagged ABCE1 in yeast even in the absence of the small ribosomal subunit. Therefore, ABCE1 must directly interact with the multifactor complex (MFC) eIF3/5/2 (Dong *et al*, 2004). Additionally, many components of the multifactor eIF3 co-immunoprecipitated with ABCE1 in *Drosophila melanogaster*. Although ribosomes were present, a direct interaction of eIF3 and ABCE1 was concluded based on depletion of eIF3 core components after ABCE1 knockdown (Andersen & Leevers, 2007). Furthermore, in a recent structure of yeast 48S late-stage initiation complexes, the N-terminus of eIF3j, a subunit of the multifactor eIF3, protrudes into the NBD1/NBD2 cleft of NBS I in ABCE1, confirming a direct interaction of ABCE1 and eIF3 on the SSU (Kratzat *et al*, 2021). Moreover, eIF3j has a functional role in ribosome recycling (Young & Guydosh, 2019). Thus, in Eukaryotes, a direct interaction of ABCE1 with eIF3 was convincingly demonstrated *in vivo*. In Archaea, no eIF3 homolog is described but the existence of a functional complex formed by ABCE1 and other initiation factors could not be excluded. However, our *in vitro* experiments do not support the hypothesis that ABCE1 forms stable complexes with initiation factors.

2.2.2 Formation of stable archaeal post-splitting/initiation complexes

As expected from structures of the eukaryotic ABCE1-initiation complex (Heuer *et al*, 2017; Mancera-Martínez *et al*, 2017) and based on the previous findings of the ABCE1 interaction analysis (Figure 14), we hypothesized an indirect interaction of ABCE1 with initiation factors and an allosteric crosstalk *via* the small ribosomal subunit in Archaea. Thus, we assembled ABCE1-initiation complexes by binding of IFs to the post-SC *in vitro* (Figure 15). In summary, binding of archaeal initiation factors to the small ribosomal subunit in the presence of ABCE1 could be demonstrated *in vitro* by three independent methods. Thus, the post-splitting complex can be decorated by initiation factors, allowing a functional role for ABCE1 in translation initiation, as suggested by numerous findings in Eukaryotes.

Stable binding of aIF2 to the post-SC was confirmed by co-migration with ABCE1 and 30S ribosomal proteins in sucrose density gradient centrifugation (Figure 15A). Co-immunoprecipitation with ABCE1 revealed that sequential binding of aIF1/1A and aIF2 to the post-SC formed a stable initiation complex (Figure 15B). Additionally, I established a native PAGE assay, in which ABCE1-bound ribosomal complexes were visualized by fluorescence. Tracer amounts of fluorescently labeled ATP molecules (Figure 24) were occluded by ABCE1^{IIEA} before forming the post-SC. aIF2/GMP-PNP/ ^{Met}tRNA$_i^{Met}$-bound ribosomal complexes and free ABCE1 were monitored in native PAGE by the fluorescent ATP occluded within the NBSs of ABCE1. Protein extraction followed by SDS-PAGE analysis confirmed the presence of aIF2 and thereby the stable ABCE1/aIF2-IC (Figure 15C).

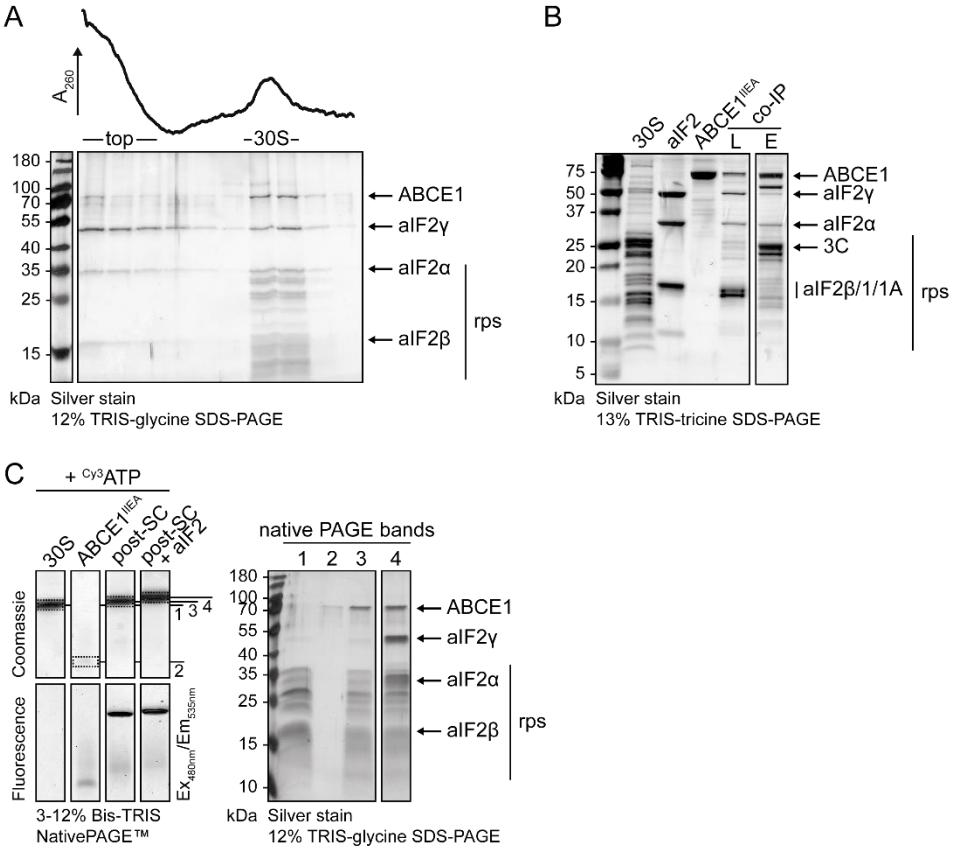

Figure 15: aIF1, aIF1A, and aIF2 bind to the post-SC forming initiation complexes with ABCE1. A) Formation of the 30S/ABCE1/aIF2-IC was verified by SDG centrifugation and SDS-PAGE. **B)** Co-immunoprecipitation of IFs and ribosomal proteins with ABCE1^{IIEA} confirmed the stable formation of the 30S/ABCE1/aIF1/aIF1A/aIF2-IC. L, IP load; E, IP eluate; 3C, 3C precision protease; rps, ribosomal proteins. **C)** Stable formation of the 30S/ABCE1/aIF2-IC was confirmed by native PAGE. ABCE1, the post-SC, and the 30S/ABCE1/aIF2-IC were visualized by occlusion of Cy3-fluorescently labeled ATP (^{Cy3}ATP) in ABCE1. Composition of ribosomal complexes in native PAGE were confirmed by protein extraction (1, 2, 3, and 4) and subsequent SDS-PAGE.

Even though we could observe IF binding to the post-SC neither a functional role of ABCE1 in translation initiation nor the trigger for ABCE1 release from the SSU could be tackled by our static binding experiments in the presence of non-hydrolyzeable nucleotide-analoga and hydrolysis-deficient ABCE1 variants. Still, this result constitutes an important puzzle piece of the molecular mechanism of ABCE1 in translation. Based on these *in vitro* assembly experiments, I conducted structural investigations of the post-SC/IC and established co-immunprecipitation experiments to elucidate the formation of this complex in *vivo*.

2.2.3 Cryo-EM analysis of archaeal mRNA translation initiation complexes following the native ribosome recycling route by ABCE1

After successful assembly of post-splitting/initiation complexes and their biochemical characterization (section 2.2.2), archaeal ABCE1-initiation complexes were structurally analyzed by cryo-EM. In accordance with formation of the stable post-SC after ribosome recycling (Kiosze-Becker *et al*, 2016; Heuer *et al*, 2017; Nürenberg-Goloub *et al*, 2018), ABCE1 was identified in low-resolution electron densities of initiation complexes. Although first misassigned as eIF3g/i (Simonetti *et al*, 2016), ABCE1 was subsequently confirmed to be part of early (43S) and late (48S) stage initiation complexes in Eukaryotes (Heuer *et al*, 2017; Mancera-Martínez *et al*, 2017). For Archaea, only low-resolution models of reconstituted 43S pre-initiation complexes lacking ABCE1 were available (Coureux *et al*, 2016). Following the native ribosome-splitting route, as described for the post-SC (2.1.1, Figure 16A), structures of archaeal ABCE1-initiation complexes were solved by cryo-EM in collaboration with the Beckmann laboratory at the LMU Munich. In parallel, new high-resolution structures of native ICs revealed the interaction of ABCE1 with eIF3j on 43S and 48S ICs in yeast and human (Simonetti *et al*, 2020; Kratzat *et al*, 2021), while structural studies of recombinantly assembled late-stage ICs in Archaea disregarded ABCE1 (Coureux *et al*, 2020).

The archaeal initiation complex was reconstituted starting with active splitting of *T. celer* 70S ribosomes by $ABCE1^{IIEA}$. Sequentially, pre-incubated aIF1/1A/mRNA (Shine-Dalgarno leadered mRNA, (Hasenöhrl *et al*, 2009)) and pre-assembled aIF2αβγ/GMP-PNP/$^{Met}tRNA_i^{Met}$ bound to the post-SC. Initiation complexes were SDG-purified and examined by cryo-EM (Figure 16A). Data were collected by Otto Berninghausen and processed by Hannah Kratzat (with help of Thomas Becker and other lab members) in the Beckmann laboratory at the LMU Munich. Over 16,000 micrographs were recorded at 75,000-fold magnification. After an initial screening and automated

particle picking (Gautomatch), almost three million particles were subjected to 2D classification. Approximately two million particles were subsequently used for 3D classification, resulting in multiple classes mainly differing in the 30S head to body movement. Further 3D classification based on ABCE1 and initiation factors, resulted in eight classes. Extended processing of three classes differing in composition, but all containing ABCE1, resulted in electron densities with intermediate resolution (overall 3.6-4.9 Å, Table S1, Figure S5). The three structural models were termed initiation complex 1-3 (IC1-3), according to the order of assembly during translation initiation (Schmitt *et al*, 2019). IC1 (3.6 Å) consisted of the post-SC and aIF1/1A, thereby representing the first step of pre-IC assembly. Structures of archaeal aIF1/1A and yeast ABCE1 were fitted into the respective densities (Figure 16B, Figure 17A). IC2 consisted of the post-SC, aIF1A, aIF2, $^{Met}tRNA_i^{Met}$, and mRNA (4.3 Å, Figure 16C). The resolution of aIF2 was very low, indicating high flexibility as previously seen (Coureux *et al*, 2016, 2020). The absence of aIF1 and the formed tRNA-mRNA stack indicated the transition to a late-stage IC (Figure 17B). IC3 consisted of the post-SC, aIF1A, $^{Met}tRNA_i^{Met}$, and mRNA (4.9 Å, Figure 17C). Although similar to IC2, only residual aIF2 density was present in IC3, which I speculated to be due to reduced presence of aIF2, as expected for the next step in initiation. Although no detailed models were built based on the obtained electron density maps, our results agree with the current understanding of eukaryotic and archaeal modes of mRNA translation initiation (Figure 18) (Schmitt *et al*, 2019). With our *in vitro* assembly approach, we could confirm the presence of ABCE1 in early and late-stage initiation complexes in Archaea, as reported for Eukaryotes (Heuer et al, 2017; Mancera-Martínez et al, 2017; Simonetti et al, 2020; Kratzat et al, 2021). Notably, no direct interactions between ABCE1 and other IC components were observed. Thus, a functional role of ABCE1 in archaeal translation initiation as well as the trigger for ABCE1 release from the archaeal post-SC remain to be elucidated.

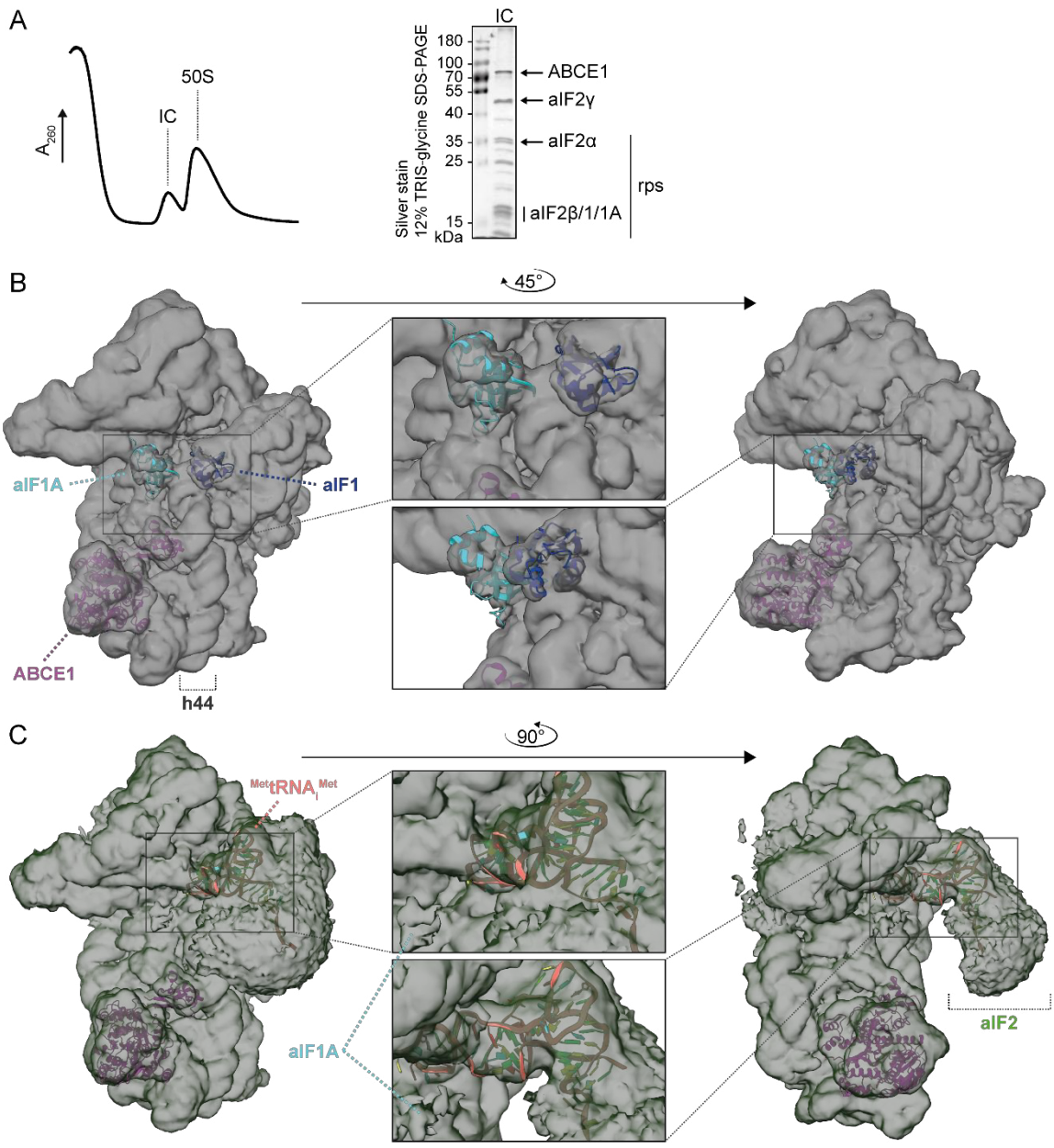

Figure 16: Cryo-EM analysis of *in vitro* assembled initiation complexes revelead diverse ICs. A) SDG purified initiation complexes, which were assembled directly after splitting of 70S ribosomes by ABCE1. The cryo-EM IC sample contained ABCE1, the 30S subunit, aIF1, aIF1A, and aIF2. **B, C)** Cryo-EM density maps of initiation complex 1 (IC1, A) and IC2 (B) at map level 0.01. Intersubunit side (left) and rotated views (right). Although all components of the IC were visible *via* SDS-PAGE/Silver Stain of the obtained sample (A), the vitrified particles and resulting electron density maps were highly diverse. This observation indicates substantial compositional variability among the analyzed complexes and high flexibility of the IC components on the SSU. **B)** IC1 consisted of the 30S subunit, ABCE1, aIF1A, and aIF1. Structures of ABCE1 (purple, PDB 5LL6), aIF1A (cyan, PDB 5JBH), and aIF1 (blue, PDB 5JBH) were fitted into the respective densities. **C)** IC2 consisted of the post-SC, aIF1A, initiator tRNA in the P site and partially aIF2. Structure of $^{Met}tRNA_i^{Met}$ (orange, PDB 5JBH) was fitted into the P site density. Additional density connected to the tRNA and was attributed to aIF2.

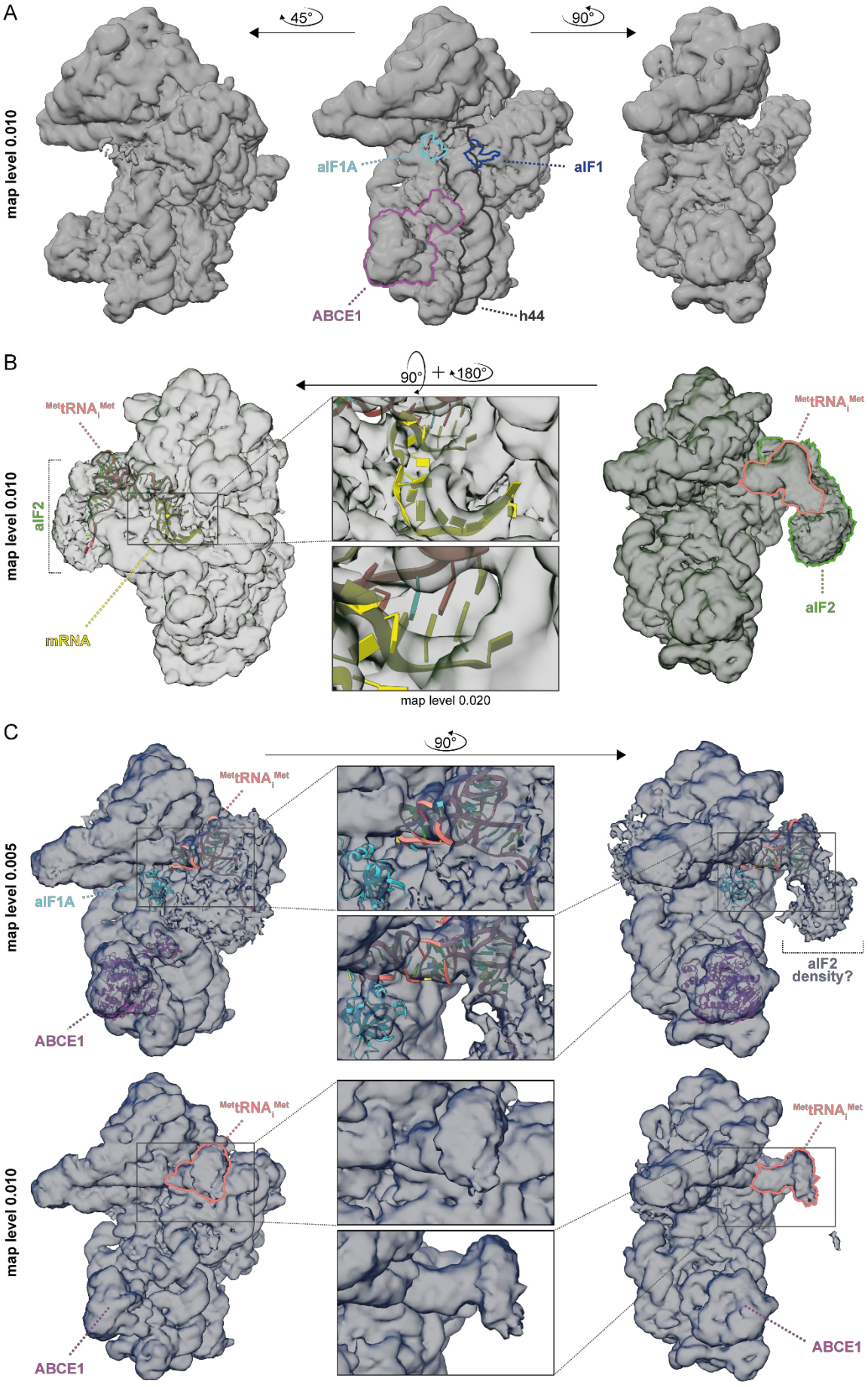
A
map level 0.010
45°
90°
aIF1A
aIF1
ABCE1
h44
B
map level 0.010
90° + 180°
MettRNAiMet
aIF2
mRNA
map level 0.020
C
map level 0.005
90°
aIF1A
ABCE1
aIF2 density?
map level 0.010
ABCE1

Figure 17: Cryo-EM density surface models of *in vitro* assembled initiation complexes show key intermediates of archael translation initiation. A) IC1 (as in Figure 16B) represents an early-stage initiation complex, which is formed by the recruitment of aIF1/1A to the post-SC directly after LSU dissociation. Intersubunit side (center) and rotated views (left and right). Positioning of ABCE1 (purple), aIF1A (cyan), and aIF1 (blue) at rRNA helix 44 (h44, gray) is outlined. **B)** IC2 (as in Figure 16C with an additional view into the mRNA tunnel) is characterized by the codon-anticodon stacking between the start codon of the mRNA (yellow) in the mRNA tunnel and the tRNA (orange) at the P site (see zoom-in). The electron density map further reveals the presence of aIF2 (green) as a stable component of this IC. **C)** Initiation complex 3 (IC3, intersubunit side on the left and rotated view on the right) consisted of the post-SC, aIF1A, and tRNA, thus pointing towards a role downstream of IC2 after aIF1 release. Resolution of aIF1A and tRNA were enhanced in comparison to IC2. Additional density at the aIF2 position was visible at lower map levels (0.005). The structure of $^{Met}tRNA_i^{Met}$ (orange, PDB 5JBH) was fitted into the tRNA density.

In other recent structures of yeast 48S late-stage initiation complexes, the N-terminus of eIF3j, a subunit of the multifactor eIF3, protrudes into the NBD1/NBD2 cleft of NBS I in ABCE1. Crosslinking showed that the eIF3j extension in this position inhibited ADP release from the semi-open NBS I. It was proposed that thereby the asymmetric state of ABCE1 (closed NBS II and semi-open NBS I) was stabilized on the 48S IC (Kratzat *et al*, 2021). It could be speculated whether eIF3/3j triggers ATP hydrolysis and subsequently traps the NBS in an intermediate state just before the release of ABCE1 from the IC. Interestingly, the C-terminal residues of the archaeal 50S stalk protein aP1 were positioned similarly to eIF3j on ABCE1 in a structure obtained by X-ray crystallography. This interaction stimulated the ATPase activity of ABCE1 on the ribosome (Imai *et al*, 2018). Thus, a multivalent interaction interface of ABCE1 seems to regulate its ATPase activity, possibly binding various factors as checkpoints during ribosome remodelling and IC assembly. Consequently, it could be speculated that aP1 or another yet unknown factor triggers ABCE1 release from the ribosome *via* this functional patch when the IC is ready for subunit joining in Archaea.

Despite the finding that ABCE1 does not have direct contacts to initiation factors on the archaeal ribosomal subunit, two additional mechanisms of interaction are plausible: (i) *via* ribosomal proteins, or (ii) *via* h44 of the 18S rRNA. Importantly, relocation of the FeSD to h44 on the post-SC and subsequent ICs resulted in flip-out of h44 bases in direct vicinity of eIF2 (Heuer *et al*, 2017). Furthermore, a/eIF1 and a/eIF1A bind at the 3'-end of h44, allowing for an allosteric crosstalk with ABCE1 *via* h44. It was speculated that ABCE1 might be released from late-stage ICs due to a slight conformational change in h44 after eIF1A release (Simonetti *et al*, 2020). Additionally, the FeSD contacts uS12, which connects to the a/eIF1A binding site potentially allowing allosteric communication (Figure 8A, B, Figure 16B) (Kiosze-Becker *et al*, 2016; Heuer *et al*, 2017; Simonetti *et al*, 2020).

Hence, it would be plausible that a potential function of ABCE1 during initiation is conserved among Eukaryotes and Archaea. However, no significant changes in the late-stage eukaryotic 48S IC was observed in presence or absence of ABCE1 (Simonetti *et al*, 2020). Consistently, we did not find any deviations in the conformation or position of h44 between the resolved early (IC1) and late stage (IC2, IC3) complexes. A possible reason might be the use of a hydrolysis deficient ABCE1 variant and the presence of non-hydrolyzeable nucleotide analoga in our sample. Because ABCE1 occupies a key position on the SSU, its conformational constraint might rigidify major conserved components of the ribosome.

Further, ABCE1 might have thermodynamic or kinetic effects on initiation factor recruitment, which cannot be assessed by structural studies. Taken together, these findings further open-up the functional complexity of ABCE1 presence on diverse ribosomal complexes during mRNA translation.

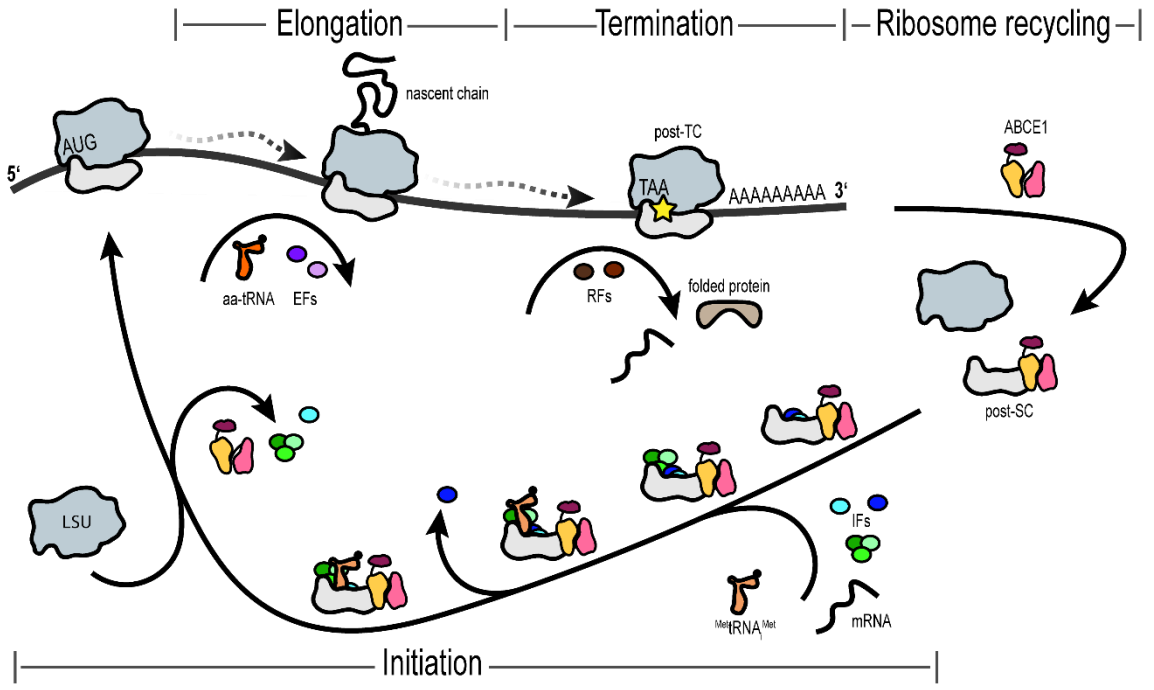

Figure 18: The sequential assembly of archaeal initiation complexes and their integration into the mRNA translation cycle. After ribosome recycling by ABCE1, initiation factors are recruited to the post-SC. First, aIF1A (cyan) and aIF1 (blue) are recruited and support mRNA binding (IC1; Figure 16B, Figure 17A). Next, heterotrimer aIF2αβγ (green) recruits the initiator tRNA ^{Met}tRNA$_i^{Met}$ (light orange) to the forming IC. After positioning of ^{Met}tRNA$_i^{Met}$ for anticodon-codon interaction with the mRNA, aIF1 is released (IC2; Figure 16C, Figure 17B). Then aIF2 is released (IC3; Figure 17C), followed by dissociation of ABCE1 and aIF1A for joining of the large subunit. Polypeptide synthesis during elongation, subsequent termination at a stop codon, and ribosome recycling follow the described mechanisms (Figure 1).

2.2.4 Co-immunoprecipitation of native ribosomal complexes paves the way to decipher translation initiation in Archaea

After successful reconstitution of the archaeal mRNA translation initiation apparatus and confirming the assembly of ABCE1-initiation complexes *in vitro* by biochemical and structural analysis, native ABCE1-ribosome complexes from *Sulfolobaceae* should be characterized. So far, studies of archaeal translation initiation focused on a reconstituted system. The eukaryotic and archaeal modes of translation initiation share a common structural basis and follow a consecutive order of IC assembly, as described in sections 2.2.2 and 2.2.3. Nevertheless, the archaeal native mode of assembly and structures of native complexes remained elusive. Hence, co-immunoprecipitation protocols for the pull-down of ribosome complexes from *S. solfataricus* and *S. acidocaldarius* cell lysates *via* recombinant ABCE1 were established. Subsequently, mass spectrometry (MS) analysis was performed to address the interactome of ABCE1. Finally, native complexes from *S. acidocaldarius* were obtained *via* pull-down of plasmid-borne ABCE1 to pave the way for structural studies of endogenous ABCE-ribosome complexes.

S. solfataricus P2 wild-type and *S. acidocaldarius* MW001 (Wagner *et al*, 2012) cells were harvested in the logarithmic growth phase to ensure the presence of translating ribosomes as targets for ABCE1. Ss ABCE1^{WT} was efficiently immunoprecipitated *via* its C-terminal FLAG® tag and complexes were specifically eluted *via* 3C precision protease cleavage (ABCE1^{WT}-3C-FLAG, Table 10, Figure 19A no lysate). ABCE1 pull-down of ribosomal proteins from *S. solfataricus* lysates was nucleotide-dependent (Figure 19A), confirming correct functional binding of ABCE1 to 30S subunits along with nucleotide occlusion and NBD closure (Kiosze-Becker *et al*, 2016; Heuer *et al*, 2017; Nürenberg-Goloub *et al*, 2018). Adapted IP conditions enhanced the typical 30S ribosomal subunit protein pattern in the IP eluate in SDS-PAGE (Figure 19B).

In collaboration with Dr. Haifei Xu of the Joazeiro laboratory at Scripps Biomedical Research Institute of the University of Florida, MS analysis of recombinant ABCE1 IP eluates from *S. solfataricus* lysates was performed. As expected, ribosomal proteins were predominant. Additionally, numerous translation factors, but also metabolic enzymes were identified (section 6.3, Table S2). Similar abundance by adjusted p-values suggested that either the pulled-down proteins were not enriched in the ABCE1 samples compared to the controls, the sample processing for MS was flawed, or that the protein concentration was too low in MS analysis. Since all biochemical methods confirmed specific 30S pull-down (Figure 19), the former could be excluded. The identification of many 50S ribosomal subunit proteins with high abundance indicated that recombinant ABCE1 not only bound

to and pulled-out 30S subunits, but also 70S ribosomes. Additionally, a *S. solfataricus* small zinc-finger protein was identified (Table S2, DUF1610 domain-containing protein, Q980V0) with 52% sequence identity to *T. celer* eS21, which we firstly identified in our atomic model of the post-SC (section 2.1.2, Figure 6). In parallel, another study also identified an eS21 homolog (termed aS21) on the *Pyrococcus abyssi* (*P. abyssi*) 30S subunit in a cryo-EM structure of an initiation complex (Coureux *et al*, 2020). Furthermore, *S. solfataricus* Q980V0 is closely related to *Haloferax volcanii* HVO_2753, which recently was extensively characterized, highlighting the high abundance and functional range of small zinc-finger proteins in Archaea (Zahn *et al*, 2021).

In *S. acidocaldarius*, a versatile genetic toolbox has been established by the Albers laboratory, which allows for affinity tagging of proteins on the genomic level and inducible expression of proteins of interest from plasmids (Wagner *et al*, 2012). The system was utilized to shift to native conditions for pull-down of archaeal ABCE1-ribosome complexes. First, pull-down conditions of recombinant Sa ABCE1^{WT} (Table 9, Table 10) from *S. acidocaldarius* cell lysates were confirmed to be equally efficient as in the previously utilized *S. solfataricus* system (Figure 19C). Although *S. solfataricus* and *S. acidocaldarius* are closely related, the pull-down of ribosomal complexes by ABCE1 was species-specific (Figure 19D). Furthermore, sucrose density gradient centrifugation analysis of the IP eluate confirmed the specific pull-down of 30S ribosomal subunits and the stable association of ABCE1 (Figure 19E).

For the analysis of endogenous ribosomal complexes, either genomically-tagged or plasmid-borne expression of ABCE1-FLAG is in principle possible. Since ABCE1 is essential in Eukaryotes and Archaea, the gene encoding for ABCE1 could not be manipulated to attach a C-terminal 3C site and FLAG® tag for IP of genomic ABCE1. Therefore, ABCE1 constructs were introduced into a *S. acidocaldarius* expression plasmid, which was kindly provided by Dr. Alejandra Recalde of the Albers laboratory at the University Freiburg, who also helped with transformation of *S. acidocaldarius*. Screening of expression conditions revealed most protein production for over-night expression of ABCE1^{WT} (Figure 20A). The utilized xylose-inducible promotor had a weaker control over protein expression in *S. acidocaldarius* compared to standard bacterial or viral promotors and thus resulted in slight background presence of ABCE1^{WT} and single catalytic glutamate variants E238A and E485A in uninduced cells (Figure 20B). Interestingly, cells transformed with ABCE1^{E485A} showed similar growth behavior and ABCE1 expression levels as WT and NBS I variant E238A (Figure 20B), although the corresponding NBS II variant E493A is lethal in yeast (Nürenberg-Goloub *et al*, 2018). MS analysis of expressed and isolated ABCE1 samples revealed identical masses for

ABCE1^{WT}, E238A, and E485A, corresponding to the wild-type mass (kindly performed by Christian Winter of the Tampé laboratory, Goethe-University Frankfurt).

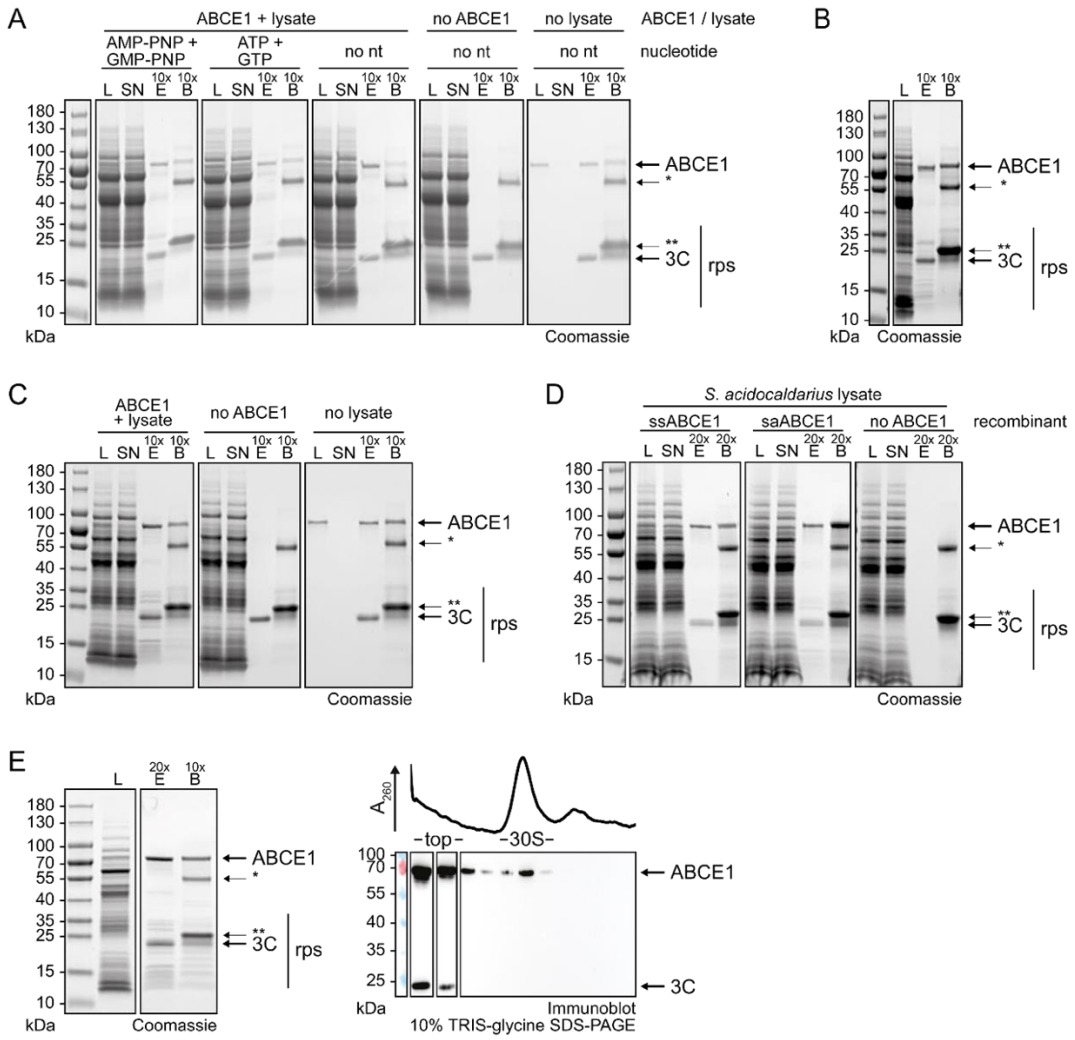

Figure 19: Pull-down of ribosomal complexes by ABCE1 from archaeal cell lysates is nucleotide dependent and species specific. 4-20% TRIS-glycine SDS-PAGE analyses of co-immunoprecipitations of ABCE1 and ribosomal complexes from archaeal lysates. L, IP load; SN, IP supernatant; E, IP eluate; B, IP beads sample; 10x/20x/60x/180x, x-fold concentration compared to L; *, IgG antibody heavy chain; **, IgG antibody light chain; 3C, 3C precision protease; rps, ribosomal proteins. **A)** Pull-down of ribosomal complexes by recombinant ssABCE1 from *S. solfataricus* cell lysates is nucleotide-dependent, confirming a specific functional interaction. **B)** IP conditions with AMP-PNP and GMP-PNP as in (A) were optimized by using lysates with a higher A_{260}. **C)** Pull-down of ribosomal complexes by recombinant saABCE1 from *S. acidocaldarius* cell lysates as in (B) served as proof-of-principle for the experimental setting before addressing endogenous complexes. **D)** Species-specific pull-down of ribosomal complexes by recombinant ABCE1 from *S. acidocaldarius* cell lysates as in (C). **E)** Co-IP as in (C) with increased eluate concentration. Stability and specificity of the pull-down of 30S/ABCE1 complexes was confirmed by SDG centrifugation analysis of the IP eluate and subsequent immunoblot of SDG samples. Immunoblot α-His 1:2,000 and α-mouse-HRP 1:10,000.

Since genomic ABCE1 is present in transformed *S. acidocaldarius*, we speculated that the plasmid-encoded dysfunctional EA variants were repaired by recombination with the genomic sequence during the growth of the cells.

Next, I aimed to optimize the yield of co-immunoprecipitated endogenous ribosomal complexes for structural studies and MS analysis. Lysates of cells, which expressed ABCE1-3C-FLAG®, were prepared as before. The amount of cell lysate needed for the pull-down was increased to the same ABCE1 levels as used in recombinant experiments. Additionally, the elution volume of ABCE1-ribosome complexes was reduced to increase the protein concentration for better visualization by Coomassie-stained SDS-PAGE and vitrification. Furthermore, AMP-PNP and GMP-PNP were added to the lysate to stabilize native ABCE1-ICs. Complexes pulled-down by plasmid-encoded, native ABCE1 were equivalent to the semi-native approach with recombinant ABCE1 (Figure 20C).

EM grids of native immunoprecipitated ABCE1-ribosome complexes were prepared by Dr. Lukas Sušac of the Tampé laboratory at the Goethe-University Frankfurt. Initial screening revealed a low concentration of 30S ribosome particles, which would only allow for intermediate resolution after processing. For solving high-resolution structures by single-particle cryo-EM in the future, it will be necessary to increase culture volumes of the ABCE1 expression in *S. acidocaldarius* and subsequently adjust the co-IP protocol to increase the concentration of pulled-down complexes. Further important factors must be critically evaluated by cryo-EM analysis of native *S. acidocaldarius* ABCE1-ribosome complexes, which are i) the use of nucleotides, ii) sample cross-linking, and iii) structural assessment of h44. The use of ATP and GTP or absence of nucleotides would allow movement of ABCE1 NBSs as seen for 48S ICs in Eukaryotes (Kratzat *et al*, 2021). However, so far, all structures of archaeal ICs have been solved in the presence of GMP-PNP and AMP-PNP (section 2.2.3, (Coureux *et al*, 2016, 2020)). Cross-linking aims to rigidify the ribosome for higher resolution (as performed for the post-SC, section 2.1.1) but increases the risk to potentially arrest non-native conformations. Therefore, published structures of the post-SC and ABCE1-ICs in Eukaryotes avoided cross-linking (Heuer *et al*, 2017; Simonetti *et al*, 2020; Kratzat *et al*, 2021). The poor or missing density for the 18S rRNA h44 in *Sulfolobaceae* 30S ribosomal subunits in cryo-EM restricted high-resolution of the *S. solfataricus* post-SC in the past (Kiosze-Becker *et al*, 2016) and intrigued us to change the source organism of the ribosomes to *T. celer* for our structural studies of the post-SC (section 2.1.1). It remains unclear why h44 could not be resolved. We speculated that h44 is intrinsically flexible or that a stress response displaces h44 upon cell cool-down or cell lysis. In conclusion, the established protocols for expression of

ABCE1 in *S. acidocaldarius* and isolation of ABCE1-ribosomal complexes by co-IP will enable further structural analysis of native ABCE1-ICs from Archaea.

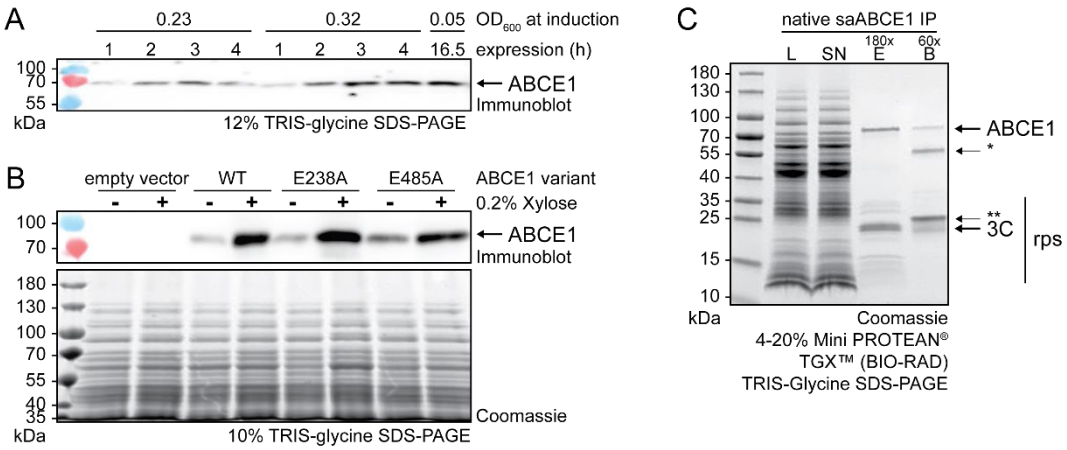

Figure 20: Native ABCE1-ribosome complexes were immunopurified from *S. acidocaldarius* for structural studies. A) Plasmid-driven homologous expression levels of ABCE1^{WT} in *S. acidocaldarius* increased with higher OD_{600} at induction and with longer expression time. The optimal conditions for pull-downs were chosen to be the induction at OD_{600} of 0.05 with 0.2% (w/v) xylose and subsequent expression for 16.5 h. Immunoblot α-FLAG® 1:2,000 and α-mouse-HRP 1:10,000. **B)** Expression levels of ABCE1 variants at optimal conditions. All three variants were efficiently expressed. Residual background expression of ABCE1 was observed in uninduced cells. Immunoblot α-FLAG® 1:2,000 and α-mouse-HRP 1:20,000. Even lysate loading was controlled by Coomassie staining. **C)** Pull-down of ribosomal complexes by native saABCE1 from *S. acidocaldarius* will allow functional and structural insights into archaeal translation in the future.

2.2.5 Binding properties of *S. solfataricus* aIF1 to the 30S subunit are similar to *S. cerevisiae* eIF1 and *P. abyssi* aIF1

After ribosome recycling, ABCE1 remains bound to the small ribosomal subunit during subsequent initiation complex assembly in yeast and higher eukaryotes (Heuer *et al*, 2017; Mancera-Martínez *et al*, 2017; Simonetti *et al*, 2020; Kratzat *et al*, 2021). In an *in vitro* reconstitution system, we confirmed that ABCE1 is also part of initiation complexes in Archaea (sections 2.2.2, 2.2.3). Furthermore, a homologous expression and co-IP approach was established to prepare native archaeal ABCE1-ICs for future structural studies (section 2.2.4). It was proposed that eIF3j and the archaeal 50S stalk protein aP1 might trigger ATP hydrolysis in ABCE1 for its release from the small subunit in Eukaryotes and Archaea, respectively (Imai *et al*, 2018; Kratzat *et al*, 2021). However, there are no functional data on whether ABCE1 affects initiation factor recruitment, or if other a/eIFs trigger the release of ABCE1 from the 30/40S subunit. We did not observe any direct interactions between ABCE1 and other IC components (see section 2.2.3) and therefore

considered deciphering possible thermodynamic effects of ABCE1 on IC assembly using biophysical methods. Thus, I sought to determine the dissociation constant of Ss aIF1 and 30S ribosomal subunits or the post-SC by fluorescence polarization (FP). Despite accurately optimized labelling and numerous FP measurements, data quality was insufficient to pursue this approach and provide new insights on the role of ABCE1 in translation initiation.

The careful choice of the labelling site and thorough optimization of the labelling strategy were key to yield a suffiencient amount of labelled aIF1 for FP measurements. Therefore, a single-cysteine variant of *S. solfataricus* aIF1 was constructed (Table 9). Two native cysteines were exchanged to serines (C6/14S) to mimic the size and polarity of cysteines and a new cysteine was introduced at position 45 (N45C) for site-specific fluorescence labeling *via* iodoacetamide or maleimide chemistry. The position was chosen by sequence and structure alignments based on a study in which *P. abyssi* aIF1 was fluorescently labeled to determine the binding affinity to 30S (Monestier *et al*, 2018). Additionally, interference with ribosome binding was excluded, as N45 is not part of the conserved binding motif of a/eIF1 to the SSU (Martin-Marcos *et al*, 2013; Coureux *et al*, 2016; Monestier *et al*, 2018).

After successful heterologous expression and affinity purification, conditions of aIF1^{N45C} fluorescence labeling with 5-iodoacetamidofluorescein (5IAF, Figure 25A) were tested in an in-solution approach. Therein, the fluorophore was directly added to aIF1 in labeling buffer and incubated in the absence of any column material. Afterwards, free 5IAF was removed by rapid gelfiltration. Almost complete labeling was observed after 30 min. Notably, aIF1 and the dye precipitated over time as seen in SDS-PAGE (Coomassie-stained), possibly induced by the organic 5IAF solvent DMSO (Figure 21A). Labeling conditions were adapted to reduce the concentration of DMSO. Furthermore, 5IAF was pre-diluted in labeling buffer before addition of aIF1. This condition improved the in-solution labeling efficiency and strongly reduced protein and label precipitation (Figure 21B, D). Importantly, 5IAF-labeled aIF1 (aIF1^{FL}) bound to 30S subunits and the post-SC in native PAGE (Figure S7B, C). Nevertheless, the amount of aIF1^{FL} was insufficient for FP titration because the in-solution labeling approach could not be scaled-up under the given protein concentration without further increase of the DMSO concentration. Therefore, an on-column labeling approach was adapted, in which aIF1 was first bound to Ni-NTA agarose *via* its N-terminal His tag before addition of the fluorophore 5IAF. Thereby, larger amounts of aIF1 could be labeled while simultaneously reducing the DMSO concentration by dilution of 5IAF before adding it to aIF1 on the column. Subsequently, aIF1^{FL} was SEC-purified to remove residual, inactivated 5IAF (Figure 21C, E). When

titrating 30S ribosomal subunits to aIF1^{FL}, the fluorescence polarization increased, indicating binding of aIF1^{FL} (Figure S6A). The fluorescence intensity also increased analogous to FP (Figure S6B), which had to be corrected (equation 2) for calculation of the fraction of bound aIF1^{FL} (f_b, equation 3). f_b was plotted against the 30S subunit concentration and fitted to obtain the dissociation constant (K_d) (equation 4, section 4.5.8.5, Figure 21F), as described (Monestier *et al*, 2018). K_d was 11 ± 5 nM, which is in good agreement with literature on *S. cerevisiae* eIF1 K_d = 16 ± 2 nM (Maag & Lorsch, 2003) and *P. abyssi* aIF1 K_d = 12 ± 4 nM (Monestier *et al*, 2018). High intrinsic deviations of replicates and general insensitivity for concentrations ≤ 10 nM 30S could not be improved in additional experiments. Furthermore, FP measurements at a Fluorolog spectrofluorometer (Horiba) with higher sensitivity did not improve data quality (Figure S6C). Since it was not possible to consistently reproduce similar data quality in FP measurements and due to unexpected fluorescence increase upon 30S subunit binding (Figure S6B), I speculated that the protein stability/fold or local environment of the fluorophore were flawed. Therefore, binding of aIF1^{FL} to the post-SC could not be addressed. Instead, optimization of FP measurements was first tackled by exchangeing the fluorophore to 7-Diethylamino-3-[N-(2-maleimidoethyl)carbamoyl]coumarin (MDCC, Figure 25B), which was previously used in FP measurements of *P. abyssi* aIF1 (Monestier *et al*, 2018). In-solution labeling of aIF1^{N45C} with MDCC was similar to labeling with 5IAF (Figure S7A). Furthermore, MDCC-labeled aIF1 also bound to 30S subunits and the post-SC in native PAGE (Figure S7B, C). A first FP test with MDCC-labeled aIF1 (Fluorolog) resulted in similar inconsistent, fluctuating data as for 5IAF-labeled aIF1. Hence, an intrinsic problem of the protein stability/fold or the labeling site was concluded. Additionally, Ss aIF1 does not contain any tryptophans, leading to imprecise concentration determination *via* A_{280}, potentially affecting the FP analysis, and contributing to high data fluctuations. We speculated that exchange of the two native cysteine residues in *S. solfataricus* aIF1, which was necessary for site-specific labeling, resulted in poor protein quality in FP.

Ultimately, a binding affinity of aIF1 to the 30S subunit could be determined in good agreement with literature. However, high errors and data fluctuations during FP measurements hindered further evaluation of the influence of ABCE1 on aIF1 recruitment to the 30S subunit. In conclusion, key functional questions remain elusive and future studies will need to establish different methodologic approaches to determine thermodynamic or kinetic parameters of IC assembly in the presence and absence of ABCE1. Importantly, the amount and concentration of the 30S subunit was a significant limiting factor. Therefore, high-quality methods like surface plasmon resonance

spectroscopy or isothermal titration calorimetry will hardly be feasible due to the demand of high 30S subunit amounts and concentrations. Since some archaeal initiation factors and ribosomes from different species are functionally interchangeable (sections 2.1.1, 2.2.3), initiation factors of a different species could be used. *P. abyssi* aIF1 and 30S subunits were suited for FP assays (Monestier *et al*, 2018). Furthermore, cell pellets for isolation of ribosomal subunits could be purchased at the Archaea center of the University of Regensburg. Thus, switching the archaeal organism could be an option to improve and advance the *in vitro* biophysical analysis of the influence of ABCE1 on IF recruitment to the SSU.

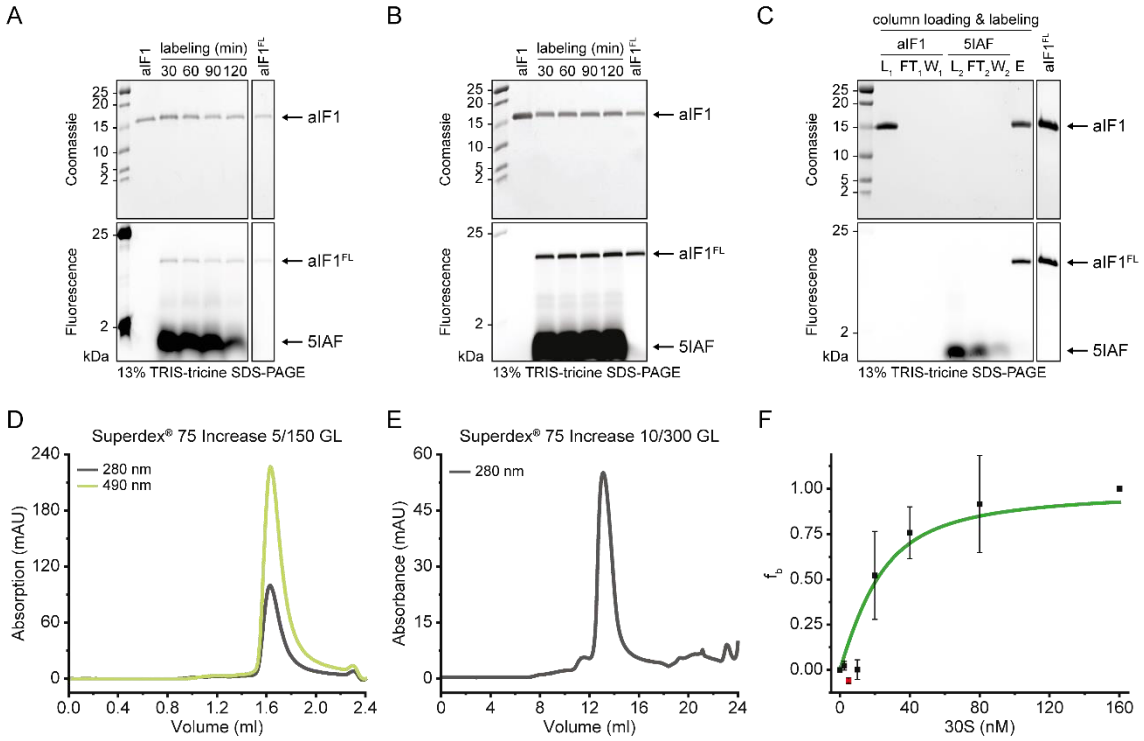

Figure 21: Improvement of aIF1 fluorescence labeling allowed for determination of the aIF1^{FL} binding affinity to 30S subunits by fluorescence polarization. A-C) 5IAF labeling of aIF1 single-cysteine variant C6/14S, N45C, following in-solution (A, B) and on-column (C) labeling approaches. Initial in-solution labeling (A) was improved by pre-dilution of 5IAF (B). Yield of aIF1^{FL} was higher for on-column labeling (C). In-gel fluorescence was recorded at $\lambda_{ex/em}$ 480/535 nm. **D)** In-solution labeled aIF1 sample was monodisperse as determined in SEC. **E)** Preparative SEC purification of on-column labeled aIF1. The main peak was pooled and used in FP measurements (C, aIF1^{FL}). **F)** Determination of the K_d of aIF1^{FL} to the 30S ribosomal subunit by fluorescence polarization using SEC-purified aIF1^{FL} (E). The bound fraction of aIF1^{FL} (f_b) was calculated *via* equation 3 (section 4.5.8.5) and plotted against the 30S subunit concentration. K_d was determined by fitting *via* equation 4 (green, section 4.5.8.5, (Monestier *et al*, 2018)). The 5 nM value was masked (red) as negative outlier. The resulting K_d = 11.2 ± 4.6 nM with R^2 = 0.92 was in good agreement with other eukaryotic and archaeal systems.

2.3 The ribosome dissociation function of the novel RQC factor MutS2 remains elusive

Cellular mechanisms for quality control of the ribosome status during mRNA translation are indispensable to rescue vacant, stalled, or collided ribosomes. They are essential for survival considering the energy cost of ribosome biogenesis and the potential toxicity of aberrant translational products (Brandman & Hegde, 2016; Buskirk & Green, 2017; Kressler *et al*, 2017; Kim & Zaher, 2022; Filbeck *et al*, 2022). After recycling of stalled ribosomes by ABCE1, the SSU can be repurposed in form of the post-SC. The obstructed LSU with P-site peptidyl tRNA is recognized by the ribosome-associated quality control factor NEMF/Rqc2, which manages nascent chain targeting for proteasomal degradation (Joazeiro, 2019; Müller *et al*, 2021). If stalling is not quickly resolved, the trailing ribosome might collide with the stalled leading ribosome, forming disomes with a specific inter-ribosome interface. Recently, two bacterial MutS-related Smr superfamily domain containing proteins with endonucleolytic RNase activity have been described to specifically rescue stalled disomes in *B*. *subtilis* (MutS2) and *E*. *coli* (SmrB) (Cerullo *et al*, 2022; Saito *et al*, 2022). SmrB was shown to cleave the mRNA template upstream of the collided disomes, thereby rescuing trailing ribosomes on the truncated mRNA *via* the tmRNA quality pathway (Saito *et al*, 2022). For MutS2, however, based on the positioning of its ATPase/clamp domain on the stalled ribosome, a mechanism was proposed that involves cleavage of the disomes *via* ATPase-driven conformational rearrangements, as described for the ribosome splitting factor ABCE1 (Cerullo *et al*, 2022). However, no functional data are available so far. I could establish the purification of recombinantly expressed MutS2 and show that the isolated protein was active in ATP and AMP-PNP binding. However, disome splitting could not be observed in initial experiments and further studies are needed on this novel translational quality control factor.

In collaboration with Federico Cerullo of the Joazeiro laboratory at ZMBH of Ruprecht-Karls-University in Heidelberg, my goal was to biochemically characterize *B*. *subtilis* MutS2 and analyze its potential function in ribosomal subunit dissociation of stalled disomes *in vitro*. MutS2^{WT} and the degenerate NBS II variant E416A were successfully expressed in *E*. *coli* and purified *via* a C-terminal His tag. Importantly, purified MutS2 was only stable in intermediate (~200 mM NaCl) salt conditions for a short time (min-h) or high salt (400 mM NaCl) conditions for a longer time (h-d) at 4 °C (Figure 22A). Ribonucleic acid contaminations could not be removed by heparin adsorption or by ion-exchange chromatography due to the instability of MutS2 in low salt conditions. SEC analysis revealed that part of the impurities precipitated with MutS2 during storage and/or under

low salt conditions. However, preparative SEC could improve future purification of MutS2 after IMAC as shown by analytical SEC for a small portion of the protein (Figure 22B).

Next, the functionality of the ATPase sites of MutS2 was addressed. Nucleotide binding of $MutS2^{WT}$ and the E416A mutant was analyzed by SEC (Figure S8A and B, respectively) and A_{260}/A_{280} ratio (Figure S8C). Both variants did not bind AMP or ADP but were able to bind AMP-PNP. $MutS2^{WT}$ showed only a slight increase of A_{260} with ATP compared to ADP and the apo state. Since A_{260} of apo $MutS2^{WT}$ was similar to the ADP condition, I speculated whether ADP or other nucleotides co-purified in the NBSs of MutS2. Reduced A_{260} of $MutS2^{WT}$ with ATP compared to AMP-PNP might be explained by partial hydrolysis during incubation for nucleotide binding. Even though the NBSs of the purified MutS2 variants were functional in AMP-PNP and ATP binding, it remains unclear whether the purified protein undergoes the essential conformational changes for ATP hydrolysis and ribosome splitting. To address the potential ribosomal subunit dissociation function of MutS2, an *in vitro* dissociation assay similar to the ABCE1 ribosome splitting assays was established (Heuer *et al*, 2017; Nürenberg-Goloub *et al*, 2018; Gouridis *et al*, 2019; Nürenberg-Goloub *et al*, 2020). First, disomes were isolated from *B*. *subtilis* ΔMutS2 cell lysates, which were grown in the presence of the antibiotic Erythromycin to stabilize the disomes (kindly provided by Federico Cerullo, Joazeiro laboratory). $MutS2^{WT}$ was incubated with disomes in the presence of different nucleotides and ribosome profiles were analyzed by SDG centrifugation (Figure S9). The disome population was unaltered under all conditions. Importantly, 70S ribosomes and disomes from *B*. *subtilis* cells could not be purified in substantial amounts. Moreover, the respective complexes were either contaminated by other ribosomal complexes due to the low resolution of the SDG or instable after purification and dissociated prior to or during subsequent experiments (Figure 22C, Figure S9). Supported by the knowledge of the Joazeiro laboratory that binding of C-terminally tagged MutS2 to disomes was strongly reduced in co-IP experiments, the C-terminal affinity tag was cleaved-off by HRV 3C precision protease (construct MutS2-3C-His_{10}, Table 10). However, disome populations remained stable under all conditions (Figure 22C, Figure S9). Complete removal of the C-terminal tag was confirmed by SDS-PAGE and immunoblot (Figure 22D). Thus, it remained elusive, whether i) leftover C-terminal 3C residues or ribonucleic acid impurities (Figure 22B) inhibited MutS2 function, ii) purified MutS2 was dysfunctional regarding ribosome binding or splitting, iii) MutS2 truly functions as a disome splitting factor *in vitro*, or iv) if other factors are involved in the process.

Taken together, my first *in vitro* studies demonstrated ATP binding activity of purified MutS2. In the future, ribosome binding and splitting must be addressed. Analysis of the

ATPase activity in the presence and absence of different ribosomes, as shown for ABCE1 (Barthelme *et al*, 2011; Nürenberg-Goloub *et al*, 2018), will give insights into the potential function of MutS2 on disomes. It will be crucial to improve the purity and stability of MutS2 and collided disomes for all functional assays.

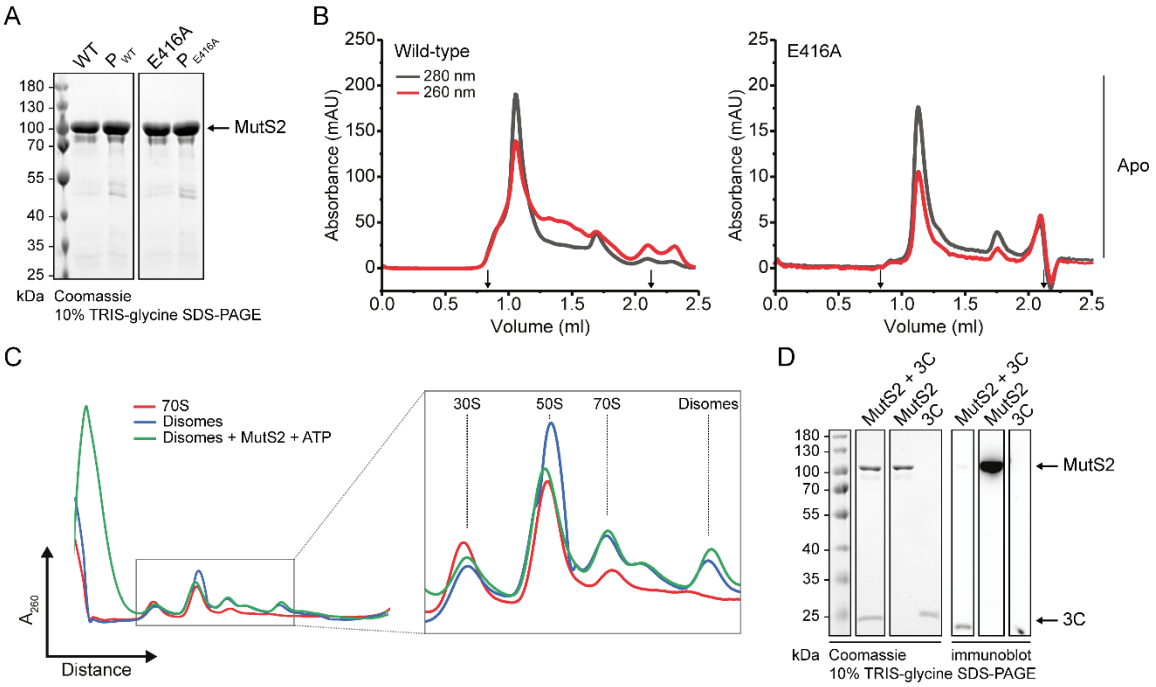

Figure 22: *B. subtilis* MutS2 did not split purified disomes *in vitro*. A) Purified MutS2 WT and the E416A variant precipitated (P) in buffer with < 400 mM NaCl at 4 °C within min-h, depending on NaCl concentration. Left lane, supernatant of the respective purified MutS2 variant; right lane, precipitate of the purified MutS2 variant. **B)** Supernatant of purified MutS2 WT contained nucleic acid contaminations. E416A precipitated to a higher degree but the supernatant was less contaminated (Superdex® 200 Increase 3.2/300 GL, Cytiva). **C)** The disome population was not affected by MutS2 WT in sucrose density gradient centrifugation analysis. The low disome stability and/or incomplete purification, as indicated by the presence of 30S, 50S, and 70S ribosomes, must be improved for further experiments. **D)** The C-terminal affinity tag of MutS2 was cleaved-off by 3C protease prior to disome analysis (C). Immunoblot α-His 1:1,000 and α-mouse-HRP 1:10,000.

3 Conclusions and outlook

The fundamental process of protein biosynthesis *via* mRNA translation is essential for the survival and reproduction of all living organisms. Decades of research unveiled the important functions of many translation factors during specific phases of mRNA translation. The identification of the conserved ribosome-splitting factor ABCE1 in Eukaryotes and Archaea revealed the final translation phase of ribosome recycling, which bridges termination to initiation and thereby closes mRNA translation into a cyclic process. Therein, ABCE1 fulfills multiple roles in different translational processes. It provides ribosomal subunits for a new translation round after canonical termination, builds a platform for translation initiation in the form of the post-SC, and rescues ribosomes after translation errors in mRNA surveillance and quality control pathways. All translational processes are tightly controlled. Accordingly, in the last years, it became a focus to understand how cells cope with errors in this intricate system. In contrast to the conserved machineries and factors involved in translation, the processes of quality control are more versatile and less well understood. Factors with specific functions are newly identified, like the bacterial collided ribosome-specific MutS2, expanding the complex functional mechanics of mRNA translation and ribosome-associated quality control across all domains of life.

During my doctoral studies, in collaboration with the Beckmann lab, I solved the high-resolution structure of the archaeal post-SC. Our work unveiled the molecular mechanism of how ABCE1 senses the ribosome *via* conserved residues in its hinge regions and how this information is integrated into the ATPase cycle. Reconstitution of the archaeal translation initiation apparatus and the assembly of initiation complexes revealed a central role of ABCE1, which confirmed recent findings in Eukaryotes, and highlighted the conserved and essential function of ABCE1 in mRNA translation beyond ribosome recycling. I established protocols for homologous expression of ABCE1 in *S. acidocaldarius* and pull-down of ribosomal complexes that will allow for straightforward structural analysis of native archaeal ABCE1-initiation complexes by cryo-EM and will give further insights into the role of ABCE1 in translation initiation. However, a potential influence of ABCE1 on the recruitment of initiation factors to the 30S subunit during IC assembly or ATPase trigger for ABCE1 release remain enigmatic. Focusing on ribosome-associated quality control in Bacteria, I was able to analyze the integrity of disomes in the presence of the newly identified RQC factor MutS2. While I could perform initial experiments to address the molecular mechanics of MutS2, a potential ribosome splitting function remained elusive. Going forward, high quality of the individual components with a

focus on disome preparation will be indispensable to unravel the MutS2 mode of function in RQC.

Future studies should answer the key question of whether there are allosteric interactions of ABCE1 and initiation factors on the small ribosomal subunit that affect the process of initiation complex assembly. Native archaeal ABCE1-initiation complexes may reveal additional factors involved during IC assembly like eIF3 in Eukaryotes. Together the data should unravel a potential trigger of ABCE1 ATPase activity and its release from the 30S subunit, and thereby elucidate the final unsolved mechanistic role of ABCE1 in mRNA translation. Regarding MutS2, characterization of the ATPase activity and conformational rearrangements in the presence of different ribosomes will allow analysis of the functional mechanics of MutS2 in RQC. Besides the bacterial di- and polysome specific factors, the field of ribosome-associated quality control will likely expand in the future by studies of the molecular mechanisms of numerous quality factors. Thereby, key quality control pathways will become the focus in mRNA translation research.

4 Material and methods

4.1 Media and buffers

4.1.1 Media

Table 1: Media for *E. coli* growth and culture.

Medium	Composition	Preparation
LB	5 g/l yeast extract 5 g/l NaCl 10 g/l tryptone	Autoclaved
LB-agar	LB 16 g/l agar-agar	LB components and agar-agar were prepared together and autoclaved.
SOB	5 g/l yeast extract 20 g/l tryptone 10.0 mM NaCl 2.5 mM KCl 10.0 mM $MgCl_2$ 10.0 mM $MgSO_4$	Prepared without Mg-salts and autoclaved. Mg-salts were separately prepared, sterile filtered, and added to the autoclaved medium.
SOC	SOB 20.0 mM glucose	Glucose was separately prepared, sterile filtered, and added to SOB medium.
TB	24 g/l yeast extract 12 g/l tryptone 0.344% glycerol 90.8 mM K_2HPO_4 9.2 mM KH_2PO_4	Phosphate salts were separately prepared, autoclaved, and added just before use.

Table 2: Media for *S. acidocaldarius* and *S. solfataricus* growth and culture.

Medium	Composition	Preparation
2x Brock	02 ml/l Brock I 20 ml/l Brock II + III 02 ml/l Fe solution 10 ml/l NZ-Amine-20 20 ml/l Dextrin-20 12 ml/l 0.5 M $CaCl_2$ 20 ml/l 1.0 M $MgCl_2$	Sterile filtered $CaCl_2$ and $MgCl_2$.
Brock I	70 g/l $CaCl_2 \cdot 2\ H_2O$	Autoclaved.
Brock II+III	130 g/l $(NH_4)_2SO_4$ 28 g/l KH_2PO_4 25 g/l $MgSO_4 \cdot 7\ H_2O$ 50 ml/l Trace element solution 2.25 ml/l H_2SO_4 (50% (v/v))	Autoclaved.
Brock-Gelrite®	200 ml Gelrite® mix 200 ml 2x Brock	2x Brock pre-heated at 75 °C. Brock-Gelrite® mix dissolved in a microwave. Then directly added to the 2x Brock, shortly mixed, and directly plated (thick, ~30-35 ml per plate).
Dextrin-20	20% (w/v) Dextrin	Autoclaved.

Fe solution	20 g/l $FeCl_3$ • 6 H_2O	Sterile filtered.
Gelrite® mix	1.2% (w/v) Gelrite®	Gelrite® hardly dissolves. Stirred very long, until almost completely dissolved before autoclaving.
Modified Brock	01 ml/l Brock I 10 ml/l Brock II + III 01 ml/l Fe solution 05 ml/l NZ-Amine-20 10 ml/l Dextrin-20 02 ml/l Uracil-5 pH adjusted to 3.0-3.5 with 50% (v/v) H_2SO_4.	Modified from (Allen, 1959; Brock *et al*, 1972). Uracil-5 was sterile filtered and stored at -20 °C. Uracil was only supplemented for non-transformed *S. acidocaldarius* cells.
NZ-Amine-20	20% (w/v) Protein-Hydrolysate N-Z-Amine® AS	Autoclaved.
Recovery solution	01 ml/l Brock I 10 ml/l Brock II + III 05 ml/l NZ-Amine-20	Sterile filtered.
Sucrose-20	20 mM sucrose	Autoclaved.
Trace element solution	9.00 g/l $Na_2B_4O_7$ • 10 H_2O 0.44 g/l $ZnSO_4$ • 7 H_2O 0.10 g/l $CuCl_2$ • 2 H_2O 0.06 g/l Na_2MoO_4 • 2 H_2O 0.06 g/l $VOSO_4$ • 2 H_2O 0.02 g/l $CoSO_4$ • 7 H_2O 3.60 g/l $MnCl_2$ • 4 H_2O	Important to stick to the order. H_2SO_4 was added until $Na_2B_4O_7$ is dissolved before adding the next component.
Uracil-5	5 mg/ml uracil	Sterile filtered. Stored at -20 °C.
Xylose-20	20% (w/v) xylose	Sterile filtered. 0.2% (w/v) in modified Brock for induction of protein expression

4.1.2 Buffers

Table 3: List of buffers and solutions.

Buffer	Composition	Preparation
10x TBE	1.0 M TRIS 1.0 M boric acid 20 mM EDTA pH 8.0	
30S-2.5 buffer	20 mM HEPES-KOH pH 7.5 60 mM KCl 2.5 mM $MgCl_2$	
5x $LP_{red.}$	250 mM TRIS-HCl pH 6.8 30% glycerol 10% (w/v) SDS 5% (v/v) BME 0.02% (w/v) bromophenol blue	Stored at -20 °C.
A30	10 mM HEPES-KOH pH 7.5 100 mM NH_4Cl 10.5 mM $Mg(OAc)_2$ 0.1 mM EDTA 4 mM BME	

AIEX A	20 mM TRIS-HCl pH 8.5 5 mM NaCl 10% (v/v) glycerol	Filtered and degassed.
AIEX B	20 mM TRIS-HCl pH 8.5 1 M NaCl 10% (v/v) glycerol	Filtered and degassed.
ATPase buffer	10 mM HEPES-KOH pH 7.5 150 mM NaCl 2.5 mM $MgCl_2$	
Blocking solution	5% (w/v) milk powder 1x DPBS 0.1% (v/v) Tween®20	Always prepared freshly. The solution was mixed ≥ 2 h at room temperature before use.
Buffer A	20 mM TRIS-HCl pH 7.5 200 mM NaCl 8 mM $MgCl_2$ 0.1 mM EDTA	
Buffer M	30 mM HEPES-KOH pH 7.5 50 mM KCl 10 mM $MgCl_2$ 0.5 mM EDTA 2 mM DTT	
Buffer M2	50 mM HEPES-KOH pH 7.5 30 mM KCl 10 mM $MgCl_2$ 2 mM DTT	
Buffer M3	50 mM HEPES-KOH pH 7.5 30 mM KCl 0.5 mM $MgCl_2$ 2 mM DTT	
Buffer S	1 mM TRIS-HCl pH 7.4 10 mM $Mg(OAc)_2$	
Concentrated Malachite Green solution	20% (v/v) H_2SO_4 0.1467% (w/v) Malachite Green	
Coupling buffer	50 mM TRIS-HCl pH 8.5 5 mM EDTA	
Developing solution	2% (w/v) Na_2CO_3 0.0156% formaldehyde 0.0084% (w/v) $Na_2S_2O_3$ • 5 H_2O)	Freshly prepared.
Disome buffer	50 mM HEPES-KOH pH 7.2 300 mM KCl 3 mM $MgCl_2$ 1 mM DTT 40 µM Erythromycin	
Fixation solution	50% (v/v) acetone 1.25% (w/v) trichloroacetic acid 0.0156% (v/v) formaldehyde	
Glycerol cushion buffer	20 mM HEPES-KOH pH 7.5 500 mM NH_4Cl 10 mM $Mg(OAc)_2$ 2 mM DTT 25% (v/v) glycerol	
High salt sucrose cushion	10 mM HEPES-KOH pH 7.5 1.1 M sucrose 1 M NH_4Cl 10.5 mM $Mg(OAc)_2$ 0.1 mM EDTA 4 mM BME	Filtered.

IMAC A	20 mM TRIS-HCl pH 8.0 300 mM NaCl 20 mM imidazole pH 8.0 4 mM BME 10% (v/v) glycerol	Filtered and degassed.
IMAC B	20 mM TRIS-HCl pH 8.0 300 mM NaCl 200 mM imidazole pH 8.0 4 mM BME 10% (v/v) glycerol	Filtered and degassed.
Impregnation solution	0.268% (w/v) $AgNO_3$ 0.37% (v/v) formaldehyde	
IP buffer	20 mM HEPES-KOH pH 7.2 60 mM KCl 10 mM $MgCl_2$	
Labeling buffer	50 mM HEPES-KOH pH 7.2 60 mM KCl 3 mM $MgCl_2$	
Lysis buffer	20 mM TRIS-HCl pH 7.5 300 mM NaCl 5 mM $MgCl_2$ 4 mM BME 30% (v/v) glycerol	
Malachite Green working solution	2 ml concentrated Malachite Green solution 40 µl Tween®20 (10% (v/v)) 550 µl Na_2MoO_4 (7.5% (w/v))	
Methionylation buffer	30 mM TRIS-HCl pH 8.0 30 mM KCl 16 mM $MgCl_2$	
native PAGE anode buffer	50 mM Bis-TRIS-HCl pH 7.0	pH adjusted cold with NaOH.
native PAGE cathode buffer	15 mM Bis-TRIS 90 mM Tricine pH 7.0	pH adjusted cold with NaOH.
PBS-T	1x DPBS 0.1% (v/v) Tween®20	DPBS: Dulbecco's Phosphate Buffered Saline without $CaCl_2$ and $MgCl_2$ (Gibco™, Thermo Scientific)
Ribosome binding buffer	20 mM HEPES-KOH pH 7.5 60 mM NH_4Cl 5 mM $Mg(OAc)_2$ 2 mM DTT	
Ribosome elution buffer	20 mM HEPES-KOH pH 7.5 500 mM NH_4Cl 10 mM $Mg(OAc)_2$ 2 mM DTT	
Ribosome extraction buffer	20 mM HEPES-KOH pH 7.5 40 mM NH_4Cl 10 mM $Mg(OAc)_2$ 1 mM DTT	
RNA loading buffer	95% (v/v) formamide 0.02% (w/v) SDS 0.02% (w/v) Bromphenol blue 0.01% (w/v) Xylene cyanol 1 mM EDTA pH 8.0	

S30 buffer	10 mM TRIS-HCl pH 7.5 60 mM KOAc 14 mM $MgCl_2$ 1 mM DTT	
SEC buffer	20 mM HEPES KOH pH 7.5 200 mM NaCl	
Separating gel buffer	1.5 M TRIS-HCl pH 8.8 0.4% (w/v) SDS	
Stacking gel buffer	0.5 M TRIS-HCl pH 6.8 0.4% (w/v) SDS	
$Storage^{ABCE1}$	20 mM TRIS-HCl pH 7.5 150 mM NaCl 10% (v/v) glycerol 4 mM BME	Filtered.
$Storage^{IFs}$	20 mM HEPES-KOH pH 7.5 200 mM KCl 10% (v/v) glycerol 4 mM BME	Filtered.
$Storage^{MutS2}$	20 mM TRIS-HCl pH 7.5 400 mM NaCl 10% glycerol	Filtered.
Subunit dissociation buffer	20 mM TRIS-HCl pH 7.5 100 mM KCl 2 mM $MgCl_2$ 1 mM DTT	
TFB-1	30 mM KOAc pH 5.8 50 mM $MnCl_2$ 100 mM RbCl 10 mM $CaCl_2$ 15% glycerol	KOAc stock solution was adjusted to pH 5.8. Buffer was sterile filtered.
TFB-2	10 mM MOPS pH 7.0 10 mM RbCl 75 mM $CaCl_2$ 15% glycerol	MOPS stock solution was adjusted to pH 7.0. Buffer was sterile filtered.
Transfer buffer	20 mM TRIS-HCl pH 7.5 190 mM glycine 0.03% (w/v) SDS 20% (v/v) MeOH	pH was adjusted cold. Methanol was freshly added before use.
TrB25	56 mM TRIS-HCl pH 8.0 250 mM KOAc 80 mM NH_4OAc 25 mM $MgCl_2$ 1 mM DTT	
Tricine gel buffer	3.0 M TRIS-HCl pH 8.5 0.3% (w/v) SDS	
TRIS-glycine SDS-PAGE running buffer	25 mM TRIS 190 mM glycine 0.1% (w/v) SDS	pH was not adjusted.
TRIS-tricine SDS-PAGE anode buffer	0.1 M TRIS-HCl pH 8.9	
TRIS-tricine SDS-PAGE cathode buffer	0.1 M TRIS 0.1 M tricine 0.1% (w/v) SDS	

4.2 Cells and reagents

4.2.1 Bacterial and archaeal strains

Table 4: List of bacterial and archaeal strains.

Strain	Genotype / Specifications	Origin / Supplier
E. coli BL21(DE3) pLysS	B F$^-$ *ompT gal dcm lon hsdS$_B$*(r_B^- m_B^-) λ(DE3 [*lacI lacUV5-T7p07 ind1 sam7 nin5*]) [*malB*$^+$]$_{K\text{-}12}$(λ^S) pLysS[*T7p20 ori*$_{p15A}$](Cm^R)	Novagen
E. coli ER1821	*E. coli* ER2566 (NEB) B F$^-$ λ$^-$ *fhuA2* [*lon*] *ompT lacZ*::T7*.1 gal sulA11* Δ(*mcrC-mrr*)*114*::IS*10* R(*mcr-73*::miniTn*10*)(Tet^S)2 R*(zgb-210*::Tn*10*)(Tet^S) *endA1* [*dcm*] transformed with pM.EsaBC4I (NEB), a pSC101 derivative, encoding the GGCC-specific R–M system EsaBC4 I, containing kanamycin resistance	(Kurosawa & Grogan, 2005) Provided by Sonja-Verena Albers.
E. coli Mach1	W Δ*recA1398 endA1 fhuA* Φ80Δ(*lac*)M15 Δ(lac)*X74* hsdR(r_K^- m_K^+)	Invitrogen
S. acidocaldarius MW001	*S. acidocaldarius* DSM639 with a deletion of 322 bp in the *pyrE* gene (*saci1597*, basepairs 91-412)	(Wagner *et al*, 2012) Provided by Prof. Dr. Sonja-Verena Albers.
S. solfataricus P2	Wild-type	Laboratory stock

4.2.2 Antibodies, labels, and standards

Table 5: List of antibodies and antibody-coupled resins.

Antibody / resins	Application	Supplier
anti-6X His tag®-HRP (rabbit), polyclonal	1:2,000 – 1:3,000 immunoblotting	Abcam (ab1187)
anti-FLAG® M2 (mouse), monoclonal	1:2,000 – 1:3,000 immunoblotting	Sigma-Aldrich (F3165)
anti-FLAG® M2 magnetic beads (mouse), monoclonal	1.3 µl / µg protein immunoprecipitation	Sigma-Aldrich (M8823)
anti-FLAG® M2 affinity gel (mouse), monoclonal	0.1 µl / pmol ABCE1 immunoprecipitation	Sigma-Aldrich (A2220)
anti-HA (rabbit), polyclonal	1:2,000 immunoblotting	Sigma-Aldrich (H6908)
anti-His_6 (mouse), monoclonal	1:1,000 – 1:2,000 immunoblotting	Sigma-Aldrich (H1029)
anti-mouse IgG-HRP (goat), polyclonal	1:10,000 – 1:20,000 immunoblotting	Sigma-Aldrich (A2554)
anti-rabbit IgG (H+L)-HRP (goat), polyclonal	1:10,000 – 1:20,000 immunoblotting	Sigma-Aldrich (AP307P)

Table 6: List of labels and fluorescent molecules.

Label	Supplier
5-Iodoacetamidofluorescein (5IAF)	Invitrogen
7-Diethylamino-3-[N-(2-maleimidoethyl)carbamoyl]coumarin (MDCC)	Sigma-Aldrich
N^6-(6-Aminohexyl)-ATP-ATTO647N	Jena Bioscience
N^6-(6-Aminohexyl)-ATP-Cy3	Jena Bioscience

Table 7: List of protein- and DNA standards.

Standard	Supplier
GeneRuler 1 kb DNA ladder	Thermo Scientific
NativeMark™ Unstained Protein Standard	Invitrogen
PageRuler™ Prestained Protein Ladder 10 to 180 kDa	Thermo Scientific
Precision Plus Protein™ Dual Xtra Prestained Protein Standards	Bio-Rad

4.3 Microbiology

4.3.1 Bacterial work

4.3.1.1 Preparation of competent *Escherichia coli* cells

4 ml lysogeny broth (LB) medium with 25 µg/ml chloramphenicol (BL21(DE3) pLysS), or 50 µg/ml kanamycin (ER1821), or without any antibiotics (Mach1) was inoculated 1:1,000 with the respective competent cells. The cells were grown overnight at 37 °C and 180 rpm. 0.5 ml of sterile-filtered Mg^{2+}-salts (1 M $MgSO_4$, 1 M $MgCl_2$) were added to 50 ml super optimal broth (SOB) medium containing the respective antibiotic and was inoculated 1:200 with the overnight culture. Cells were grown at 30 °C and 180 rpm to an OD_{600} of 0.5. The culture was cooled on ice for 10 min and the cells were pelleted at 2,500 *g* for 15 min at 4 °C. The cells were made chemically competent by the calcium chloride method (based on (Mandel & Higa, 1970)). The cell pellet was carefully resuspended in 2 ml ice-cold transformation buffer 1 (TFB-1), then filled up to 25 ml with TFB-1 and incubated for 30-60 min on ice. The cells were pelleted again at 2,500 *g* for 15 min at 2 °C, resuspended in 1 ml ice-cold transformation buffer 2 (TFB-2), and then filled up to 2.5 ml with TFB-2. Finally, the cells were aliquoted on ice, shock-frozen in liquid nitrogen, and stored at −80 °C.

4.3.1.2 Heat-shock transformation of competent *E. coli* cells

50 µl chemically competent *E. coli* cells were thawed on ice and incubated with 1 µl plasmid DNA (20-300 ng) for 10 min. After a 1 min heat-shock at 42 °C, the cells were cooled on ice for 5 min and then recovered in 500 µl super optimal broth with catabolite repression (SOC) medium for 60 min at 37 °C and 350 rpm. Afterwards, the cells were pelleted at 800 *g* for 3 min, resuspended in one third of the medium, and spread onto LB-agar plates with respective antibiotics. Plates were incubated at 37°C overnight or room temperature for three days.

4.3.1.3 Plasmid DNA propagation

Mach1 chemically competent *E. coli* cells were heat-shock transformed with the respective plasmid DNA (section 4.3.1.2). Single colonies were picked from the LB-agar plates, transferred into 4 ml LB medium with respective antibiotics, and grown overnight at 37 °C and 180 rpm. Plasmid DNA was prepared using the NucleoSpin® Plasmid EasyPure kit (Macherey-Nagel) according to the manufacturer's instructions with few changes. The ethanol-washing step was performed twice. The spin-column was dried for 5 min at 70 °C.

Plasmid DNA was eluted with pre-warmed 20 mM TRIS-HCl pH 8.0 by incubation at 70 °C for 5 min and subsequent spin-down for 1 min at 16,100 *g*.

4.3.1.4 Plasmid DNA methylation

For successful transformation of *S. acidocaldarius*, plasmid DNA needed to be specifically methylated. ER1821 chemically competent *E. coli* cells, containing the needed machinery for correct methylation (Table 4), were heat-shock transformed and plasmid DNA was isolated as described (section 4.3.1.3) using kanamycin and carbenicillin for selection.

4.3.1.5 Heterologous protein expression in *E. coli*

All archaeal proteins and *Bacillus subtilis* (Bs) MutS2 were expressed in *E. coli* BL21(DE3) pLysS cells. Multiple colonies were picked from respective LB-agar plates (section 4.3.1.2), transferred to LB medium with 25 µg/ml chloramphenicol (cam) and 100 µg/ml carbenicillin (carb) or 50 µg/ml kanamycin (kan) and grown overnight at 37 °C and 180 rpm (Table 8). Terrific broth (TB) medium with the same antibiotics was inoculated 1:40 with overnight culture and grown to an OD_{600} of 0.6-0.8 at 37 °C and 180 rpm. After induction with Isopropyl-β-D-galactopyranoside (IPTG), proteins were expressed for 20 h at 20 °C and 180 rpm (Table 8). The cells were harvested by centrifugation for 15 min at 5,000 *g* and 4 °C. Cell pellets were shock-frozen in liquid nitrogen and stored at −20 °C.

Table 8: Parameters for heterologous protein expression in *E. coli*.

Protein	IPTG [mM]	Antibiotics
Bs MutS2	1.0	cam, carb
Sa ABCE1	0.75	cam, carb
Ss ABCE1	0.75	cam, carb
Ss aIF1	0.75	cam, carb

4.3.2 Archaeal work

4.3.2.1 Growth of *Saccharolobus solfataricus*

S. solfataricus was cultured in modified Brock medium at 78 °C to generate cell mass for purification of ribosomal subunits. First, a pre-culture of 50 ml modified Brock medium was inoculated with 200 µl cryo-stock cells (section 4.3.2.2) at room temperature. The pre-culture was incubated for 3-4 days at 78 °C and 180 rpm until an OD_{600} of 0.4-0.6. Next, the pre-culture was transferred into 400 ml fresh and pre-warmed modified Brock

medium. The middle-culture was grown for 1-2 days at 78 °C and 180 rpm until an OD_{600} of 0.4-0.6. Finally, 1 L of fresh and pre-warmed modified Brock medium was inoculated with 50 ml middle-culture. The main-culture was grown for 3-4 days until an OD_{600} of 0.4-0.6. The cells were harvested by rapidly cooling the culture on ice before removing the medium at 5,000 *g* for 20 min. The cell pellet was resuspended in ribosome extraction buffer to a theoretical OD_{600} of 150-200. The cell suspension was slowly dropped into liquid nitrogen and the forming spherules were stored at -80 °C.

4.3.2.2 Preparation of *S. solfataricus* glycerol stocks

50 ml pre-warmed modified Brock medium was inoculated with 0.5 ml of a running culture ($OD_{600} \approx 0.4$). The culture was grown at 78 °C and 180 rpm until an OD_{600} of 0.4. The culture was rapidly cooled on ice and the medium was removed at 5,000 *g* for 20 min. The cell pellet was resuspended in ice-cold modified Brock medium with 15% (v/v) glycerol. 200 µl aliquots were shock-frozen in liquid nitrogen and stored at -80 °C.

4.3.2.3 Growth of *Sulfolobus acidocaldarius*

S. acidocaldarius MW001 (kindly provided by Sonja-Verena Albers) was cultured in modified Brock medium at 75 °C and 180 rpm to prepare glycerol stocks (section 4.3.2.4), competent cells (section 4.3.2.5), or homologously express a plasmid-encoded Sa ABCE1 (section 4.3.2.7). *S. acidocaldarius* was mostly grown in pre-, middle-, and main-cultures, similar to *S. solfataricus* (section 4.3.2.1).

4.3.2.4 Preparation of *S. acidocaldarius* glycerol stocks

10 ml *S. acidocaldarius* MW001 was grown until an OD_{600} of 0.5. Preparation of glycerol stocks was performed at room temperature and sterile. The medium was removed at 3,000 g for 20 min. Cells were resuspended in a 1 ml modified Brock medium with 50% (v/v) glycerol. To reduce shearing forces, the front part of the 1 ml pipette tip was cut-off for resuspension. Without being shock-frozen, 50 µL aliquots were stored at -80 °C.

4.3.2.5 Preparation of competent *S. acidocaldarius* cells

50 ml modified Brock medium was inoculated with 50 µl *S. acidocaldarius* MW001 glycerol stock at room temperature and grown at 75 °C and 180 rpm for 2-3 days. 50 ml pre-warmed modified Brock medium was inoculated with pre-culture to an OD_{600} of 0.05. The main culture was grown until an OD_{600} of 0.3. The culture was rapidly cooled on ice and the medium was removed at 2,500 *g* for 20 min and 2 °C. The cell pellet of 25 ml culture was carefully resuspended in ice-cold sucrose-20 (using cut-off pipette tips) and

then filled-up to 30 ml. The sucrose was removed at 2,500 *g* for 20 min and 2 °C. The cells were washed two more times. Finally, cells were resuspended to a theoretical OD_{600} of 20 in ice-cold sucrose-20. Without being shock-frozen, 50 µL aliquots were stored at -80 °C.

4.3.2.6 Transformation of competent *S. acidocaldarius* cells

Competent *S. acidocaldarius* cells were thawed on ice. 500 ng methylated plasmid DNA was added to the cells and incubated on ice for 30 min and then transferred into pre-cooled 0.1 cm electroporation cuvettes. Cells were electroporated at 2,200 V with a single pulse (Agr protocol) using a MicroPulser (Bio-Rad). 400 µL room temperature recovery solution was directly added into the cuvette. Cells and recovery solution were quickly mixed, then transferred into a 1.5 ml tube and cells were recovered at 75 °C and 300 rpm for 30 min. 100 µL of recovered cells were spread onto Brock-Gelrite® plates using a glass capillary. Plates were incubated in a closed box with wet tissues, to prevent them from drying out, at 75 °C for 1 week. Remain. Single colonies were carefully spread onto pre-warmed fresh Brock-Gelrite® plates and incubated at 75 °C for 2-7 days.

4.3.2.7 Homologous expression of ABCE1 in *S. acidocaldarius*

Single colonies of *S. acidocaldarius* MW001 transformed with Sa ABCE1 WT, E238A, or E485A (containing a C-terminal His_{10}-3C-FLAG tag) were picked from Brock-Gelrite® plates (transformed by Dr. Alejandra Recalde, laboratory of Prof. Dr. Sonja-Verena Albers, Albert-Ludwigs-University Freiburg) to inoculate pre-cultures (section 4.3.2.3). Main cultures were inoculated to an OD_{600} of 0.05 and expression was induced with 0.2% (w/v) xylose. ABCE1 was expressed for 18 h at 75 °C and 180 rpm. The cells were harvested at 3,000 *g* and 4 °C for 20 min. The cell pellets were shock-frozen in liquid nitrogen and stored at -80 °C.

4.3.2.8 Preparation of archaeal cell lysates for immunoprecipitation

For preparation of archaeal cell lysates for immunoprecipitation (IP) with spiked-in proteins, 2-4 g archaeal cell pellets (section 4.3.2.1) were resuspended in 10 ml IP buffer with 200 U RiboLock RNase Inhibitor (Thermo Scientific), 200 U DNase I (RNase-free, Roche) and 1x Protease-Inhibitor Mix HP (Serva). The cells were lysed either by ultra-sonication (3x 1 min pulses, output control 4, 50% duty cycle, Branson Ultrasonics™ Sonifier™ Modell 250) on ice with 1 min cooling intervals in-between pulses or by 2% (w/v) n-Dodecyl-beta-maltoside (DDM) detergent for 3 h at room temperature. Cell debris was removed for 30 min at 100,000 *g* and 4 °C. IP buffer was added to the lysate to adjust A_{260}

to 10-15. 500 µl (A_{260} = 15) or 750 µl (A_{260} = 10) aliquots were shock-frozen in liquid nitrogen and stored at -80 °C.

S. acidocaldarius lysates of homologous ABCE1 expression were prepared by resuspending the cell pellet to a theoretical OD_{600} of 30 and lysis *via* 2% (w/v) DDM.

4.4 Molecular genetics

4.4.1 Molecular cloning

Proteins were expressed from a standard *E. coli* expression plasmid pSVA4 (kindly provided by Dr. Elina Nürenberg-Goloub, Figure 23). Protein sequences were inserted *via* *NcoI* and *BamHI*, *HindIII*, or *XhoI* restriction sites. C-terminal affinity tags were exchanged *via* *BamHI* and *HindIII* or *XhoI*. Sequence of an aIF1 cysteine variant with N-terminal affinity tags was ordered from Integrated DNA Technologies (IDT) and inserted into pRSETB *via* *NdeI* and *HindIII* (Table 9). Due to inconsistent expression, aIF1 awas transferred into pSVA4 *via* *NcoI* and *HindIII*. Sa ABCE1 was amplified from *S. acidocaldarius* genomic DNA (kindly provided by Prof. Dr. Sonja-Verena Albers). For homologous expression of ABCE1 in *S. acidocaldarius*, Sa ABCE1 variants were inserted into pSVAxylFX (kindly provided by Prof. Dr. Sonja-Verena Albers) *via* *NcoI* and *BamHI* by standard restriction and ligation protocols (Figure 23). ABCE1 variants were generated by two-step megaprimer PCR (based on (Barik, 1996)). A primer containing the mutation (Table 9) and a second consensus primer were used to generate a ~200 bp megaprimer, which was analyzed by agarose gel electrophoresis (section 4.4.2) prior to whole plasmid amplification in a second PCR step. Plasmid PCR products were treated with *DpnI*, amplified in *E. coli* (section 4.3.1.3), and sequenced at Microsynth Seqlab.

Table 9: List of primers and sequences to generate protein variants and constructs. Base mutations are colored red, restriction sites are blue, overhangs are brown, and affinity tags are green.

Construct	Sequence 5' – 3'	Specifications
Sa ABCE1 E238A	GAAGAAGGTGCGTCAAATATG	Reverse
Sa ABCE1 E485A	GAGGAAGGTGCATCCAAAAC	Forward
Sa ABCE1 genome F	GACATACCATGGTGAGAGTTGCTGTAATAAATTATGATTATTGTAAACC	Forward
Sa ABCE1 genome R	GACATAGGATCCTGTAGATTCCTCTTCCCTAGAGATTTTCATAG	Reverse
Ss ABCE1 L353Y	CTACTACTAACTGAAAATCACCATACTTCTTGATTATCTTAGTCC	Reverse
Ss ABCE1 R565E	GAGGTAACGTTCGAGAGAGATGCAGAG	Forward
Ss ABCE1 S580E	CTAGAGTAAATAAGATTGGGGAATACTTAGATAGAGTCCAG	Forward
Ss ABCE1 Y592/593A	CAGAAAGAAAGAGGAGATGCTGCCTCCTTGGTTCTTTCTAC	Forward
Ss aIF1 C6/14S, N45C with N-terminal His_6-3C-FLAG tag	TAAGCACATATGCATCATCATCATCATCATCTGGAAGTGCTGTTTCAGGGCCCGGATTATAAAGATGATGATGATAAAGCAGAAAATCTGTCTGGTGGTCTTCCACCAGACATATCTGAGCAACTTTCTAAGGAAGAACAATTTATTAAAATTAAAGTTGAAAAAAGAAGATATGGAAAAGAGGTCACAATAATAGAAGGATTAGGAGGTTGTGATTCTGAACTTAAAAAAATAGCTTCTGAACTTAAATCCAAATTAGCAGCAGGAGGTACAGTAAAAGATGGAAAGATACTTATTCAAAGGGATCATAAAGAAAAAGTTAGGGAGATCCTAATAAAAATGGGATATGCAGAATCCAATATTCTAGTTATTTGATAATGAAAGCTTTAAGCA	Forward, gene block ordered at IDT

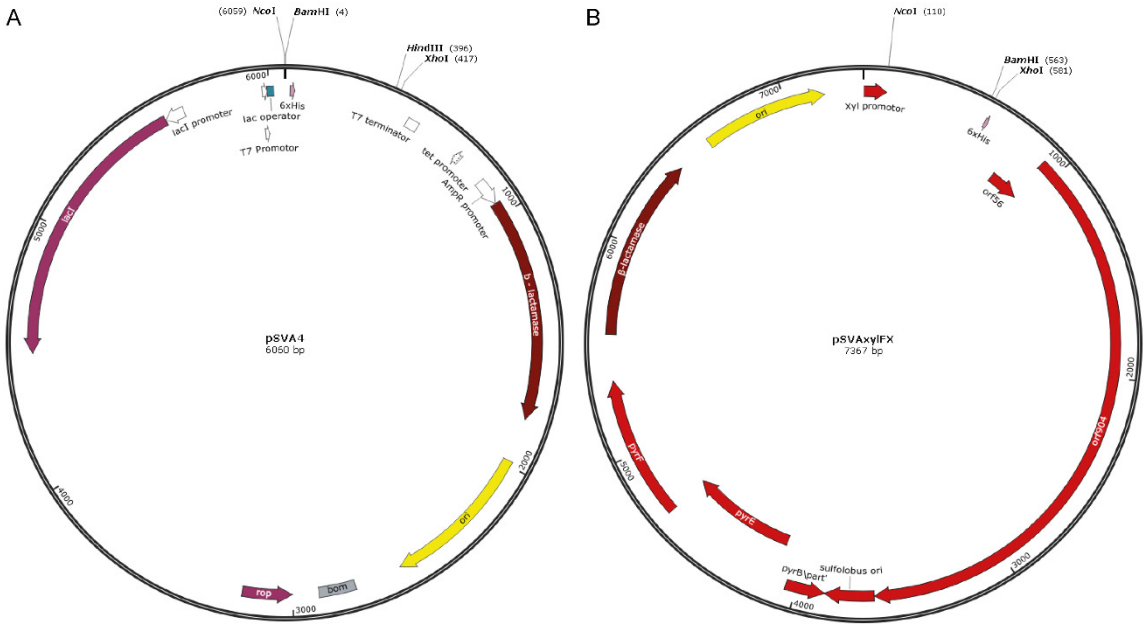

Figure 23: Features of expression plasmids. Both plasmid maps were created with SnapGene® version 2.3.2. **A)** The pSVA4 *E. coli* expression plasmid contains bacterial lac operon features for IPTG-induced expression of the target gene in *E. coli*: a multiple cloning site (exemplary restriction sites: *NcoI*, *BamHI*, *HindIII*, *XhoI*) flanked by T7 promotor and T7 terminator for insertion of the target sequence, β-lactamase as ampicillin resistance marker, and an origin of replication. Protein sequences were inserted *via NcoI* and *BamHI*, *HindIII*, or *XhoI* by standard restriction and ligation protocols. **B)** The pSVAxylFX *S. acidocaldarius* expression plasmid. contains a bacterial origin of replication and β-lactamase as ampicillin resistance marker for propagation in *E. coli*. For xylose-induced protein expression in *S. acidocaldarius*, the inducible Xyl promotor is placed directly in front of a multiple cloning site (exemplary restriction sites: *NcoI*, *BamHI*, *XhoI*). ABCE1 sequence was inserted *via NcoI* and *BamHI*, and the C-terminal His_{10}-3C-FLAG tag was inserted *via BamHI* and *XhoI* by standard restriction and ligation protocols.

4.4.2 Agarose gel electrophoresis

DNA fragments were analyzed with 1% (w/v) agarose in 1x TAE. Electrophoresis was performed in 1x TAE at 100 V for 30-90 min depending on fragment sizes. DNA was stained with ethidium-bromide for 30 min at room temperature and then visualized by UV light.

4.5 Protein and RNA biochemistry

4.5.1 Protein purification

All proteins expressed in *E. coli* were purified *via* a poly-histidine affinity tag by immobilized metal ion affinity chromatography (IMAC). ABCE1 and aIF1 were additionally purified by anion exchange chromatography (AIEX).

Table 10: Properties of purified proteins computed with ExPASy ProtParam (Duvaud *et al*, 2021)**.** Generated mutations did not significantly affect the biophysical properties of the proteins.

Protein	Variant	Affinity tag	ε (A_{280}) ($M^{-1}cm^{-1}$)	MW (kDa)	pI
Bs MutS2	E416A	C-term. 3C-His_{10}	24,870	89.9	6.1
	WT	C-term. 3C-His_{10}	24,870	89.9	6.0
Sa ABCE1	WT	C-term. His_{10}-3C-FLAG	63,190	71.8	7.0
Ss ABCE1	E238/485A	C-term. His_6	58,220	69.3	8.3
	L353Y	C-term. His_6	59,710	69.4	7.9
	R565E	C-term. His_6	58,220	69.4	7.2
	S580E	C-term. His_6	58,220	69.4	7.6
	WT	C-term. 3C-His_6-FLAG	59,710	70.8	6.7
	WT	C-term. His_6	58,220	69.4	7.9
	Y592/593A	C-term. His_6	55,240	69.2	7.9
Ss aIF1	C6/14S, N45C	N-term. His_6-3C-FLAG	4,470	13.7	6.4

4.5.1.1 Cell lysis and precipitation of *E. coli* host proteins

E. coli cell pellets (section 4.3.1.5) were resuspended with two-fold volume of lysis buffer and disrupted by ultra-sonication in three-times 1.5 min pulses (output control 6, duty cycle 60%, Branson Ultrasonics™ Sonifier™ Modell 250) on ice, with 1 min cooling in-between pulses. Cell debris was removed by ultra-centrifugation for 30 min at 130,000 *g* and 4 °C. For purification of archaeal proteins, the lysate was incubated at 65 °C for 10 min to precipitate *E. coli* host proteins, which were removed after cooling on ice by another ultra-centrifugation step. The lysate was filtered through a 200 µM filter.

4.5.1.2 Immobilized metal ion affinity chromatography

Proteins were purified by IMAC using a 5 ml HisTrap™ HP column (Cytiva) on an ÄKTA Prime Plus fast-protein liquid chromatography (FPLC) system (GE Healthcare) at room temperature for archaeal proteins or an ÄKTA Go FPLC system (Cytiva) at 8 °C for bacterial MutS2. The column was loaded with lysate and unbound proteins were removed

by washing with IMAC A until A_{280} almost reached baseline levels. Low-affinity binding proteins were removed with 20% (v/v) IMAC B for two column volumes. For MutS2 purification, the washing step was performed with IMAC B with 1M NaCl for additional removal of nucleic acids. Finally, proteins were eluted with 100% (v/v) IMAC B. 1 ml fractions containing the protein of interest (based on single A_{280} peak and/or SDS-PAGE analysis) were pooled and exchanged to AIEX A or storage buffer by 10DG gravity flow desalting columns (Bio-Rad).

4.5.1.3 Ion exchange chromatography

Anion exchange chromatography for purification of Ss ABCE1, aIF1, and aIF1A was performed at room temperature using an ÄKTA Prime Plus FPLC system (GE Healthcare). IMAC-purified cell lysate in AIEX A buffer was loaded by hand onto a 1 ml HiTrap Q HP column (Cytiva). The column was washed with three column volumes AIEX A. Proteins were eluted from the column with a linear gradient of 0-60% AIEX B for ABCE1, or 0-100% AIEX B for aIFs, in 80 ml. The column was washed with 10 column volumes 100% AIEX B to remove remaining highly charged biomolecules from the column. 0.5 ml fractions of the eluate were collected. Samples were analyzed by SDS-PAGE and the A_{280} peak of the protein of interest. The buffer was exchanged to storage buffer *via* 10DG desalting columns (Bio-Rad). Proteins were concentrated in Amicon® centrifugation filters (Merck) with the respective molecular weight cut-off, aliquoted, shock-frozen in liquid nitrogen, and stored at -80 °C.

4.5.2 Purification of tRNA

E. coli tRNA was purified from a 1 l MRE600 cell pellet in which initiator tRNA ($tRNA_i^{Met}$) was over-expressed (kindly provided by Dr. Elina Nürenberg-Goloub, Tampé laboratory, Goethe-University Frankfurt). Protocols for tRNA extraction by phenol and further purification by precipitation and AIEX were adapted with minor changes (Zubay, 1962; Stolboushkina *et al*, 2013).

All steps very carried out on ice. The cell pellet was resuspended in 12 ml buffer S and mixed 1:1 (v/v) with water saturated phenol (stabilized with 0.1% 8-Hydroxychinoline) for 1 h. Phases were separated for 30 min at 12,500 *g*. The hydrophilic phase was transferred into a fresh tube, mixed with 1/10 volume of 20% (w/v) KOAc pH 5.2 and 2x volumes EtOH absolute, and incubated at -20 °C for 3 h. Nucleic acids were pelleted for 30 min at 12,500 *g*. The pellet was dried, resuspended in 6 ml ice-cold 1 M NaCl, and incubated on

ice for 1 h. Higher molecular weight nucleic acids were pelleted as described and the tRNA-containing supernatant was transferred into a fresh tube. The nucleic acid pellet was resuspended, and the last step was repeated. tRNA-containing supernatant was mixed with 2x volumes EtOH absolute, precipitated over night at -20 °C, pelleted as described, and resuspended in 600 µl 2 M TRIS-HCl pH 8.8. tRNA was deaminoacylated for 3 h at 37 °C, shortly chilled on ice and then precipitated with 200 µl 5 M NaCl and 2x volumes EtOH absolute over night at -20 °C. The tRNA was pelleted as described, dried, resuspended in 3.9 ml 300 mM KOAc pH 7.0 and thoroughly mixed with 2.1 ml isopropanol for 30 min at room temperature. After centrifugation, the supernatant was transferred into a fresh tube and the last extraction step was repeated with the pellet. The supernatants were mixed with 0.45x volume isopropanol, pelleted, resuspended in 600 µl ddH_2O, and tRNA was again precipitated with 3x volumes EtOH absolute and 1/10 volume 3 M KOAc pH 5.2 overnight at -20 °C. Pelleted tRNA was resuspended in 1 ml buffer A and loaded onto a 5 ml HiTrap® Q HP AIEX column, (Cytiva), which was pre-equilibrated with buffer A. The column was washed with multiple column volumes buffer A and tRNA was eluted with a linear 200 – 750 mM NaCl gradient. 0.5 ml fractions were analyzed by Urea-PAGE (section 4.5.3.3) and tRNA concentration was determined at A_{260} (ε_{260} = 606,060 $M^{-1}cm^{-1}$). tRNA-containing fractions were shock-frozen in liquid nitrogen and stored at -80 °C.

4.5.3 Polyacrylamide gel electrophoresis

4.5.3.1 SDS-PAGE

Gels for protein sample analysis by discontinuous sodium dodecyl sulfate polyacrylamide gel electrophoresis (SDS-PAGE) (Laemmli, 1970) were prepared as depicted in Table 11 and Table 12. Protein samples were mixed with 5x SDS-PAGE loading buffer (5x $LP_{red.}$) and denatured for 10 min at 95 °C. Proteins were separated by TRIS-glycine or TRIS-tricine SDS-PAGE at 100-180 V for 45-90 min. Samples with a broad molecular weight range were analyzed using 4-20% Mini-PROTEAN® TGX™ Precast Protein Gels (Bio-Rad) in a TRIS-glycine SDS-PAGE. PageRuler™ Prestained Protein Ladder 10 to 180 kDa (Thermo Scientific) was used for molecular weight approximation in TRIS-glycine SDS-PAGE and Precision Plus Protein™ Dual Xtra Prestained Protein Standards (Bio-Rad) in TRIS-tricine SDS-PAGE. Separated proteins were visualized by Coomassie staining using InstantBlue™ Protein Stain (Expedeon) according to the manufacturer's

instructions, silver staining (section 4.5.3.4), immunoblotting (section 4.5.3.5), or in-gel fluorescence (section 4.5.3.6).

Table 11: Composition of polyacrylamide gels for TRIS-glycine SDS-PAGE.

Component	**Separating gel**		**Stacking gel**
	12%	10%	4.4%
Rotiphorese® Gel 30 (37.5 : 1, acrylamide : bisacrylamide) (Carl Roth)	9.4 ml	8.0 ml	1.3 ml
Separation gel buffer	8.0 ml	8.0 ml	-
Stacking gel buffer	-	-	2.2 ml
ddH_2O	6.4 ml	7.8 ml	5.4 ml
10% (w/v) APS	120 µl	120 µl	90 µl
TEMED	60 µl	60 µl	30 µl

Table 12: Composition of polyacrylamide gels for TRIS-tricine SDS-PAGE.

Component	**13% separating gel**	**4.4% stacking gel**
Rotiphorese® Gel 40 (19 : 1, acrylamide : bisacrylamide) (Carl Roth)	7.5 ml	1.1 ml
Tricine gel buffer	7.5 ml	2.5
86% (v/v) glycerol	3.0 ml	-
ddH_2O	4.7 ml	6.6 ml
10% (w/v) APS	100 µl	80 µl
TEMED	50 µl	40 µl

4.5.3.2 Clear native PAGE

Ribosomal complexes (post-splitting- or initiation complexes) were analyzed by clear native PAGE. Due to the high negative charge of the ribosomal RNA, ribosomal complexes easily migrated in the native polyacrylamide gel without addition of a charge donor like Coomassie brilliant blue in blue native PAGE.

5 pmol 30S were incubated with 3-fold excess of ABCE1 and/or initiation factors for 10 min at 65 °C in 20 mM HEPES-KOH pH 7.5, 60 mM KCl, 2.5 mM $MgCl_2$, in a total volume of 10 µl. The samples were spun down for 5 min at 16,100 *g* and the supernatant was added to 1 µl 50% (v/v) glycerol, which allowed the sample to sink down into the gel pockets during PAGE loading. Clear native PAGE was performed using 3-12% Bis-TRIS NativePAGE™ Gels (Invitrogen) in an XCell SureLock Mini-Cell Electrophoresis System (Thermo Scientific) with 90 mM tricine, 15 mM Bis-TRIS pH 7.0 as cathode buffer and

50 mM Bis-TRIS-HCl pH 7.0 as anode buffer. Electrophoresis was performed for 2.0-2.5 h at 150 V on ice or at 4 °C.

ABCE1-containing samples were incubated with 300-fold excess of ATP or AMP-PNP. In aIF2-containing samples, additionally 300-fold excess of GTP or GMP-PNP was used. Furthermore, ABCE1 was visualized in complex with 30S subunits in clear native PAGE by occlusion of fluorescently labeled ATP. Therefore, ABCE1 was first incubated with a 1/10 molar deficit of N^6-(6-Aminohexyl)-ATP-ATTO647N (^{ATTO647N}ATP) or N^6-(6-Aminohexyl)-ATP-Cy3 (^{Cy3}ATP, Jena Bioscience, Figure 24, Table 6), then with unlabeled ATP before addition of 30S ribosomes. In-gel fluorescence of ^{fluorescent}ATP-ABCE1 co-localized with the distinctive band of 30S ribosomes visualized by InstantBlue™ staining.

The size of 30S complexes was estimated in native PAGE to be ~1 MDa using NativeMark™ Unstained Protein Standard (Invitrogen) as a reference.

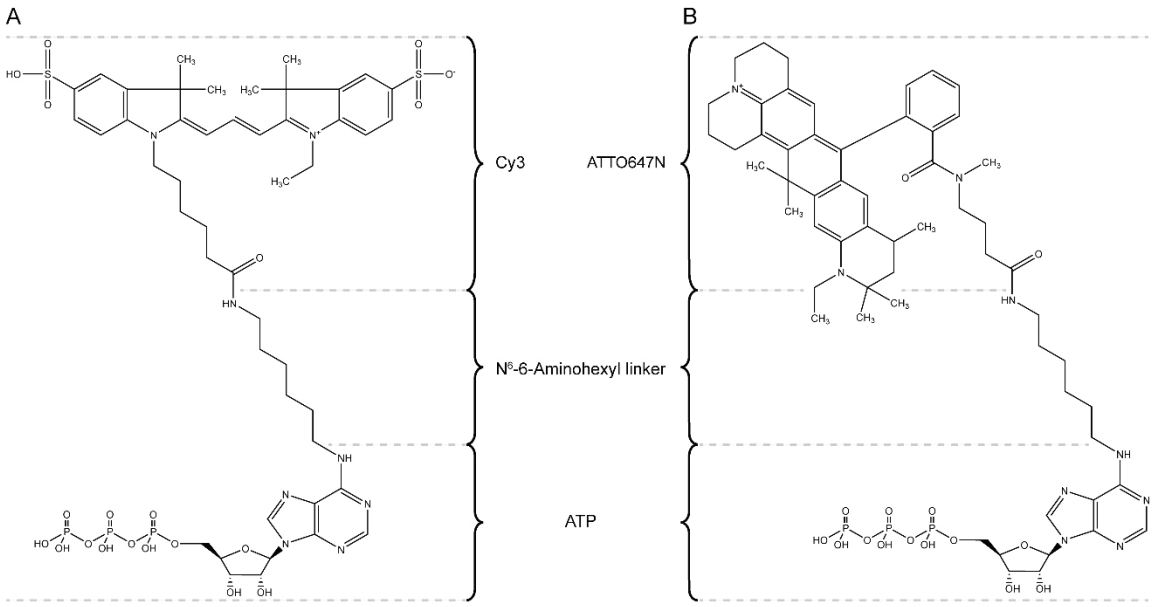

Figure 24: Chemical structures of fluorescently labeled ATP derivates. The fluorophores are attached to the N^6 of the ATP adenosine *via* a 6-Aminohexyl linker. **A)** N^6-(6-Aminohexyl)-ATP-ATTO647N (^{ATTO647N}ATP). **B)** N^6-(6-Aminohexyl)-ATP-Cy3 (^{Cy3}ATP).

4.5.3.3 Urea-PAGE

Urea-containing polyacrylamide gels were prepared according to Table 13. tRNA samples were mixed 1:1 (v/v) with RNA loading buffer and heated 10 min at 75 °C. Electrophoresis was performed in 1x TBE at 180 V. tRNA was stained with 0.1% (w/v) toluidine blue.

Table 13: Composition of polyacrylamide gels for urea PAGE.

Component	Composition
Rotiphorese® Gel 40 (19 : 1, acrylamide : bisacrylamide) (Carl Roth)	5.0 ml
Urea	12.0 g
10x TBE	2.5 ml
ddH_2O	Added to 25 ml
10% (w/v) APS	125 µl
TEMED	25 µl

4.5.3.4 Silver staining

Small amounts of proteins were visualized after SDS-PAGE following a standard silver staining protocol. All steps were performed at room temperature with gentle shaking. Proteins were fixed within the polyacrylamide gel in fixation solution (50% (v/v) acetone, 1.25% (w/v) trichloroacetic acid, 0.0156% (v/v) formaldehyde) for ≥ 10 min or overnight. The gel was rinsed three times with ddH_2O for ≥ 5 s. After a washing step of ≥ 5 min with ddH_2O, the gel was rinsed again. Next, the gel was pre-treated first with 50% (v/v) acetone for 5 min and then 1 min with 0.0332% (w/v) $Na_2S_2O_3$ • 5 H_2O. After rinsing, the gel was treated with impregnation solution (0.268% (w/v) $AgNO_3$, 0.37% (v/v) formaldehyde) for 8 min. After a final rinsing step, the gel was treated with developing solution (2% (w/v) Na_2CO_3, 0.0156% (v/v) formaldehyde, 0.0084% (w/v) $Na_2S_2O_3$ • 5 H_2O) for 5-60s until protein bands were clearly visible. The staining reaction was stopped with 1% (v/v) glacial acetic acid for ≥ 2 min.

4.5.3.5 Immunoblotting

For semi-dry blotting, transfer buffer was freshly prepared and pre-cooled on ice. Proteins were transferred onto a nitrocellulose membrane. For this, pre-soaked Whatman filter paper (in transfer buffer), membrane, polyacrylamide gel, and another pre-soaked Whatman filter paper were stacked from bottom to top. Proteins were transferred at 12 V for 30 min. The membrane was blocked in blocking solution for ≥ 45 min at room temperature. Primary antibodies were prepared in blocking solution and incubated on the membrane overnight at 4 °C. The membrane was washed three times 10 min with ≥ 20 ml PBS-T. Secondary antibodies were prepared in blocking solution and incubated on the membrane for ≥ 1 h at room temperature. The membrane was washed again and proteins

were visualized *via* enhanced chemiluminescence (ECL) using the Clarity Western ECL Substrate (Bio-Rad) according to the manufacturer's instructions.

4.5.3.6 In-gel fluorescence

Fluorescently labeled proteins and occluded fluorescently labeled ATP in ABCE1 were visualized after PAGE using a Vilber Fusion FX imaging system with respective excitation and emission filters.

4.5.4 Methionylation of initiator tRNA

E. coli initiator tRNA ($tRNA_i^{Met}$, section 4.5.2) was freshly methionylated prior to biochemical assays. 40 µg $tRNA_i^{Met}$ were methionylated with 1:1 (w/w) methionine-tRNA synthetase (MetRS, kindly provided by Dr. Elina Nürenberg-Goloub) and 100 µM L-methionine in the presence of 10 mM ATP in methionylation buffer for 15 min at 37 °C. MetRS was removed by IMAC using 10% (v/v) Ni-NTA agarose (Qiagen). The buffer of the $^{Met}tRNA_i^{Met}$-containing flow-through was exchanged to the respective assay buffer by Zeba™ Spin 7 K MWCO 0.5 ml Desalting Columns (Thermo Scientific). Concentration of $^{Met}tRNA_i^{Met}$ was determined by A_{260} (ε_{260} = 606,060 $M^{-1}cm^{-1}$).

4.5.5 Site-specific fluorescence labeling of aIF1

aIF1 was site-specifically labeled at a cysteine sidechain (C6/14S, N45C) either by iodoacetamide or maleimide chemistry using 5-Iodoacetamidofluorescein (5IAF) (Figure 25A) or 7-Diethylamino-3-[N-(2-maleimidoethyl)carbamoyl]coumarin (MDCC) (Figure 25B), respectively. A_{280} and absorption of the fluorophore at its absorption maximum (A_λ) and at 280 nm (A_{280}(FL)) were measured to determine the degree of labeling (DOL). The extinction coefficients of 5IAF and MDCC (ε_{FL}) were given as 73,000 $M^{-1}cm^{-1}$ and 46,800 $M^{-1}cm^{-1}$, respectively:

$$\mathrm{DOL} = \frac{A_\lambda \cdot \varepsilon_P}{(A_{280} - (A_\lambda \cdot C_F)) \cdot \varepsilon_{FL}} \text{ with } C_F = \frac{A_{280}(FL)}{A_\lambda}.$$

Labeled aIF1 ($aIF1^{FL}$) was analyzed by in-gel fluorescence and SEC (sections 4.5.3.6 and 4.5.6.3).

4.5.5.1 In-solution labeling

Storage buffer of 100 µl 60 µM aIF1 was exchanged to labeling buffer by Zeba™ Spin 7 K MWCO 0.5 ml Desalting Columns (Thermo Scientific). Directly prior to labeling, 10-fold molar excess of TRIS(2-carboxyethyl)phosphine (TCEP) was added to aIF1 and incubated for 15 min at 25 °C to ensure complete reduction of the sulfhydryl-group. 5IAF or MDCC (both prepared in dimethyl sulfoxide (DMSO)) were added to reach a final 10-fold molar excess of label while not exceeding 8% (v/v) DMSO. Labeling was performed for 1-2 h at 25 °C. The reaction was stopped by addition of excess BME to neutralize remaining active label for 5 min at 25 °C. Free label was removed and the buffer was exchanged to SEC buffer by Zeba™ Spin 7 K MWCO 0.5 ml desalting columns (Thermo Scientific).

4.5.5.2 On-column labeling

500 µl Ni Sepharose® 6 Fast Flow (Cytiva) were placed into an empty 5 ml gravity flow column and equilibrated twice with ten column volumes labeling buffer. 1 ml 70 µM aIF1 was prepared in labeling buffer and bound to the Ni Sepharose® by its N-terminal His_6 tag. The matrix was washed again twice with ten column volumes of labeling buffer to remove residual BME of the storage buffer. 2 ml 175 µM 5IAF in labeling buffer was added in a five-fold molar excess over aIF1. Labeling was performed in an overhead rotor in the dark for 2 h at room temperature. Free label was removed by washing twice with ten column volumes of labeling buffer. $aIF1^{FL}$ was eluted with 400 mM imidazole (in labeling buffer) and collected in 250 µl fractions. Concentrations were determined by absorption. Residual free label in pooled fractions was quenched with 10 mM BME for 10 min at room temperature. $aIF1^{FL}$ was purified by SEC (section 4.5.6). SEC fractions were pooled and $aIF1^{FL}$ was concentrated using Amicon® Ultra 3 K MWCO centrifugal filters (Merck).

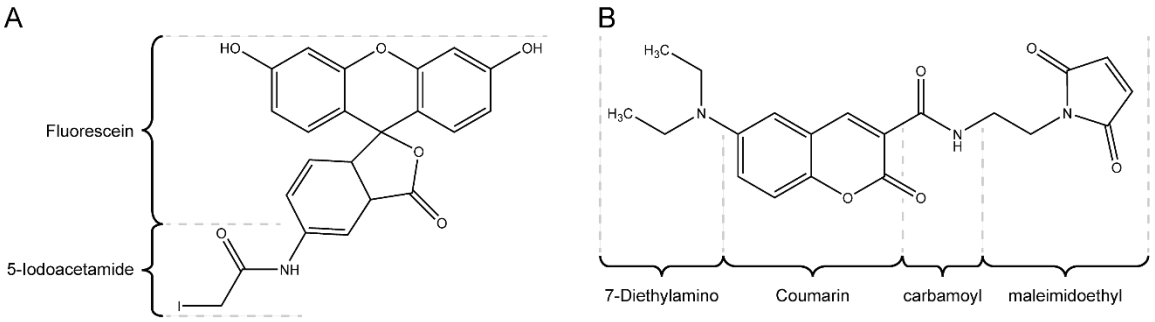

Figure 25: Chemical structures of fluorescence labels. A) 5-Iodoacetamidofluorescein (5IAF). **B)** 7-Diethylamino-3-[N-(2-maleimidoethyl)carbamoyl]coumarin (MDCC).

4.5.6 Size exclusion chromatography

All qualitative size exclusion chromatography (SEC) runs were performed on an ÄKTA Ettan FPLC system (GE Healthcare). Quantitative purification *via* SEC was carried out on ÄKTA GO (Cytiva) or ÄKTA Purifier (GE Healthcare) FPLC systems at 8 °C.

4.5.6.1 Protein quality control

For standard protein quality control after purification, SEC was performed with 50 µl of 10-20 µM protein in SEC buffer, except for MutS2, which was performed in SEC buffer with 400 mM NaCl. ABCE1 and MutS2 were analyzed on a Superdex® 200 Increase 3.2/300 GL column (Cytiva). aIF1 was analyzed on a Superdex® 75 Increase 5/150 GL column (Cytiva).

4.5.6.2 $tRNA_i^{Met}$ binding by aIF2

50 µl 2.5 µM aIF2αβγ heterotrimer was formed in presence of 1 mM GMP-PNP for 3 min at 65 °C. 1.25 µM $tRNA_i^{Met}$ or $^{Met}tRNA_i^{Met}$ was bound for 5 min at 65 °C. The sample was centrifuged for 10 min at 16,100 *g* and 4 °C before it was analyzed on Superdex® 200 Increase 3.2/300 GL column (Cytiva).

4.5.6.3 Purification of labeled aIF1

Fluorescently labeled aIF1 ($aIF1^{FL}$) was purified and analyzed by SEC. After in-solution labeling, 20 µl of $aIF1^{FL}$ was diluted to 50 µl in SEC buffer and analyzed qualitatively on a Superdex® 75 Increase 5/150 GL column (Cytiva). After on-column labeling, $aIF1^{FL}$ was purified by SEC on a Superdex® 75 Increase 10/300 GL column (Cytiva). Residual free label was removed and peak fractions of $aIF1^{FL}$ were pooled and concentrated for use in functional assays.

4.5.6.4 Nucleotide-binding by MutS2

30 µM MutS2 WT or 5 µM MutS2 E416A was incubated with 10-15-fold molar excess ATP, AMP-PNP, ADP, or AMP for 2 min at 35 °C in a total volume of 50 µl in SEC buffer with 400 mM NaCl. Nucleotide-binding was analyzed by A_{260} on a Superdex® 200 Increase 3.2/300 GL column (Cytiva).

4.5.7 Preparation of ribosomes

4.5.7.1 *Thermococcus celer* 70S ribosomes and 30S subunits

Frozen *T. celer* cell pellets were purchased from the Centre of Microbiology and Archaea, University of Regensburg, Germany. Cell pellets were resuspended in 2.5-fold volume S30 buffer and lysed using a Branson Sonifier. Cell debris was removed by centrifugation two times for 30 min at 34,000 *g* and 4 °C. The supernatant was loaded on a high-salt sucrose cushion, and ribosomes were pelleted at 200,000 *g* for 15 h at 4 °C. For 70S preparation, pelleted ribosomes were resuspended in S30 buffer and gradient purified (10-40% (w/v) sucrose, S30 buffer) for 14 h at 68,000 *g*. Fractions were collected using a Piston Gradient Fractionator (Biocomp) recording the A_{260} profile. The buffer of 70S ribosomes containing fractions was exchanged to TrB25 *via* Econo-Pac 10DG Desalting Columns (Bio-Rad), and 70S were concentrated using a 100K Amicon® Ultra filter (Merck). For 30S subunit purification (for 30S ribosome binding assays), high-salt sucrose cushion-pelleted ribosomes were resuspended in buffer A30 and loaded onto a HiPrep 16/60 Sephacryl S-400 HR size exclusion chromatography column (GE Healthcare). Ribosome fractions were collected and pelleted through a low magnesium sucrose cushion in buffer A30 (2.5 mM $Mg(OAc)_2$) for subunit dissociation. Ribosomes were resuspended in S30 buffer and gradient purified. 30S subunit fractions were pooled, the buffer exchanged to S30, and concentrated. Concentration of ribosomes was determined by A_{260} (70S ribosomes $\varepsilon_{260} = 5.6\times10^7\ M^{-1}cm^{-1}$, 30S subunits $\varepsilon_{260} = 1.4\times10^7\ M^{-1}cm^{-1}$) following Lambert-Beer ($c = \frac{A}{\varepsilon \times d}$). Ribosomes and subunits were shock-frozen in liquid nitrogen and stored at -80 °C.

4.5.7.2 *Saccharolobus solfataricus* 30S subunits

30S ribosomal subunits were prepared from *S. solfataricus* cells by ion exchange chromatography using cysteine-charged Sulfolink® resin (Thermo Scientific) and sucrose density gradient centrifugation. The Sulfolink® resin was charged once and used for multiple purifications. For charging, 10 ml of a 50% Sulfolink® coupling gel slurry were transferred into two 15 ml tubes and washed three times 5 min at 850 *g* with coupling buffer. The resin was mixed with 50 mM L-cysteine (5 ml per tube) by slowly rotating for 1 h at room temperature and washed again three times with coupling buffer. After washing three times in ribosome binding buffer, the loaded columns were stored at 4 °C. Binding buffer was removed directly before use. For purification of ribosomes, cells were resuspended in buffer M and lysed by ultra sonication. The lysate was cleared at 30,000 *g* and 4 °C for 30 min. The supernatant was added to charged Sulfolink® resin and

ribosomes were bound for 15 min on ice. The flow-through was removed at 1000 *g* for 1 min. Batch-binding was repeated with the flow-through. The resin was washed three times with 5 ml binding buffer. Ribosomes were eluted with two times 1 ml ribosome elution buffer and pelleted through a glycerol cushion at 100,000 *g* for 15 h at 4 °C (2-3 ml of elution fractions per 1 ml of glycerol cushion buffer). The pellet was resuspended in 100 µl elution buffer by gentle disruption with a glass rod. Aggregates were removed at 16,100 *g* for 10 min. Ribosomal subunits were separated by 10-30% (w/v) sucrose density gradient centrifugation in subunit dissociation buffer. Gradients were harvested, 30S subunit-containing fractions were pooled, the buffer was exchanged, ribosomal subunits were concentrated, concentration of 30S subunits was estimated, and 30S subunits were stored as described (section 4.5.7.1).

4.5.7.3 *Bacillus subtilis* 70S ribosomes and disomes

The cell pellet of a 250 ml culture of *B. subtilis* ΔMutS2 grown in the presence of Erythromycin (kindly provided by Federico Cerullo, Joazeiro Lab) was resuspended 1:1 (v/v) in disome buffer with 20 mM $MgCl_2$, 1x Protease Inhibitor Mix HP (Serva), 1,000 U RiboLock RNase Inhibitor (Thermo Scientific), and 500 U DNase I (RNase-free, Roche). Cells were lysed by ultra-sonication (4x 1 min pulses, output control 5, 50% duty cycle, Branson Ultrasonics™ Sonifier™ Modell 250) and cell debris was removed for 20 min at 80,000 *g* and 4 °C. Ribosomes were pelleted through a 10% (w/v) sucrose cushion in disome buffer with 20 mM $MgCl_2$ (1.5 ml cushion plus 2.0 ml lysate) for 1 h at 300,000 g and 4 °C. Ribosome pellets were resuspended in 100 µl disome buffer with 20 mM MgCl2 and ribosomes were separated by 15-45% (w/v) sucrose density gradient centrifugation for 16 h at 68,000 *g* and 4 °C. Gradients were fractionated as described. If 70S ribosomes and disomes could not be separated after the first SDG, the second half of the overloaded 70S ribosome peak was pooled, pelleted again for 1 h at 300,000 g, resuspended, and separated again *via* SDG. 70S ribosomes and disomes were pooled separately. The buffer was exchanged, ribosomes were concentrated, and stored as described (section 4.5.7.1). The concentration of disomes was estimated by A_{260} assuming that the extinction coefficient of disomes was twice the value of 70S ribosomes.

4.5.8 Biochemical activity assays

4.5.8.1 Malachite Green ATPase

ATP turnover by ABCE1 was determined by a colorimetric Malachite Green-based assay (adapted from (Baykov *et al*, 1988)). Samples were measured in triplicates. 1–2 µM

ABCE1 was incubated with 2 mM Mg-ATP in ATPase buffer for 8 min at 80°C in a total volume of 25 µl. The reaction was immediately stopped by addition of 175 µl ice-cold 20 mM H_2SO_4. 50 µl Malachite Green working solution was added per sample and incubated for 2–5 min at room temperature until color change. A_{620} was recorded in a CLARIOstar plate reader (BMG Labtech). Additionally, controls for residual phosphate (samples without ATP) and ATP auto-hydrolysis at 80 °C (samples without ABCE1) were measured. ATP turnover (ATP per ABCE1 and minute) was determined. First, raw data was blank-corrected (buffer only) and ATP auto-hydrolysis and residual phosphate were subtracted. Then, the amount of produced phosphate was calculated from the slope of a phosphate standard curve (0, 0.1875, 0.375, 0.75, 1.5, 3.0, 6.0, and 12.0 nmol K_2HPO_4). Final turnover numbers were calculated as the quotient of total produced phosphate and ABCE1 quantity and per time of reaction. Bar diagrams represent mean ± SD of two-four independent experiments.

4.5.8.2 70S ribosome splitting

T. celer 70S ribosomes (7.5 pmol) were split into 30S and 50S ribosomal subunits by ABCE1 with aRF1, aPelota, and aIF6 (75 pmol each). The reaction was performed in the presence of 22.5 nmol AMP-PNP or ATP in S30 buffer at 65 °C for 15 min in a total volume of 20 µl. Higher molecular weight aggregates were removed for 10 min at 16,100 *g* and 4 °C. Ribosomal subunits were separated *via* 10–40% (w/v) sucrose density gradient in S30 buffer. Splitting efficiency was evaluated as the ratio of the 50S subunit peak area *versus* the 70S ribosome peak area of the A_{254} gradient profile. Calculated ratios were normalized to the mean value of wild-type ABCE1. Splitting experiments were performed at least three times per ABCE1 variant. Bars represent mean ± SD.

4.5.8.3 30S subunit binding

S. solfataricus or *T. celer* 30S subunits (17.0 pmol) were incubated with ABCE1 (8.5 pmol) in the presence of AMP-PNP, ADP (8.5 nmol), or in the absence of any nucleotide, in S30 buffer in a total volume of 20 µl for 10 min at 65°C. Higher molecular weight aggregates were removed *via* spin down for 10 min at 16,100 *g* and 4°C. Samples were loaded onto a 10-40% (w/v) sucrose density gradient in S30 buffer, as described. 0.5 ml fractions were collected and proteins were precipitated overnight at -20°C with 1.0 ml acetone. Precipitated proteins were pelleted for 1 h at 16,100 *g* and 4 °C. The supernatant was removed and residual acetone was evaporated at 65 °C for 10 min. The pellet was resuspended in 25 µl SDS loading dye. ABCE1 co-migration with 30S subunits was analyzed by SDS-PAGE and immunoblotting.

4.5.8.4 Disome stability

260 µg MutS2 WT was incubated with 60 µg 3C protease in disome buffer (V_{tot} = 58 µl) for 35 min at 35 °C to remove the C-terminal affinity tag of MutS2. 0.1 µM disomes were pre-incubated with 5.0 µM MutS2 (cleaved-off or intact C-terminal affinity tag) for 3 min at 30 °C. 1.0 mM nucleotides (ATP, AMP-PNP, or ADP) were added (V_{tot} = 25 µl in disome buffer) and samples were incubated for 15 min at 30 °C. Precipitates were removed for 10 min at 20,000 *g*. Samples were analyzed on 15-45% (w/v) sucrose density gradients in disome buffer with 10 mM $MgCl_2$ for 16 h at 20,000 rpm (SW41Ti rotor, Beckman Coulter).

4.5.8.5 Fluorescence polarization

aIF1 binding to 30S was analyzed by measuring fluorescence polarization either in a 96-well plate with different 30S subunit concentrations in a ClarioStar® Plus plate reader (BMG Labtech) or in a cuvette by adding 30S subunits to labeled aIF1 on a Fluorolog®-3 spectrofluorometer (HORIBA). In the ladder, 50 nM $aIF1^{FL}$ (50 µl sample) was measured in a micro fluorescence cuvette for ~300 s at 65 °C. 30S subunit binding was performed by addition of 15-fold molar excess of 30S subunits (in 1 µl), quick mixing, and returning the sample into the heated (65 °C) measuring chamber for subsequent ~300 s of measurement. For the 96-well plate format, 100 nM $aIF1^{FL}$ was added to a 30S dilution series (0-160 nM) in V_{tot} = 175 µl in IP buffer. Binding was performed for 10 min at 65 °C. After cool-down on ice, samples were centrifuged at 21,000 *g* for 10 min. Samples were split into 50 µl technical triplicates in a Proxiplate™-96 F (PerkinElmer). Buffer and fluorophore only (100 nM BME-deactivated 5IAF) controls were performed accordingly. For determination of the dissociation constant K_d, fluorescence polarization (P) was first converted to fluorescence anisotropy (r) by

(1) $$r = \frac{2P}{3-P}.$$

Fluorescence anisotropy was corrected for fluorescence intensity increase upon binding of $aIF1^{FL}$ to 30S subunits. The correction factor (Q) was calculated as the ratio of fluorescence intensity of the sample with the highest (I_{max}) and lowest (I_0) 30S subunit concentration by

(2) $$Q = \frac{I_{max}}{I_0}.$$

The fraction of $aIF1^{FL}$ bound to 30S subunits (f_b) was calculated with the anisotropy (r), anisotropy of free $aIF1^{FL}$ (r_0), anisotropy of fully bound $aIF1^{FL}$ (r_{max}, highest 30S subunit concentration) and the correction factor (Q) by

(3) $f_b = \frac{r - r_0}{(r - r_0) - Q(r_{max} - r)}$.

The 30S subunit-bound fraction of aIF1^{FL} (f_b) was plotted against the 30S subunit concentration. Data were fitted and the K_d was determined using a quadratic single site binding model in Origin® 2021 (OriginLab)

(4) $f_b = \frac{1}{2[aIF1^{FL}]}\left(\left([aIF1^{FL}] + [30S] + K_d\right) - \sqrt{([aIF1^{FL}] + [30S] + K_d)^2 - 4[aIF1^{FL}][30S]}\right)$,

as previously described (Monestier *et al*, 2018).

4.5.9 *In vitro* assembly of mRNA translation complexes

4.5.9.1 *In vitro* assembly of the post-splitting complex for cryo-EM

Post-splitting complexes were generated *in vitro* by mimicking the physiological translation route. Purified *T. celer* 70S ribosomes (1 nmol) were split with ABCE1^{IIEA} (8 µM), aPelota, and aRF1 (5 µM each) in the presence of 0.5 mM AMP-PNP in buffer M2 at 65 °C for 15 min. Samples were shortly cooled on ice and then cross-linked with 1% (v/v) formaldehyde for 30 min on ice. Aggregates were removed for 15 min at 16,100 *g* and 4 °C. Samples were loaded onto a 10–30% (w/v) SDG in buffer M3 and ribosomal particles were separated by centrifugation for 13.5 h at 78,000 *g* and 4 °C. 30S subunit-containing fractions were pooled and the sucrose was removed *via* gravity flow desalting columns (Sephadex® G-25, GE Healthcare). Ribosomal complexes were diluted to 50-70 nM (determined *via* A_{260}) for quality control by negative stain-EM. Cryo-EM samples were applied onto 2 nm pre-coated Quantifoil R3/3 holey carbon-supported grids and immediately vitrified using a Vitrobot mark IV (FEI). Data collection, processing, and model building (by Hanna Kratzat, Beckmann lab, LMU Munich) is described in detail in (Nürenberg-Goloub *et al*, 2020).

4.5.9.2 *In vitro* assembly of post-splitting/initiation complexes

ABCE1-30S post-splitting complexes were decorated *in vitro* with initiation factors, mRNA (kindly provided by Dr. Elina Nürenberg-Goloub), and $^{Met}tRNA_i^{Met}$. Successful initiation complex assembly was confirmed by co-IP, native PAGE, and cryo-EM. Samples were prepared in 100 µl with 2 µM *T. celer* 30S subunits, 4 µM Ss ABCE1 and aIFs, 1 mM nucleotides, 20 µM mRNA, and 4 µM $^{Met}tRNA_i^{fMet}$. First, the post-SC, aIF2αβγ/GMP-PNP/ $^{Met}tRNA_i^{Met}$, and aIF1/aIF1A/mRNA were separately pre-assembled in IP buffer for 3 min at 65 °C. Components were combined and initiation complexes were assembled for 15 min

at 65 °C. For IP, samples were diluted to 500 µl (SDS-PAGE sample L) and bound to 40 µl equilibrated anti-FLAG® M2 affinity gel (Sigma-Aldrich) for 1 h at room temperature in an overhead rotor. The affinity gel agarose was carefully washed twice with 20 column volumes IP buffer (wash W). ABCE1 was specifically eluted by addition of 5 µg 3C protease (kindly provided by Dr. Elina Nürenberg-Goloub) in 50 µl IP buffer for 30 min at 35 °C and 400 rpm in a shaker (eluate E). The eluate was removed, the beads were washed again, prepared in SDS-loading buffer, and heated for 10 min at 95 °C together with the other PAGE samples for SDS-PAGE analysis.

4.5.9.3 *In vitro* assembly of initiation complexes for cryo-EM

First, the post-SC was formed as described in 4.5.9.1. aIF2αβγ/GMP-PNP/^{Met}tRNA$_i^{Met}$ and aIF1/aIF1A/mRNA were separately pre-assembled and then incubated with the post-SC as described in 4.5.9.2. Finally, the sample was cross-linked and processed for cryo-EM as described in 4.5.9.1.

4.5.10 Pull-down of ABCE1 complexes from Archaea

All immunoprecipitation (IP) experiments were performed at room temperature. ABCE1 was pulled-down from archaeal lysates *via* its C-terminal FLAG tag using anti-FLAG M2 magnetic beads (Sigma-Aldrich). Beads were equilibrated three times with ten column volumes of IP buffer. For each pull-down experiment of ABCE1 plus lysate, lysate only (without addition of ABCE1) and ABCE1 only (without addition of lysate) controls were performed to attest ABCE1-specific pull-down of proteins from the archaeal cell lysates.

4.5.10.1 Pull-down of recombinant ABCE1 from *Sulfolobaceae* lysates

Recombinant Ss or Sa ABCE1 WT (80 µg) was prepared in 50 µl with 10 mM AMP-PNP and GMP-PNP (final nucleotide concentration in the sample was 1 mM) in IP buffer with additional 5 mM $MgCl_2$ and incubated for 3 min at 65 °C. 500 µl *S. solfataricus* or *S. acidocaldarius* lysates (A_{260} = 15) were added and incubated for 15 min at 65 °C. After rapid cool-down on ice, aggregates were removed for 8 min at 20,000 *g*. The sample was added to 80 µl equilibrated magnetic beads (SDS-PAGE sample load (L)) and antibody binding was performed for 1.5 h at room temperature slowly rotating. The unbound supernatant (SN) was removed and the beads were washed three times with ten column volumes of IP buffer. 50 µl (1/10 volume) of 0.3 µg/µl 3C precision protease was added to the beads to specifically elute ABCE1 for 1.5 h at 35 °C and 500 rpm in a shaker. The eluate (E) was analyzed by SDS-PAGE and mass spectrometry or sucrose density gradient centrifugation. The beads were washed again, 50 µl 2x SDS-loading buffer was

added, and heated for 10 min at 95 °C for SDS-PAGE analysis of non-eluted ABCE1 and unspecific-bound proteins (B).

4.5.10.2 Pull-down of native ABCE1 from *S. acidocaldarius* lysates

Anti-FLAG® immunoprecipitation of homologously expressed ABCE1 was performed as described (section 4.5.10.1) with minor changes. AMP-PNP and GMP-PNP were added to 4.5 ml *S. acidocaldarius* lysate (A_{260} = 15) for a final concentration of 1 mM each. 100 µl anti-FLAG® M2 magnetic beads, equilibrated four times with 10 column volumes, were used. Elution was performed in 1/60 lysate volume with a total amount of 16.5 µg 3C precision protease.

4.6 Bioinformatics tools and software

Plasmid maps, DNA sequences, and primers were designed in SnapGene® 2.3.2. Data analysis and plotting (SDG profiles, peak integration, SEC chromatograms, column diagrams, FP plots, and K_d fits) were performed with Origin® (versions 2017-2021, OriginLab). Gels and immunoblots were analyzed with ImageJ (Schneider *et al*, 2012). Cryo-EM density surface and IC protein structure models were generated with UCSF ChimeraX (Pettersen *et al*, 2021; Goddard *et al*, 2018). ABCE1 and MutS2 protein structures were generated with PyMOL™ 1.9. Figures were designed in Adobe Illustrator® 2021.

5 References

Alkalaeva EZ, Pisarev AV, Frolova LY, Kisselev LL & Pestova TV (2006) In vitro reconstitution of eukaryotic translation reveals cooperativity between release factors eRF1 and eRF3. *Cell* 125: 1125–36

Allen MB (1959) Studies with cyanidium caldarium, an anomalously pigmented chlorophyte. *Arch Mikrobiol* 32: 270–7

Andersen DS & Leevers SJ (2007) The essential Drosophila ATP-binding cassette domain protein, Pixie, binds the 40S ribosome in an ATP-dependent manner and is required for translation initiation. *J Biol Chem* 282: 14752–60

Andreev DE, O'Connor PBF, Loughran G, Dmitriev SE, Baranov P v. & Shatsky IN (2017) Insights into the mechanisms of eukaryotic translation gained with ribosome profiling. *Nucleic Acids Res* 45: 513–26

Armache J-P, Anger AM, Márquez V, Franckenberg S, Fröhlich T, Villa E, Berninghausen O, Thomm M, Arnold GJ, Beckmann R, *et al* (2013) Promiscuous behaviour of archaeal ribosomal proteins: implications for eukaryotic ribosome evolution. *Nucleic Acids Res* 41: 1284–93

Aspesi A & Ellis SR (2019) Rare ribosomopathies: insights into mechanisms of cancer. *Nat Rev Cancer* 19: 228–38

Ban N, Beckmann R, Cate JH, Dinman JD, Dragon F, Ellis SR, Lafontaine DL, Lindahl L, Liljas A, Lipton JM, *et al* (2014) A new system for naming ribosomal proteins. *Curr Opin Struct Biol* 24: 165–9

Barik S (1996) Site-directed mutagenesis in vitro by megaprimer PCR. *Methods Mol Biol* 57: 203–15

Barthelme D, Dinkelaker S, Albers SV, Londei P, Ermler U & Tampé R (2011) Ribosome recycling depends on a mechanistic link between the FeS cluster domain and a conformational switch of the twin-ATPase ABCE1. *Proc Natl Acad Sci USA* 108: 3228–33

Barthelme D, Scheele U, Dinkelaker S, Janoschka A, MacMillan F, Albers SV, Driessen AJM, Stagni MS, Bill E, Meyer-Klaucke W, *et al* (2007) Structural organization of essential iron-sulfur clusters in the evolutionarily highly conserved ATP-binding cassette protein ABCE1. *J Biol Chem* 282: 14598–607

Bassani F, Romagnoli A, Cacciamani T, Amici A, Benelli D, Londei P, Märtens B, Bläsi U & la Teana A (2018) Modification of translation factor aIF5A from Sulfolobus solfataricus. *Extremophiles* 22: 769–80

Baykov AA, Evtushenko OA & Avaeva SM (1988) A malachite green procedure for orthophosphate determination and its use in alkaline phosphatase-based enzyme immunoassay. *Anal Biochem* 171: 266–70

Becker T, Armache J-P, Jarasch A, Anger AM, Villa E, Sieber H, Motaal BA, Mielke T, Berninghausen O & Beckmann R (2011) Structure of the no-go mRNA decay complex Dom34–Hbs1 bound to a stalled 80S ribosome. *Nat Struct Mol Biol* 18: 715–20

Becker T, Franckenberg S, Wickles S, Shoemaker CJ, Anger AM, Armache J-P, Sieber H, Ungewickell C, Berninghausen O, Daberkow I, *et al* (2012) Structural basis of highly conserved ribosome recycling in Eukaryotes and Archaea. *Nature* 482: 501–6

Behrmann E, Loerke J, Budkevich TV, Yamamoto K, Schmidt A, Penczek PA, Vos MR, Bürger J, Mielke T, Scheerer P, *et al* (2015) Structural snapshots of actively translating human ribosomes. *Cell* 161: 845–57

Belardinelli R, Sharma H, Peske F, Wintermeyer W & Rodnina MV (2016) Translocation as continuous movement through the ribosome. *RNA Biol* 13: 1197–203

Benelli D, Maone E & Londei P (2003) Two different mechanisms for ribosome/mRNA interaction in archaeal translation initiation. *Mol Microbiol* 50: 635–43

Bengtson MH & Joazeiro CAP (2010) Role of a ribosome-associated E3 ubiquitin ligase in protein quality control. *Nature* 467: 470–3

Bieri P, Greber BJ & Ban N (2018) High-resolution structures of mitochondrial ribosomes and their functional implications. *Curr Opin Struct Biol* 49: 44–53

Bisbal C, Martinand C, Silhol M, Lebleu B & Salehzada T (1995) Cloning and characterization of a RNase L inhibitor. *J Biol Chem* 270: 13308–17

Borg A, Pavlov M & Ehrenberg M (2016) Complete kinetic mechanism for recycling of the bacterial ribosome. *RNA* 22: 10–21

Boussaid I & Fontenay M (2022) Translation defects in ribosomopathies. *Curr Opin Hematol* 29: 119–25

Brandman O & Hegde RS (2016) Ribosome-associated protein quality control. *Nat Struct Mol Biol* 23: 7–15

Brandman O, Stewart-Ornstein J, Wong D, Larson A, Williams CC, Li G-W, Zhou S, King D, Shen PS, Weibezahn J, *et al* (2012) A ribosome-bound quality control complex triggers degradation of nascent peptides and signals translation stress. *Cell* 151: 1042–54

Brenneis M, Hering O, Lange C & Soppa J (2007) Experimental characterization of cis-acting elements important for translation and transcription in halophilic Archaea. *PLoS Genet* 3: e229

Brock TD, Brock KM, Belly RT & Weiss RL (1972) Sulfolobus: a new genus of sulfur-oxidizing Bacteria living at low pH and high temperature. *Arch Mikrobiol* 84: 54–68

Brown A, Shao S, Murray J, Hegde RS & Ramakrishnan V (2015) Structural basis for stop codon recognition in eukaryotes. *Nature* 524: 493–6

Burby PE & Simmons LA (2017) MutS2 promotes homologous recombination in Bacillus subtilis. *J Bacteriol* 199: e00682-16

Buskirk AR & Green R (2017) Ribosome pausing, arrest and rescue in bacteria and eukaryotes. *Philos Trans R Soc London, Ser B* 372: 20160183

Caliskan N, Peske F & Rodnina MV (2015) Changed in translation: mRNA recoding by −1 programmed ribosomal frameshifting. *Trends Biochem Sci* 40: 265–74

Cannone JJ, Subramanian S, Schnare MN, Collett JR, D'Souza LM, Du Y, Feng B, Lin N, Madabusi L v., Müller KM, *et al* (2002) The comparative RNA web (CRW) site: an online database of comparative sequence and structure information for ribosomal, intron, and other RNAs. *BMC Bioinf* 3: 2

Carter AP, Clemons WM, Brodersen DE, Morgan-Warren RJ, Hartsch T, Wimberly BT & Ramakrishnan V (2001) Crystal structure of an initiation factor bound to the 30S ribosomal subunit. *Science (1979)* 291: 498–501

Cerullo F, Filbeck S, Patil PR, Hung HC, Xu H, Vornberger J, Hofer FW, Schmitt J, Kramer G, Bukau B, *et al* (2022) Bacterial ribosome collision sensing by a MutS DNA repair ATPase paralogue. *Nature* 603: 509–14

Chavatte L, Seit-Nebi A, Dubovaya V & Favre A (2002) The invariant uridine of stop codons contacts the conserved NIKSR loop of human eRF1 in the ribosome. *EMBO J* 21: 5302–11

Chen J, Lu G, Lin J, Davidson AL & Quiocho FA (2003) A tweezers-like motion of the ATP-binding cassette dimer in an ABC transport cycle. *Mol Cell* 12: 651–61

Chen L, Muhlrad D, Hauryliuk V, Cheng Z, Lim MK, Shyp V, Parker R & Song H (2010) Structure of the Dom34–Hbs1 complex and implications for no-go decay. *Nat Struct Mol Biol* 17: 1233–40

Chen S, Oldham ML, Davidson AL & Chen J (2013) Carbon catabolite repression of the maltose transporter revealed by X-ray crystallography. *Nature* 499: 364–8

Chen Z, Dong J, Ishimura A, Daar I, Hinnebusch AG & Dean M (2006) The essential vertebrate ABCE1 protein interacts with eukaryotic initiation factors. *J Biol Chem* 281: 7452–7

Choe Y-J, Park S-H, Hassemer T, Körner R, Vincenz-Donnelly L, Hayer-Hartl M & Hartl FU (2016) Failure of RQC machinery causes protein aggregation and proteotoxic stress. *Nature* 531: 191–5

Coelho CMA, Kolevski B, Bunn C, Walker C, Dahanukar A & Leevers SJ (2005) Growth and cell survival are unevenly impaired in pixie mutant wing discs. *Development* 132: 5411–24

Cooper HL, Park MH, Folk JE, Safer B & Braverman R (1983) Identification of the hypusine-containing protein hy+ as translation initiation factor eIF-4D. *Proc Natl Acad Sci USA* 80: 1854–7

Coureux P-D, Lazennec-Schurdevin C, Bourcier S, Mechulam Y & Schmitt E (2020) Cryo-EM study of an archaeal 30S initiation complex gives insights into evolution of translation initiation. *Commun Biol* 3: 58

Coureux P-D, Lazennec-Schurdevin C, Monestier A, Larquet E, Cladière L, Klaholz BP, Schmitt E & Mechulam Y (2016) Cryo-EM study of start codon selection during archaeal translation initiation. *Nat Commun* 7: 13366

Crick F (1970) Central dogma of molecular biology. *Nature* 227: 561–3

Dassa E & Bouige P (2001) The ABC of ABCs: a phylogenetic and functional classification of ABC systems in living organisms. *Res Microbiol* 152: 211–29

Dean M, Rzhetsky A & Allikmets R (2001) The human ATP-binding cassette (ABC) transporter superfamily. *Genome Res* 11: 1156–66

Defenouillère Q, Yao Y, Mouaikel J, Namane A, Galopier A, Decourty L, Doyen A, Malabat C, Saveanu C, Jacquier A, *et al* (2013) Cdc48-associated complex bound to 60S particles is required for the clearance of aberrant translation products. *Proc Natl Acad Sci USA* 110: 5046–51

De S & Mühlemann O (2022) A comprehensive coverage insurance for cells: revealing links between ribosome collisions, stress responses and mRNA surveillance. *RNA Biol* 19: 609–21

Dever TE, Dinman JD & Green R (2018) Translation elongation and recoding in Eukaryotes. *Cold Spring Harbor Perspect Biol* 10: a032649

Dever TE & Green R (2012) The elongation, termination, and recycling phases of translation in Eukaryotes. *Cold Spring Harbor Perspect Biol* 4: a013706

Doamekpor SK, Lee J-W, Hepowit NL, Wu C, Charenton C, Leonard M, Bengtson MH, Rajashankar KR, Sachs MS, Lima CD, *et al* (2016) Structure and function of the yeast listerin (Ltn1) conserved N-terminal domain in binding to stalled 60S ribosomal subunits. *Proc Natl Acad Sci USA* 113: 4151–60

Doerfel LK, Wohlgemuth I, Kothe C, Peske F, Urlaub H & Rodnina MV (2013) EF-P is essential for rapid synthesis of proteins containing consecutive proline residues. *Science (1979)* 339: 85–8

Doma MK & Parker R (2006) Endonucleolytic cleavage of eukaryotic mRNAs with stalls in translation elongation. *Nature* 440: 561–4

Dong J, Lai R, Nielsen K, Fekete CA, Qiu H & Hinnebusch AG (2004) The essential ATP-binding cassette protein RLI1 functions in translation by promoting preinitiation complex assembly. *J Biol Chem* 279: 42157–68

D'Orazio KN, Wu CC-C, Sinha N, Loll-Krippleber R, Brown GW & Green R (2019) The endonuclease Cue2 cleaves mRNAs at stalled ribosomes during no go decay. *Elife* 8: e49117

Dubiez E, Aleksandrov A, Lazennec-Schurdevin C, Mechulam Y & Schmitt E (2015) Identification of a second GTP-bound magnesium ion in archaeal initiation factor 2. *Nucleic Acids Res* 43: 2946–57

Duvaud S, Gabella C, Lisacek F, Stockinger H, Ioannidis V & Durinx C (2021) Expasy, the Swiss bioinformatics resource portal, as designed by its users. *Nucleic Acids Res* 49: W216-27

van den Elzen AMG, Schuller A, Green R & Séraphin B (2014) Dom34-Hbs1 mediated dissociation of inactive 80S ribosomes promotes restart of translation after stress. *EMBO J* 33: 265–76

Fernández IS, Bai X-C, Hussain T, Kelley AC, Lorsch JR, Ramakrishnan V & Scheres SHW (2013) Molecular architecture of a eukaryotic translational initiation complex. *Science (1979)* 342: 1240585

Ferretti MB & Karbstein K (2019) Does functional specialization of ribosomes really exist? *RNA* 25: 521–38

Filbeck S, Cerullo F, Pfeffer S & Joazeiro CAP (2022) Ribosome-associated quality-control mechanisms from bacteria to humans. *Mol Cell* 82: 1451–66

French SL, Santangelo TJ, Beyer AL & Reeve JN (2007) Transcription and translation are coupled in Archaea. *Mol Biol Evol* 24: 893–5

Frischmeyer PA, van Hoof A, O'Donnell K, Guerrerio AL, Parker R & Dietz HC (2002) An mRNA surveillance mechanism that eliminates transcripts lacking termination codons. *Science (1979)* 295: 2258–61

Frolova L, le Goff X, Zhouravleva G, Davydova E, Philippe M & Kisselev L (1996) Eukaryotic polypeptide chain release factor eRF3 is an eRF1- and ribosome-dependent guanosine triphosphatase. *RNA* 2: 334–41

Frolova L, Seit-Nebi A & Kisselev L (2002) Highly conserved NIKS tetrapeptide is functionally essential in eukaryotic translation termination factor eRF1. *RNA* 8: 129–36

Frolova L, Tsivkovskii R, Sivolobova G, Oparina N, Serpinsky O, Blinov V, Tatkov S & Kisselev L (1999) Mutations in the highly conserved GGQ motif of class 1 polypeptide release factors abolish ability of human eRF1 to trigger peptidyl-tRNA hydrolysis. *RNA* 5: 1014–20

Fu Z, Kaledhonkar S, Borg A, Sun M, Chen B, Grassucci RA, Ehrenberg M & Frank J (2016) Key intermediates in ribosome recycling visualized by time-resolved cryoelectron microscopy. *Structure* 24: 2092–101

Gao N, Zavialov AV, Li W, Sengupta J, Valle M, Gursky RP, Ehrenberg M & Frank J (2005) Mechanism for the disassembly of the posttermination complex inferred from cryo-EM studies. *Mol Cell* 18: 663–74

Gay DM, Lund AH & Jansson MD (2022) Translational control through ribosome heterogeneity and functional specialization. *Trends Biochem Sci* 47: 66–81

des Georges A, Hashem Y, Unbehaun A, Grassucci RA, Taylor D, Hellen CUT, Pestova TV & Frank J (2014) Structure of the mammalian ribosomal pre-termination complex associated with eRF1•eRF3•GDPNP. *Nucleic Acids Res* 42: 3409–18

Gerovac M & Tampé R (2019) Control of mRNA translation by versatile ATP-driven machines. *Trends Biochem Sci* 44: 167–80

Gingras A-C, Raught B & Sonenberg N (1999) eIF4 initiation factors: effectors of mRNA recruitment to ribosomes and regulators of translation. *Annu Rev Biochem* 68: 913–63

Glover ML, Burroughs AM, Monem PC, Egelhofer TA, Pule MN, Aravind L & Arribere JA (2020) NONU-1 encodes a conserved endonuclease required for mRNA translation surveillance. *Cell Rep* 30: 4321–31.e4

Goddard TD, Huang CC, Meng EC, Pettersen EF, Couch GS, Morris JH & Ferrin TE (2018) UCSF ChimeraX: meeting modern challenges in visualization and analysis. *Protein Sci* 27: 14–25

Gouridis G, Hetzert B, Kiosze-Becker K, de Boer M, Heinemann H, Nürenberg-Goloub E, Cordes T & Tampé R (2019) ABCE1 controls ribosome recycling by an asymmetric dynamic conformational equilibrium. *Cell Rep* 28: 723–34.e6

Goyal A, Belardinelli R, Maracci C, Milón P & Rodnina MV (2015) Directional transition from initiation to elongation in bacterial translation. *Nucleic Acids Res* 43: 10700–12

Greber BJ & Ban N (2016) Structure and function of the mitochondrial ribosome. *Annu Rev Biochem* 85: 103–32

Gromadski KB, Schümmer T, Strømgaard A, Knudsen CR, Kinzy TG & Rodnina MV (2007) Kinetics of the interactions between Yeast elongation factors 1A and 1Bα, guanine nucleotides, and aminoacyl-tRNA. *J Biol Chem* 282: 35629–37

Groothuizen FS & Sixma TK (2016) The conserved molecular machinery in DNA mismatch repair enzyme structures. *DNA Repair (Amst)* 38: 14–23

Grossmann N, Vakkasoglu AS, Hulpke S, Abele R, Gaudet R & Tampé R (2014) Mechanistic determinants of the directionality and energetics of active export by a heterodimeric ABC transporter. *Nat Commun* 5: 5419

Gualerzi CO & Pon CL (2015) Initiation of mRNA translation in bacteria: structural and dynamic aspects. *Cell Mol Life Sci* 72: 4341–67

Guenneugues M, Caserta E, Brandi L, Spurio R, Meunier S, Pon CL, Boelens R & Gualerzi CO (2000) Mapping the fMet-tRNAfMet binding site of initiation factor IF2. *EMBO J* 19: 5233–40

Guo H (2018) Specialized ribosomes and the control of translation. *Biochem Soc Trans* 46: 855–69

Gutierrez E, Shin B-S, Woolstenhulme CJ, Kim J-R, Saini P, Buskirk AR & Dever TE (2013) eIF5A promotes translation of polyproline motifs. *Mol Cell* 51: 35–45

Hasenöhrl D, Benelli D, Barbazza A, Londei P & Bläsi U (2006) Sulfolobus solfataricus translation initiation factor 1 stimulates translation initiation complex formation. *RNA* 12: 674–82

Hasenöhrl D, Fabbretti A, Londei P, Gualerzi CO & Bläsi U (2009) Translation initiation complex formation in the crenarchaeon Sulfolobus solfataricus. *RNA* 15: 2288–98

Hayes CS & Sauer RT (2003) Cleavage of the A site mRNA codon during ribosome pausing provides a mechanism for translational quality control. *Mol Cell* 12: 903–11

Hellen CUT (2018) Translation termination and ribosome recycling in Eukaryotes. *Cold Spring Harbor Perspect Biol* 10: a032656

Heuer A, Gerovac M, Schmidt C, Trowitzsch S, Preis A, Kötter P, Berninghausen O, Becker T, Beckmann R & Tampé R (2017) Structure of the 40S-ABCE1 post-splitting complex in ribosome recycling and translation initiation. *Nat Struct Mol Biol* 24: 453–60

Hofmann S, Januliene D, Mehdipour AR, Thomas C, Stefan E, Brüchert S, Kuhn BT, Geertsma ER, Hummer G, Tampé R, *et al* (2019) Conformation space of a heterodimeric ABC exporter under turnover conditions. *Nature* 571: 580–3

van Hoof A, Frischmeyer PA, Dietz HC & Parker R (2002) Exosome-mediated recognition and degradation of mRNAs lacking a termination codon. *Science (1979)* 295: 2262–4

Hopfner K (2016) Architectures and mechanisms of ATP binding cassette proteins. *Biopolymers* 105: 492–504

Hürlimann LM, Hohl M & Seeger MA (2017) Split tasks of asymmetric nucleotide-binding sites in the heterodimeric ABC exporter EfrCD. *FEBS J* 284: 1672–87

Huter P, Arenz S, Bock L v., Graf M, Frister JO, Heuer A, Peil L, Starosta AL, Wohlgemuth I, Peske F, *et al* (2017) Structural basis for polyproline-mediated ribosome stalling and rescue by the translation elongation factor EF-P. *Mol Cell* 68: 515–27.e6

Ikeuchi K, Tesina P, Matsuo Y, Sugiyama T, Cheng J, Saeki Y, Tanaka K, Becker T, Beckmann R & Inada T (2019) Collided ribosomes form a unique structural interface to induce Hel2-driven quality control pathways. *EMBO J* 38: e100276

Imai H, Abe T, Miyoshi T, Nishikawa S, Ito K & Uchiumi T (2018) The ribosomal stalk protein is crucial for the action of the conserved ATPase ABCE1. *Nucleic Acids Res* 46: 7820–30

Ivanova N, Pavlov MY, Felden B & Ehrenberg M (2004) Ribosome rescue by tmRNA requires truncated mRNAs. *J Mol Biol* 338: 33–41

Jackson RJ, Hellen CUT & Pestova TV (2010) The mechanism of eukaryotic translation initiation and principles of its regulation. *Nat Rev Mol Cell Biol* 11: 113–27

Jin H, Kelley AC, Loakes D & Ramakrishnan V (2010) Structure of the 70S ribosome bound to release factor 2 and a substrate analog provides insights into catalysis of peptide release. *Proc Natl Acad Sci USA* 107: 8593–8

Joazeiro CAP (2019) Mechanisms and functions of ribosome-associated protein quality control. *Nat Rev Mol Cell Biol* 20: 368–83

Johnson E, Nguyen PT, Yeates TO & Rees DC (2012) Inward facing conformations of the MetNI methionine ABC transporter: implications for the mechanism of transinhibition. *Protein Sci* 21: 84–96

Julián P, Milón P, Agirrezabala X, Lasso G, Gil D, Rodnina MV & Valle M (2011) The cryo-EM atructure of a complete 30S translation initiation complex from Escherichia coli. *PLoS Biol* 9: e1001095

Juszkiewicz S, Chandrasekaran V, Lin Z, Kraatz S, Ramakrishnan V & Hegde RS (2018) ZNF598 Is a quality control sensor of collided ribosomes. *Mol Cell* 72: 469–81.e7

Karcher A, Schele A & Hopfner KP (2008) X-ray structure of the complete ABC enzyme ABCE1 from Pyrococcus abyssi. *J Biol Chem* 283: 7962–71

Karousis ED & Mühlemann O (2019) Nonsense-mediated mRNA decay begins where translation ends. *Cold Spring Harbor Perspect Biol* 11: a032862

Karzai AW, Susskind MM & Sauer RT (1999) SmpB, a unique RNA-binding protein essential for the peptide-tagging activity of SsrA (tmRNA). *EMBO J* 18: 3793–9

Keiler KC (2008) Biology of trans-translation. *Annu Rev Microbiol* 62: 133–51

Keiler KC, Waller PRH & Sauer RT (1996) Role of a peptide tagging system in degradation of proteins synthesized from damaged messenger RNA. *Science (1979)* 271: 990–3

Kim KQ & Zaher HS (2022) Canary in a coal mine: collided ribosomes as sensors of cellular conditions. *Trends Biochem Sci* 47: 82–97

Kim SJ, Yoon JS, Shishido H, Yang Z, Rooney LA, Barral JM & Skach WR (2015) Translational tuning optimizes nascent protein folding in cells. *Science (1979)* 348: 444–8

Kiosze-Becker K, Ori A, Gerovac M, Heuer A, Nürenberg-Goloub E, Rashid UJ, Becker T, Beckmann R, Beck M & Tampé R (2016) Structure of the ribosome post-recycling complex probed by chemical cross-linking and mass spectrometry. *Nat Commun* 7: 13248

Kisselev LL & Buckingham RH (2000) Translational termination comes of age. *Trends Biochem Sci* 25: 561–6

Klein I, Sarkadi B & Váradi A (1999) An inventory of the human ABC proteins. *Biochim Biophys Acta* 1461: 237–62

Klinge S, Voigts-Hoffmann F, Leibundgut M & Ban N (2012) Atomic structures of the eukaryotic ribosome. *Trends Biochem Sci* 37: 189–98

Kobayashi K, Kikuno I, Kuroha K, Saito K, Ito K, Ishitani R, Inada T & Nureki O (2010) Structural basis for mRNA surveillance by archaeal Pelota and GTP-bound EF1α complex. *Proc Natl Acad Sci USA* 107: 17575–9

Kobayashi K, Saito K, Ishitani R, Ito K & Nureki O (2012) Structural basis for translation termination by archaeal RF1 and GTP-bound EF1α complex. *Nucleic Acids Res* 40: 9319–28

Kögel A, Keidel A, Bonneau F, Schäfer IB & Conti E (2022) The human SKI complex regulates channeling of ribosome-bound RNA to the exosome via an intrinsic gatekeeping mechanism. *Mol Cell* 82: 756–69.e8

Kolosov P, Frolova L, Seit-Nebi A, Dubovaya V, Kononenko A, Oparina N, Justesen J, Efimov A & Kisselev L (2005) Invariant amino acids essential for decoding function of polypeptide release factor eRF1. *Nucleic Acids Res* 33: 6418–25

Korkhov VM, Mireku SA & Locher KP (2012) Structure of AMP-PNP-bound vitamin B12 transporter BtuCD–F. *Nature* 490: 367–72

Korostelev A, Zhu J, Asahara H & Noller HF (2010) Recognition of the amber UAG stop codon by release factor RF1. *EMBO J* 29: 2577–85

Kostova KK, Hickey KL, Osuna BA, Hussmann JA, Frost A, Weinberg DE & Weissman JS (2017) CAT-tailing as a fail-safe mechanism for efficient degradation of stalled nascent polypeptides. *Science (1979)* 357: 414–7

Kratzat H, Mackens-Kiani T, Ameismeier M, Potocnjak M, Cheng J, Dacheux E, Namane A, Berninghausen O, Herzog F, Fromont-Racine M, *et al* (2021) A structural inventory of native ribosomal ABCE1-43S pre-initiation complexes. *EMBO J* 40: e105179

Kressler D, Hurt E & Baßler J (2017) A puzzle of life: crafting ribosomal subunits. *Trends Biochem Sci* 42: 640–54

Kurosaki T, Popp MW & Maquat LE (2019) Quality and quantity control of gene expression by nonsense-mediated mRNA decay. *Nat Rev Mol Cell Biol* 20: 406–20

Kurosawa N & Grogan DW (2005) Homologous recombination of exogenous DNA with the Sulfolobus acidocaldarius genome: properties and uses. *FEMS Microbiol Lett* 253: 141–9

Laemmli UK (1970) Cleavage of structural proteins during the assembly of the head of bacteriophage T4. *Nature* 227: 680–5

Lake JA (1976) Ribosome structure determined by electron microscopy of Escherichia coli small subunits, large subunits and monomeric ribosomes. *J Mol Biol* 105: 131–59

Lamers MH, Perrakis A, Enzlin JH, Winterwerp HHK, de Wind N & Sixma TK (2000) The crystal structure of DNA mismatch repair protein MutS binding to a G·T mismatch. *Nature* 407: 711–7

Lammens K, Bemeleit DJ, Möckel C, Clausing E, Schele A, Hartung S, Schiller CB, Lucas M, Angermüller C, Söding J, *et al* (2011) The Mre11:Rad50 structure shows an ATP-dependent molecular clamp in DNA double-strand break repair. *Cell* 145: 54–66

LaRiviere FJ, Wolfson AD & Uhlenbeck OC (2001) Uniform binding of aminoacyl-tRNAs to elongation factor Tu by thermodynamic compensation. *Science (1979)* 294: 165–8

Laurberg M, Asahara H, Korostelev A, Zhu J, Trakhanov S & Noller HF (2008) Structural basis for translation termination on the 70S ribosome. *Nature* 454: 852–7

Locher KP (2016) Mechanistic diversity in ATP-binding cassette (ABC) transporters. *Nat Struct Mol Biol* 23: 487–93

Lomakin IB, Stolboushkina EA, Vaidya AT, Zhao C, Garber MB, Dmitriev SE & Steitz TA (2017) Crystal structure of the human ribosome in complex with DENR-MCT-1. *Cell Rep* 20: 521–8

Londei P (2015) Translation initiation models in prokaryotes and eukaryotes. In *eLS* pp 1–7. Wiley

Lytvynenko I, Paternoga H, Thrun A, Balke A, Müller TA, Chiang CH, Nagler K, Tsaprailis G, Anders S, Bischofs I, *et al* (2019) Alanine tails signal proteolysis in bacterial ribosome-associated quality control. *Cell* 178: 76-90.e22

Maag D, Algire MA & Lorsch JR (2006) Communication between eukaryotic translation initiation factors 5 and 1A within the ribosomal pre-initiation complex plays a role in start site selection. *J Mol Biol* 356: 724–37

Maag D & Lorsch JR (2003) Communication between eukaryotic translation initiation factors 1 and 1A on the yeast small ribosomal subunit. *J Mol Biol* 330: 917–24

Mancera-Martínez E, Brito Querido J, Valasek LS, Simonetti A & Hashem Y (2017) ABCE1: a special factor that orchestrates translation at the crossroad between recycling and initiation. *RNA Biol* 14: 1279–85

Mandel M & Higa A (1970) Calcium-dependent bacteriophage DNA infection. *J Mol Biol* 53: 159–62

Maone E, di Stefano M, Berardi A, Benelli D, Marzi S, la Teana A & Londei P (2007) Functional analysis of the translation factor aIF2/5B in the thermophilic archaeon Sulfolobus solfataricus. *Mol Microbiol* 65: 700–13

Martin-Marcos P, Nanda J, Luna RE, Wagner G, Lorsch JR & Hinnebusch AG (2013) β-Hairpin loop of eukaryotic initiation factor 1 (eIF1) mediates 40S ribosome binding to regulate initiator tRNAMet recruitment and accuracy of AUG selection in vivo. *J Biol Chem* 288: 27546–62

Matsuo Y, Ikeuchi K, Saeki Y, Iwasaki S, Schmidt C, Udagawa T, Sato F, Tsuchiya H, Becker T, Tanaka K, *et al* (2017) Ubiquitination of stalled ribosome triggers ribosome-associated quality control. *Nat Commun* 8: 159

Melnikov S, Mailliot J, Shin B-S, Rigger L, Yusupova G, Micura R, Dever TE & Yusupov M (2016) Crystal structure of Hypusine-containing translation factor eIF5A bound to a rotated eukaryotic ribosome. *J Mol Biol* 428: 3570–6

Mills EW & Green R (2017) Ribosomopathies: there's strength in numbers. *Science (1979)* 358: eaan2755

Milón P, Carotti M, Konevega AL, Wintermeyer W, Rodnina MV & Gualerzi CO (2010) The ribosome-bound initiation factor 2 recruits initiator tRNA to the 30S initiation complex. *EMBO Rep* 11: 312–6

Milón P, Maracci C, Filonava L, Gualerzi CO & Rodnina MV (2012) Real-time assembly landscape of bacterial 30S translation initiation complex. *Nat Struct Mol Biol* 19: 609–15

Milón P & Rodnina MV (2012) Kinetic control of translation initiation in bacteria. *Crit Rev Biochem Mol Biol* 47: 334–48

Mitchell SF & Lorsch JR (2008) Should I stay or should I go? Eukaryotic translation initiation factors 1 and 1A control start codon recognition. *J Biol Chem* 283: 27345–9

Mitkevich VA, Kononenko AV, Petrushanko IY, Yanvarev DV, Makarov AA & Kisselev LL (2006) Termination of translation in eukaryotes is mediated by the quaternary eRF1•eRF3•GTP•Mg2+ complex. The biological roles of eRF3 and prokaryotic RF3 are profoundly distinct. *Nucleic Acids Res* 34: 3947–54

Monestier A, Lazennec-Schurdevin C, Coureux PD, Mechulam Y & Schmitt E (2018) Role of aIF1 in Pyrococcus abyssi translation initiation. *Nucleic Acids Res* 46: 11061–74

Moore SD & Sauer RT (2007) The tmRNA system for translational surveillance and ribosome rescue. *Annu Rev Biochem* 76: 101–24

Müller C, Crowe-McAuliffe C & Wilson DN (2021) Ribosome rescue pathways in Bacteria. *Front Microbiol* 12: 652980

Newstead S, Fowler PW, Bilton P, Carpenter EP, Sadler PJ, Campopiano DJ, Sansom MSP & Iwata S (2009) Insights into how nucleotide-binding domains power ABC transport. *Structure* 17: 1213–22

Nürenberg E & Tampé R (2013) Tying up loose ends: ribosome recycling in Eukaryotes and Archaea. *Trends Biochem Sci* 38: 64–74

Nürenberg-Goloub E (2018) Molecular mechanism of the ribosome recycling factor ABCE1. [PhD Thesis, Institute of Biochemistry, Goethe-University Frankfurt]

Nürenberg-Goloub E, Heinemann H, Gerovac M & Tampé R (2018) Ribosome recycling is coordinated by processive events in two asymmetric ATP sites of ABCE1. *Life Sci Alliance* 1: e201800095

Nürenberg-Goloub E, Kratzat H, Heinemann H, Heuer A, Kötter P, Berninghausen O, Becker T, Tampé R & Beckmann R (2020) Molecular analysis of the ribosome recycling factor ABCE1 bound to the 30S post-splitting complex. *EMBO J* 39: e103788

Nürenberg-Goloub E & Tampé R (2019) Ribosome recycling in mRNA translation, quality control, and homeostasis. *Biol Chem* 401: 47–61

Obmolova G, Ban C, Hsieh P & Yang W (2000) Crystal structures of mismatch repair protein MutS and its complex with a substrate DNA. *Nature* 407: 703–10

Passmore LA, Schmeing TM, Maag D, Applefield DJ, Acker MG, Algire MA, Lorsch JR & Ramakrishnan V (2007) The eukaryotic translation initiation factors eIF1 and eIF1A induce an open conformation of the 40S ribosome. *Mol Cell* 26: 41–50

Pavlov MY, Watts RE, Tan Z, Cornish VW, Ehrenberg M & Forster AC (2009) Slow peptide bond formation by proline and other N-alkylamino acids in translation. *Proc Natl Acad Sci USA* 106: 50–4

Pedullà N, Palermo R, Hasenöhrl D, Bläsi U, Cammarano P & Londei P (2005) The archaeal eIF2 homologue: functional properties of an ancient translation initiation factor. *Nucleic Acids Res* 33: 1804–12

Peske F, Kuhlenkoetter S, Rodnina MV & Wintermeyer W (2014) Timing of GTP binding and hydrolysis by translation termination factor RF3. *Nucleic Acids Res* 42: 1812–20

Peske F, Rodnina MV & Wintermeyer W (2005) Sequence of steps in ribosome recycling as defined by kinetic analysis. *Mol Cell* 18: 403–12

Petrov AS, Gulen B, Norris AM, Kovacs NA, Bernier CR, Lanier KA, Fox GE, Harvey SC, Wartell RM, Hud NV, *et al* (2015) History of the ribosome and the origin of translation. *Proc Natl Acad Sci USA* 112: 15396–401

Pettersen EF, Goddard TD, Huang CC, Meng EC, Couch GS, Croll TI, Morris JH, Ferrin TE & Thomas Ferrin CE (2021) UCSF ChimeraX: structure visualization for researchers, educators, and developers. *Protein Sci* 30: 70–82

Pisarev AV, Hellen CUT & Pestova TV (2007) Recycling of eukaryotic posttermination ribosomal complexes. *Cell* 131: 286–99

Pisareva VP, Skabkin MA, Hellen CUT, Pestova TV & Pisarev AV (2011) Dissociation by Pelota, Hbs1 and ABCE1 of mammalian vacant 80S ribosomes and stalled elongation complexes. *EMBO J* 30: 1804–17

Pisarev AV, Skabkin MA, Pisareva VP, Skabkina OV, Rakotondrafara AM, Hentze MW, Hellen CUT & Pestova TV (2010) The role of ABCE1 in eukaryotic posttermination ribosomal recycling. *Mol Cell* 37: 196–210

Preis A, Heuer A, Barrio-Garcia C, Hauser A, Eyler DE, Berninghausen O, Green R, Becker T & Beckmann R (2014) Cryoelectron microscopic structures of eukaryotic translation termination complexes containing eRF1-eRF3 or eRF1-ABCE1. *Cell Rep* 8: 59–65

Procko E, Ferrin-O'Connell I, Ng S-L & Gaudet R (2006) Distinct structural and functional properties of the ATPase sites in an asymmetric ABC transporter. *Mol Cell* 24: 51–62

Prunetti L, Graf M, Blaby IK, Peil L, Makkay AM, Starosta AL, Papke RT, Oshima T, Wilson DN & de Crécy-Lagard V (2016) Deciphering the translation initiation factor 5A modification pathway in halophilic Archaea. *Archaea* 2016: 1–14

Rees DC, Johnson E & Lewinson O (2009) ABC transporters: the power to change. *Nat Rev Mol Cell Biol* 10: 218–27

Rodnina MV (2013) The ribosome as a versatile catalyst: reactions at the peptidyl transferase center. *Curr Opin Struct Biol* 23: 595–602

Rodnina MV (2018) Translation in Prokaryotes. *Cold Spring Harbor Perspect Biol* 10: a032664

Rodnina MV, Fischer N, Maracci C & Stark H (2017) Ribosome dynamics during decoding. *Philos Trans R Soc London, Ser B* 372: 20160182

Saini P, Eyler DE, Green R & Dever TE (2009) Hypusine-containing protein eIF5A promotes translation elongation. *Nature* 459: 118–21

Saito K, Kobayashi K, Wada M, Kikuno I, Takusagawa A, Mochizuki M, Uchiumi T, Ishitani R, Nureki O & Ito K (2010) Omnipotent role of archaeal elongation factor 1 alpha (EF1α) in translational elongation and termination, and quality control of protein synthesis. *Proc Natl Acad Sci USA* 107: 19242–7

Saito K, Kratzat H, Campbell A, Buschauer R, Burroughs AM, Berninghausen O, Aravind L, Green R, Beckmann R & Buskirk AR (2022) Ribosome collisions induce mRNA cleavage and ribosome rescue in bacteria. *Nature* 603: 503–8

Saito S, Hosoda N & Hoshino S (2013) The Hbs1-Dom34 protein complex functions in non-stop mRNA decay in mammalian cells. *J Biol Chem* 288: 17832–43

Saurin W, Hofnung M & Dassa E (1999) Getting in or out: early segregation between importers and exporters in the evolution of ATP-binding cassette (ABC) transporters. *J Mol Evol* 48: 22–41

Schmeing TM, Voorhees RM, Kelley AC, Gao Y-G, Murphy FV, Weir JR & Ramakrishnan V (2009) The crystal structure of the ribosome bound to EF-Tu and aminoacyl-tRNA. *Science (1979)* 326: 688–94

Schmidt C, Becker T, Heuer A, Braunger K, Shanmuganathan V, Pech M, Berninghausen O, Wilson DN & Beckmann R (2016) Structure of the hypusinylated eukaryotic translation factor eIF-5A bound to the ribosome. *Nucleic Acids Res* 44: 1944–51

Schmitt E, Coureux P-D, Kazan R, Bourgeois G, Lazennec-Schurdevin C & Mechulam Y (2020) Recent advances in archaeal translation initiation. *Front Microbiol* 11: 584152

Schmitt E, Coureux P-D, Monestier A, Dubiez E & Mechulam Y (2019) Start codon recognition in eukaryotic and archaeal translation initiation: a common structural core. *Int J Mol Sci* 20: 939

Schmitt E, Panvert M, Lazennec-Schurdevin C, Coureux P-D, Perez J, Thompson A & Mechulam Y (2012) Structure of the ternary initiation complex aIF2–GDPNP–methionylated initiator tRNA. *Nat Struct Mol Biol* 19: 450–4

Schneider CA, Rasband WS & Eliceiri KW (2012) NIH Image to ImageJ: 25 years of image analysis. *Nat Methods* 9: 671–5

Schramm F, Borst A, Linne U & Soppa J (2021) Elucidation of the translation initiation factor interaction network of Haloferax volcanii reveals coupling of transcription and translation in Haloarchaea. *Front Microbiol* 12: 742806

Schuller AP, Wu CC-C, Dever TE, Buskirk AR & Green R (2017) eIF5A functions globally in translation elongation and termination. *Mol Cell* 66: 194-205.e5

Shao S, Brown A, Santhanam B & Hegde RS (2015) Structure and assembly pathway of the ribosome quality control complex. *Mol Cell* 57: 433–44

Shao S, Murray J, Brown A, Taunton J, Ramakrishnan V & Hegde RS (2016) Decoding mammalian ribosome-mRNA states by translational GTPase complexes. *Cell* 167: 1229–40.e15

Shaw JJ & Green R (2007) Two distinct components of release factor function uncovered by nucleophile partitioning analysis. *Mol Cell* 28: 458–67

Shen PS, Park J, Qin Y, Li X, Parsawar K, Larson MH, Cox J, Cheng Y, Lambowitz AM, Weissman JS, *et al* (2015) Rqc2p and 60S ribosomal subunits mediate mRNA-independent elongation of nascent chains. *Science (1979)* 347: 75–8

Shine J & Dalgarno L (1974) The 3′-terminal sequence of Escherichia coli 16S ribosomal RNA: complementarity to nonsense triplets and ribosome binding sites. *Proc Natl Acad Sci USA* 71: 1342–6

Shine J & Dalgarno L (1975) Determinant of cistron specificity in bacterial ribosomes. *Nature* 254: 34–8

Shirokikh NE & Preiss T (2018) Translation initiation by cap-dependent ribosome recruitment: Recent insights and open questions. *Wiley Interdiscip Rev RNA* 9: e1473

Shoemaker CJ, Eyler DE & Green R (2010) Dom34:Hbs1 promotes subunit dissociation and peptidyl-tRNA drop-off to initiate no-go decay. *Science (1979)* 330: 369–72

Shoemaker CJ & Green R (2011) Kinetic analysis reveals the ordered coupling of translation termination and ribosome recycling in yeast. *Proc Natl Acad Sci USA* 108: 1392–8

Sievers A, Beringer M, Rodnina MV & Wolfenden R (2004) The ribosome as an entropy trap. *Proc Natl Acad Sci USA* 101: 7897–901

Simms CL, Yan LL & Zaher HS (2017) Ribosome collision is critical for quality control during no-go decay. *Mol Cell* 68: 361–73.e5

Simonetti A, Brito Querido J, Myasnikov AG, Mancera-Martinez E, Renaud A, Kuhn L & Hashem Y (2016) eIF3 peripheral subunits rearrangement after mRNA binding and start-codon recognition. *Mol Cell* 63: 206–17

Simonetti A, Guca E, Bochler A, Kuhn L & Hashem Y (2020) Structural insights into the mammalian late-stage initiation complexes. *Cell Rep* 31: 107497

Sitron CS & Brandman O (2019) CAT tails drive degradation of stalled polypeptides on and off the ribosome. *Nat Struct Mol Biol* 26: 450–9

Skabkin MA, Skabkina OV, Dhote V, Komar AA, Hellen CUT & Pestova TV (2010) Activities of Ligatin and MCT-1/DENR in eukaryotic translation initiation and ribosomal recycling. *Genes Dev* 24: 1787–801

Skabkin MA, Skabkina OV, Hellen CUT & Pestova TV (2013) Reinitiation and other unconventional posttermination events during eukaryotic translation. *Mol Cell* 51: 249–64

Smith PC, Karpowich N, Millen L, Moody JE, Rosen J, Thomas PJ & Hunt JF (2002) ATP binding to the motor domain from an ABC transporter drives formation of a nucleotide sandwich dimer. *Mol Cell* 10: 139–49

Song H, Mugnier P, Das AK, Webb HM, Evans DR, Tuite MF, Hemmings BA & Barford D (2000) The crystal structure of human eukaryotic release factor eRF1—mechanism of stop codon recognition and peptidyl-tRNA hydrolysis. *Cell* 100: 311–21

Steitz TA (2008) A structural understanding of the dynamic ribosome machine. *Nat Rev Mol Cell Biol* 9: 242–53

Stolboushkina E, Nikonov S, Nikulin A, Bläsi U, Manstein DJ, Fedorov R, Garber M & Nikonov O (2008) Crystal structure of the intact archaeal translation initiation factor 2 demonstrates very high conformational flexibility in the α- and β-subunits. *J Mol Biol* 382: 680–91

Stolboushkina E, Nikonov S, Zelinskaya N, Arkhipova V, Nikulin A, Garber M & Nikonov O (2013) Crystal structure of the archaeal translation initiation factor 2 in complex with a GTP analogue and met-tRNAfMet. *J Mol Biol* 425: 989–98

Strunk BS, Novak MN, Young CL & Karbstein K (2012) A translation-like cycle is a quality control checkpoint for maturing 40S ribosome subunits. *Cell* 150: 111–21

Sundaramoorthy E, Leonard M, Mak R, Liao J, Fulzele A & Bennett EJ (2017) ZNF598 and RACK1 regulate mammalian ribosome-associated quality control function by mediating regulatory 40S ribosomal ubiquitylation. *Mol Cell* 65: 751–60.e4

Tahmasebi S, Khoutorsky A, Mathews MB & Sonenberg N (2018) Translation deregulation in human disease. *Nat Rev Mol Cell Biol* 19: 791–807

Taylor D, Unbehaun A, Li W, Das S, Lei J, Liao HY, Grassucci RA, Pestova TV & Frank J (2012) Cryo-EM structure of the mammalian eukaryotic release factor eRF1–eRF3-associated termination complex. *Proc Natl Acad Sci USA* 109: 18413–8

la Teana A, Benelli D, Londei P & Bläsi U (2013) Translation initiation in the crenarchaeon Sulfolobus solfataricus: eukaryotic features but bacterial route. *Biochem Soc Trans* 41: 350–5

Terenin IM, Dmitriev SE, Andreev DE & Shatsky IN (2008) Eukaryotic translation initiation machinery can operate in a bacterial-like mode without eIF2. *Nat Struct Mol Biol* 15: 836–41

Thomas C, Aller SG, Beis K, Carpenter EP, Chang G, Chen L, Dassa E, Dean M, Duong Van Hoa F, Ekiert D, *et al* (2020) Structural and functional diversity calls for a new classification of ABC transporters. *FEBS Lett* 594: 3767–75

Thomas C & Tampé R (2020) Structural and mechanistic principles of ABC transporters. *Annu Rev Biochem* 89: 605–36

Thrun A, Garzia A, Kigoshi-Tansho Y, Patil PR, Umbaugh CS, Dallinger T, Liu J, Kreger S, Patrizi A, Cox GA, *et al* (2021) Convergence of mammalian RQC and C-end rule proteolytic pathways via alanine tailing. *Mol Cell* 81: 2112–22.e7

Tolstrup N, Sensen CW, Garrett RA & Clausen IG (2000) Two different and highly organized mechanisms of translation initiation in the archaeon Sulfolobus solfataricus. *Extremophiles* 4: 175–9

Tsuboi T, Kuroha K, Kudo K, Makino S, Inoue E, Kashima I & Inada T (2012) Dom34:Hbs1 plays a general role in quality-control systems by dissociation of a stalled ribosome at the 3′ end of aberrant mRNA. *Mol Cell* 46: 518–29

Ude S, Lassak J, Starosta AL, Kraxenberger T, Wilson DN & Jung K (2013) Translation elongation factor EF-P alleviates ribosome stalling at polyproline stretches. *Science (1979)* 339: 82–5

Voorhees RM & Ramakrishnan V (2013) Structural basis of the translational elongation cycle. *Annu Rev Biochem* 82: 203–36

Voorhees RM, Schmeing TM, Kelley AC & Ramakrishnan V (2010) The mechanism for activation of GTP hydrolysis on the ribosome. *Science (1979)* 330: 835–8

Wagner M, van Wolferen M, Wagner A, Lassak K, Meyer BH, Reimann J & Albers SV (2012) Versatile genetic tool box for the crenarchaeote Sulfolobus acidocaldarius. *Front Microbiol* 3: 214

Watson JD & Crick FHC (1953) Molecular structure of nucleic acids: a structure for deoxyribose nucleic Acid. *Nature* 171: 737–8

Weixlbaumer A, Grünberger F, Werner F & Grohmann D (2021) Coupling of transcription and translation in Archaea: cues from the bacterial world. *Front Microbiol* 12: 661827

Weixlbaumer A, Jin H, Neubauer C, Voorhees RM, Petry S, Kelley AC & Ramakrishnan V (2008) Insights into translational termination from the structure of RF2 bound to the ribosome. *Science (1979)* 322: 953–6

Woese CR (1968) The fundamental nature of the genetic code: prebiotic interactions between polynucleotides and polyamino acids or their derivatives. *Proc Natl Acad Sci USA* 59: 110–7

Woese CR (2001) Translation: in retrospect and prospect. *RNA* 7: 1055–67

Woolstenhulme CJ, Parajuli S, Healey DW, Valverde DP, Petersen EN, Starosta AL, Guydosh NR, Johnson WE, Wilson DN & Buskirk AR (2013) Nascent peptides that block protein synthesis in Bacteria. *Proc Natl Acad Sci USA* 110: 878–87

Wurtzel O, Sapra R, Chen F, Zhu Y, Simmons BA & Sorek R (2010) A single-base resolution map of an archaeal transcriptome. *Genome Res* 20: 133–41

Wu Z, Wang Y, Lim J, Liu B, Li Y, Vartak R, Stankiewicz T, Montgomery S & Lu B (2018) Ubiquitination of ABCE1 by NOT4 in response to mitochondrial damage links co-translational quality control to PINK1-directed mitophagy. *Cell Metab* 28: 130–44.e7

Xu B, Liu L & Song G (2022) Functions and regulation of translation elongation factors. *Front Mol Biosci* 8: 816398

Xue S & Barna M (2012) Specialized ribosomes: a new frontier in gene regulation and organismal biology. *Nat Rev Mol Cell Biol* 13: 355–69

Yi Z, Sanjeev M & Singh G (2021) The branched nature of the nonsense-mediated mRNA decay pathway. *Trends Genet* 37: 143–59

Yonashiro R, Tahara EB, Bengtson MH, Khokhrina M, Lorenz H, Chen K-C, Kigoshi-Tansho Y, Savas JN, Yates JR, Kay SA, *et al* (2016) The Rqc2/Tae2 subunit of the ribosome-associated quality control (RQC) complex marks ribosome-stalled nascent polypeptide chains for aggregation. *Elife* 5: e11794

Young DJ & Guydosh NR (2019) Hcr1/eIF3j is a 60S ribosomal subunit recycling accessory factor in vivo. *Cell Rep* 28: 39-50.e4

Young DJ, Makeeva DS, Zhang F, Anisimova AS, Stolboushkina EA, Ghobakhlou F, Shatsky IN, Dmitriev SE, Hinnebusch AG & Guydosh NR (2018) Tma64/eIF2D, Tma20/MCT-1, and Tma22/DENR recycle post-termination 40S subunits in vivo. *Mol Cell* 71: 761–74.e5

Young DJ, Meydan S & Guydosh NR (2021) 40S ribosome profiling reveals distinct roles for Tma20/Tma22 (MCT-1/DENR) and Tma64 (eIF2D) in 40S subunit recycling. *Nat Commun* 12: 2976

Zahn S, Kubatova N, Pyper DJ, Cassidy L, Saxena K, Tholey A, Schwalbe H & Soppa J (2021) Biological functions, genetic and biochemical characterization, and NMR structure determination of the small zinc finger protein HVO_2753 from Haloferax volcanii. *FEBS J* 288: 2042–62

Zaitseva J, Jenewein S, Jumpertz T, Holland IB & Schmitt L (2005) H662 is the linchpin of ATP hydrolysis in the nucleotide-binding domain of the ABC transporter HlyB. *EMBO J* 24: 1901–10

Zhang G & Ignatova Z (2011) Folding at the birth of the nascent chain: coordinating translation with co-translational folding. *Curr Opin Struct Biol* 21: 25–31

Zhouravleva G, Frolova L, le Goff X, le Guellec R, Inge-Vechtomov S, Kisselev L & Philippe M (1995) Termination of translation in eukaryotes is governed by two interacting polypeptide chain release factors, eRF1 and eRF3. *EMBO J* 14: 4065–72

Zimmerman C, Klein KC, Kiser PK, Singh AR, Firestein BL, Riba SC & Lingappa JR (2002) Identification of a host protein essential for assembly of immature HIV-1 capsids. *Nature* 415: 88–92

Zinoviev A, Ayupov RK, Abaeva IS, Hellen CUT & Pestova TV (2020) Extraction of mRNA from stalled ribosomes by the Ski complex. *Mol Cell* 77: 1340–9.e6

Zubay G (1962) The isolation and fractionation of soluble ribonucleic acid. *J Mol Biol* 4: 347–56

Zutz A, Hoffmann J, Hellmich UA, Glaubitz C, Ludwig B, Brutschy B & Tampé R (2011) Asymmetric ATP hydrolysis cycle of the heterodimeric multidrug ABC transport complex TmrAB from Thermus thermophilus. *J Biol Chem* 286: 7104–15

6 Supplementary information

6.1 The post-splitting complex

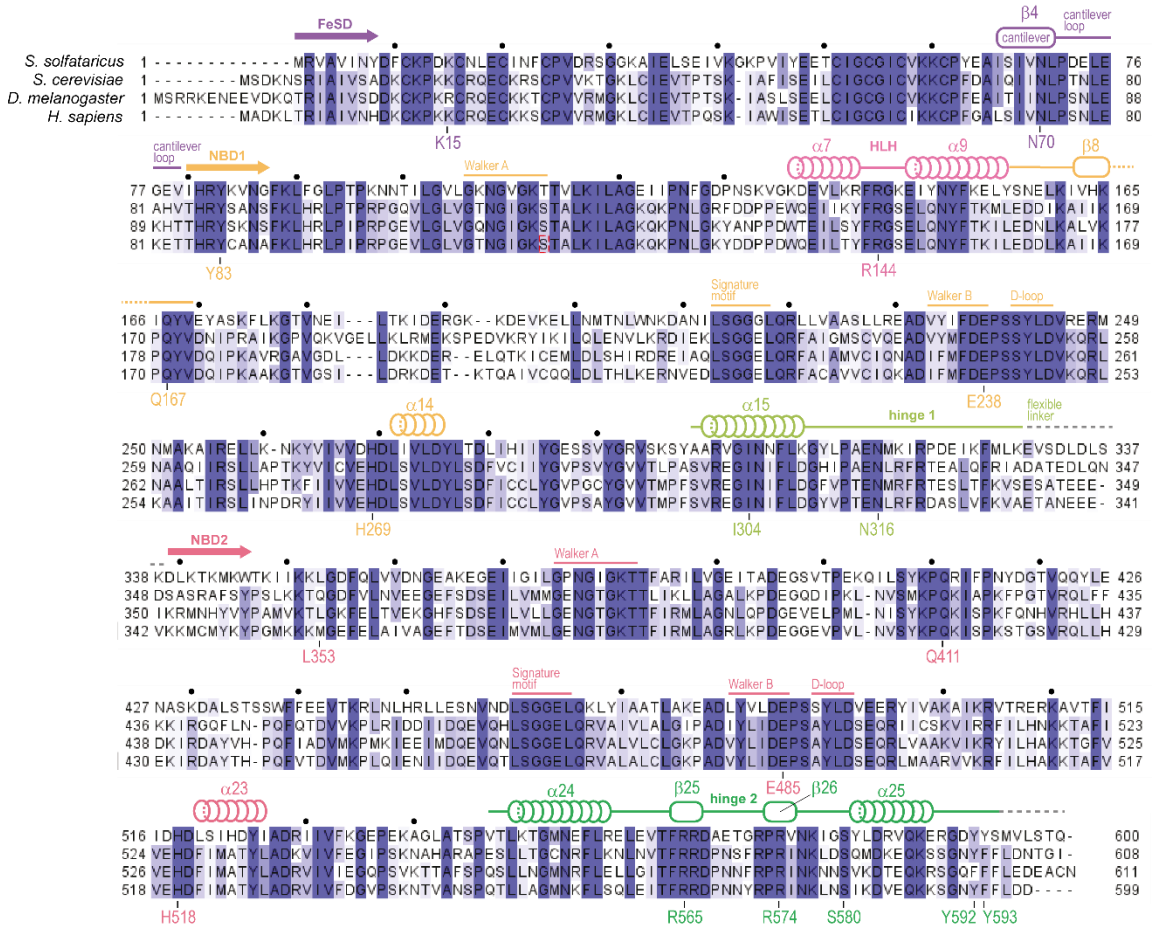

Figure S1: Sequence alignment of ABCE1 from different species (Nürenberg-Goloub *et al*, 2020)**.** *S. solfataricus*, *S. cerevisiae*, *D. melanogaster*, and *H. sapiens* ABCE1 display strong sequence conservation, illustrated by the shades of blue. Numbering according to Ss ABCE1. Domains are indicated by arrows. Loops are represented by lines, α-helices by tubes and β-sheets by boxes. Conserved motifs, important secondary structure elements (numbered according to (Karcher *et al*, 2008)) and colored according to Figure 4), and residues are indicated.

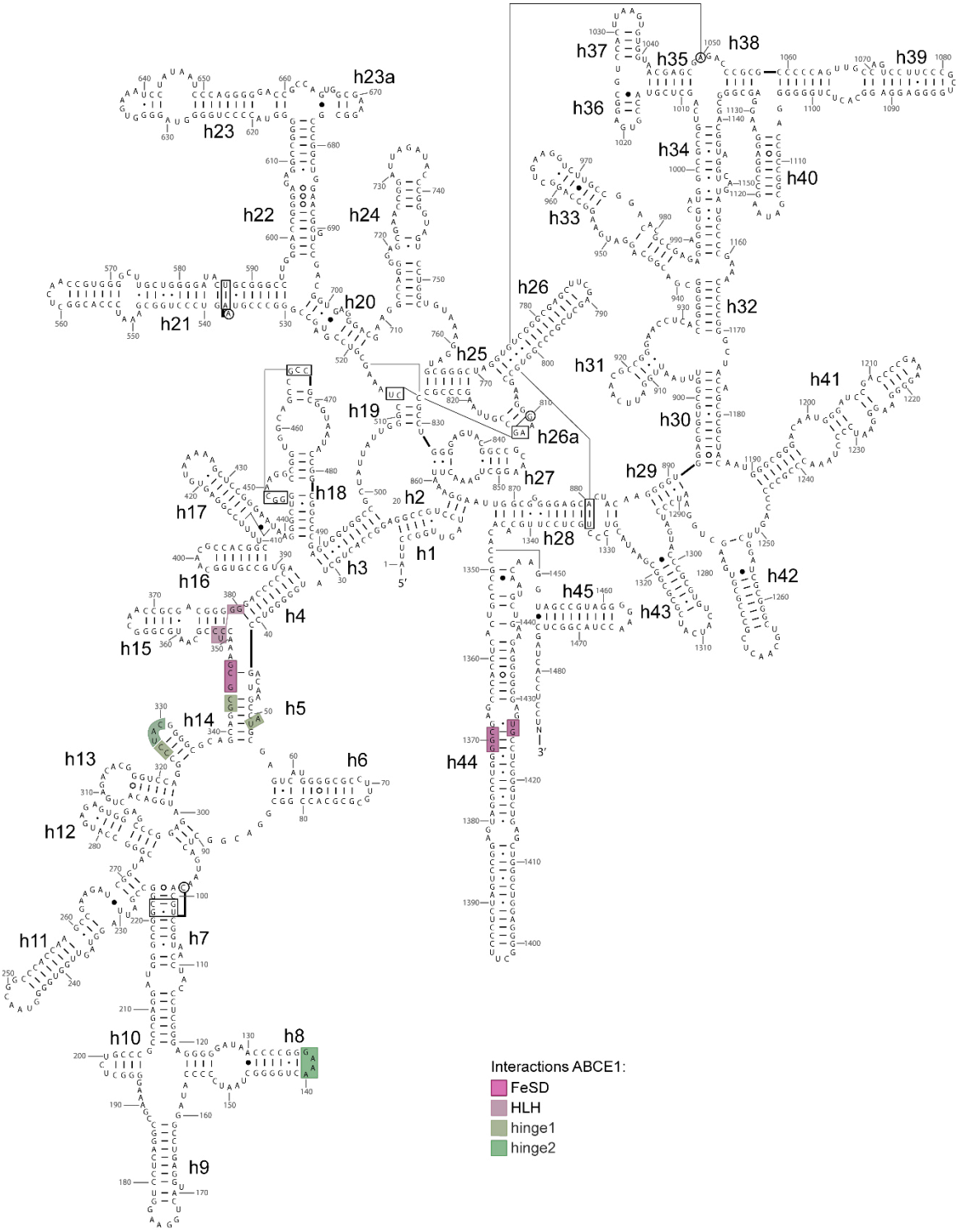

Figure S2: Secondary structure of *T. celer* 16S rRNA (Nürenberg-Goloub *et al*, 2020)**.** 1487 nucleic acid residues form the *T. celer* 16S rRNA (Cannone *et al*, 2002). ABCE1-domain interactions with the 16S rRNA are colored according to the domain architecture of ABCE1 in Figure 4. FeSD contacts G345, C346, and G347 of h5 and C1369, G1370, G1371, G1426, and U1427 of h44. HLH motif binds to C352, U253, C354, and G379 of h15 and G380 of h4. Hinge 1 contacts h5 at A51, U52, G343, and C344 and h14 at C326 and C327. Hinge 2 anchors to the ribosome at G137, A138, A139, and A140 of h8 and U328, A329, and C330 of h14.

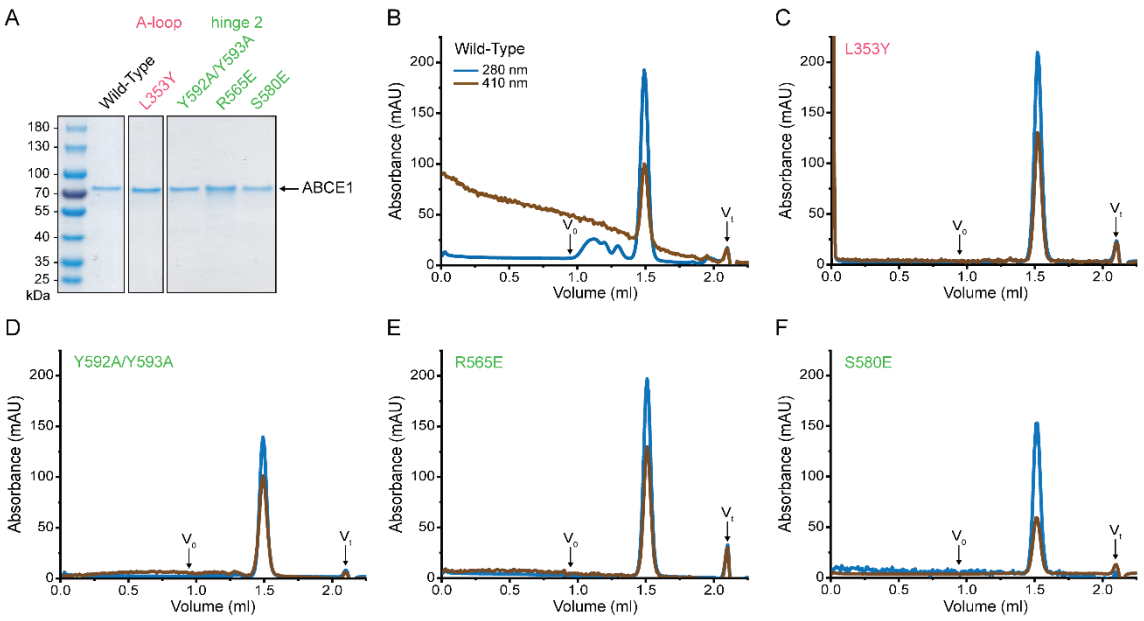

Figure S3: Quality control of *S. solfataricus* ABCE1 variants for post-SC functional studies (Nürenberg-Goloub *et al*, 2020)**. A)** Quality of purified ABCE1 variants is assured by single protein bands at the expected molecular weight in TRIS-glycine SDS-PAGE. **B-F)** All ABCE1 variants elute in single symmetric peaks in size-exclusion-chromatography confirming monodisperse protein samples. Absorbance at 410 nm attests correct assembly of the iron-sulfur clusters (Barthelme *et al*, 2007).

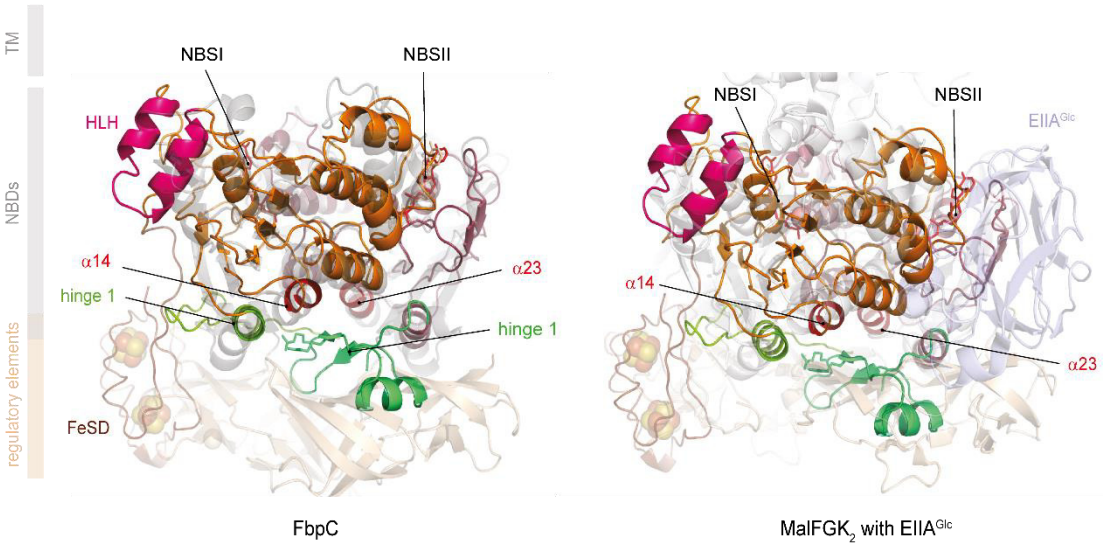

Figure S4: Structural alignment of ABCE1 with bacterial ABC-importers (Nürenberg-Goloub *et al*, 2020)**.** Superposition of the NBDs from ABCE1, the iron uptake transporter FbpC (left) of *Neisseria gonorrhoeae* (PDB 3FVQ) (Newstead *et al*, 2009), and the maltose transporter $MalFGK_2$ (right) in complex with the glucose-specific phosphotransferase enzyme $EIIA^{Glc}$ from *E. coli* (4JBW) (Chen *et al*, 2013). The hinge regions of ABCE1 are located at the same position as the regulatory elements of the ABC-importers. Thus, hinge 1 and hinge 2 may fulfill regulatory functions in ribosome sensing and communication to the NBSs *via* α14 and α23, in accordance with the evolution of the ubiquitous ABC-protein system.

6.2 Cryo-EM analysis of *in vitro* assembled archaeal post-splitting/initiation complexes

Table S1: Details of initiation complexes solved by cryo-EM. All data were processed and provided by Hannah Kratzat.

Initiation complexes	IC composition	Number of particles	Overall resolution [Å]
IC1	Post-SC aIF1A aIF1	293,010	3.6
IC2	Post-SC aIF1A aIF2 $^{Met}tRNA_i^{fMet}$ mRNA	48,051	4.3
IC3	Post-SC aIF1A $^{Met}tRNA_i^{fMet}$ mRNA	30,912	4.9

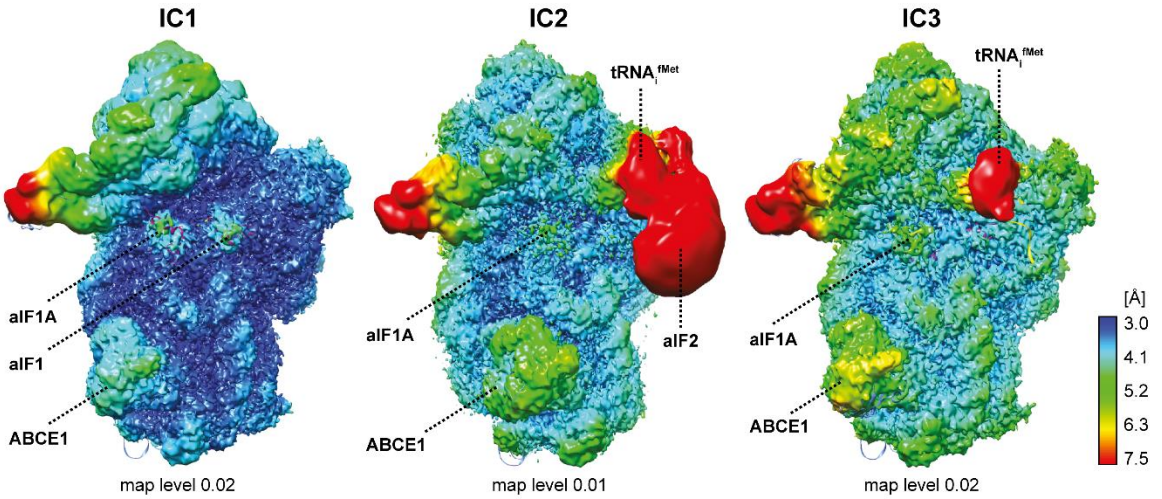

Figure S5: Local resolution of ABCE1-initiation complexes highlight the rigidity of the 30S core and flexibility of exposed regions. Intersubunit side view of the initiation complexes. Cryo-EM density is colored according to local resolution. High resolution (blue, ~3.0 Å) is in the core (body) of the 30S subunit, while low resolution (red, ~7.5 Å) is in the flexible 30S head beak, aIF2, and part of the tRNA. Contact sides to the 30S subunit of ABCE1, aIF1, and aIF1A are higher resolved than their solvent-facing side.

6.3 Mass spectrometry analysis of recombinant ABCE1 co-IP

Table S2: Mass spectrometry results of recombinant ssABCE1 pull-down from *S. solfataricus* cell lysates (selection of identified proteins) in collaboration with Dr. Haifei Xu, Joazeiro laboratory, Scripps Biomedical Research Institute, University of Florida. Co-IPs were performed with (sample) or without (control) recombinant ssABCE1 (n = 3 each). Identified proteins were sorted by relative abundance increase (ratio of sample to control) of the mean of three independent samples. All MS data were analyzed and provided by the Joazeiro laboratory.

Accession	Protein description	Abundance sample/control	P-Value sample/control	Adj. P-Value sample/control
Q980W3	30S ribosomal protein S8e	81,79	0,01007	0,27674
Q980Q5	30S ribosomal protein S28e	62,34	0,01037	0,27674
Q97ZH4	LSU ribosomal protein S30E (Rps30E)	60,71	0,00289	0,27674
Q9UX87	30S ribosomal protein S5	59,37	0,00935	0,27674
Q980K7	30S ribosomal protein S17e	48,41	0,00430	0,27674
Q9UXA0	30S ribosomal protein S3	48,00	0,01243	0,27674
P55858	50S ribosomal protein L7Ae	45,74	0,00579	0,27674
Q9UX98	30S ribosomal protein S17	44,38	0,01741	0,27674
Q97ZQ5	30S ribosomal protein S14	43,83	0,01327	0,27674
Q97Z80	30S ribosomal protein S27e	42,37	0,02446	0,27674
Q980A8	30S ribosomal protein S15	37,29	0,01420	0,27674
P95993	30S ribosomal protein S2	37,05	0,01716	0,27674
Q980F7	30S ribosomal protein S19e	36,06	0,01854	0,27674
Q9UXD4	30S ribosomal protein S3Ae	35,80	0,01431	0,27674
P58190	50S ribosomal protein L31e	35,24	0,00798	0,27674
Q9UX92	30S ribosomal protein S8	34,46	0,01489	0,27674
Q97ZY7	30S ribosomal protein S27ae	32,64	0,02414	0,27674
Q9UX94	30S ribosomal protein S4e	32,36	0,01931	0,27674
Q980K5	RNase L inhibitor / ABCE1	30,41	0,00074	0,21681
Q980A6	30S ribosomal protein S6e	29,24	0,01341	0,27674
P95987	30S ribosomal protein S4	26,76	0,01938	0,27674
P39573	30S ribosomal protein S12	22,25	0,01613	0,27674
P95988	30S ribosomal protein S11	22,18	0,02272	0,27674
Q980V0	DUF1610 domain-containing protein	21,96	0,01503	0,27674
Q9UXA3	30S ribosomal protein S19	21,58	0,02288	0,27674
Q97ZY6	30S ribosomal protein S24	21,43	0,00705	0,27674
P58084	50S ribosomal protein L29	20,11	0,01402	0,27674
Q97ZZ6	30S ribosomal protein S25e	19,97	0,02402	0,27674
Q9UX89	50S ribosomal protein L19e	19,29	0,01289	0,27674
Q9UX86	50S ribosomal protein L30	17,77	0,02206	0,27674
Q97Z81	50S ribosomal protein L44e	16,96	0,02280	0,27674
Q9UX90	50S ribosomal protein L32e	16,87	0,01195	0,27674
P95986	30S ribosomal protein S13	16,50	0,02383	0,27674
P95990	50S ribosomal protein L18e	16,47	0,01444	0,27674

Q9UX85	50S ribosomal protein L15	15,75	0,00860	0,27674
P95991	50S ribosomal protein L13	15,29	0,00863	0,27674
Q9UX97	50S ribosomal protein L14	14,86	0,01408	0,27674
P35027	30S ribosomal protein S10	14,75	0,02084	0,27674
Q9UX91	50S ribosomal protein L6	14,59	0,01170	0,27674
Q9UX95	50S ribosomal protein L24	14,54	0,02368	0,27674
Q980R3	50S ribosomal protein L30e	14,19	0,02185	0,27674
P95992	30S ribosomal protein S9	14,12	0,03031	0,28149
Q9UXA2	50S ribosomal protein L22	13,95	0,02357	0,27674
Q9UXD0	50S ribosomal protein L15e	13,30	0,01009	0,27674
Q9UXA6	50S ribosomal protein L4	13,20	0,02017	0,27674
Q9UXE0	50S ribosomal protein L21e	12,89	0,01443	0,27674
Q97ZR1	Ribosomal protein S26E (Rps26E)	11,91	0,01457	0,27674
P35026	30S ribosomal protein S7	11,56	0,01770	0,27674
P58222	50S ribosomal protein L18Ae	11,53	0,02783	0,27738
Q9UX88	50S ribosomal protein L18	11,17	0,02389	0,27674
Q980T2	Archaeal Rqc2 homolog	10,60	0,00003	0,03212
Q980C1	50S ribosomal protein L14e	10,44	0,02381	0,27674
Q980J7	50S ribosomal protein L10e	10,36	0,02682	0,27692
P96038	50S ribosomal protein L1	9,86	0,01431	0,27674
Q9UXA8	50S ribosomal protein L3	9,28	0,02958	0,28149
P96039	50S ribosomal protein L10	9,08	0,00522	0,27674
P30925	Elongation factor 2	7,65	0,17543	0,28149
P35021	Elongation factor 1 alpha	6,37	0,18039	0,28149
Q980G0	Translation initiation factor 6	5,89	0,03847	0,28149
Q97ZX6	Translation factor SUI1 homolog / aIF1	5,33	0,02619	0,27674
Q7LXS9	FeS assembly P domain-containing protein	4,96	0,04811	0,28149
Q97ZW4	Iron-sulfur cluster carrier protein	4,56	0,06026	0,28149
Q97Z79	Translation initiation factor 2 alpha	4,08	0,06374	0,28149
Q64214	Elongation factor 1 beta	4,07	0,14200	0,28149
Q97ZE8	Translation initiation factor 5A	3,47	0,30141	0,33772
Q980A5	Translation initiation factor 2 gamma	3,25	0,06251	0,28149
Q97W62	Translation initiation factor 1A	2,02	0,22297	0,28149

6.4 Binding properties of aIF1^{FL} to the 30S subunit

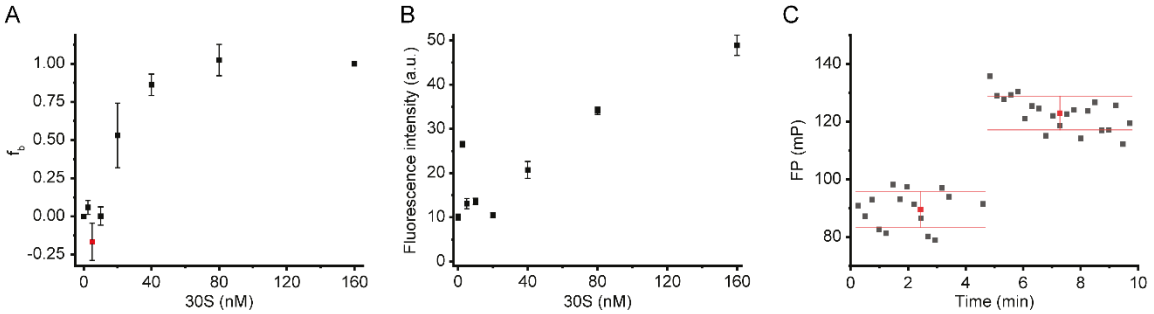

Figure S6: Fluorescence polarization and intensity increased upon binding of 5IAF-labeled aIF1 to the 30S subunit. A) Fluorescence polarization of 5IAF-labeled aIF1 binding to 30S increased with higher 30S concentration (96-well format, plate reader). The fraction of bound aIF1^{FL} to 30S (f_b) was calculated without correction for fluorescence intensity (Q = 1, equation 3, section 4.5.8.5) and plotted against the 30S subunit concentration. A negative data point is colored red. **B)** Fluorescence intensity increased with higher 30S concentration. Samples from (A) (96-well format, plate reader). **C)** Fluorescence polarization of 5IAF-labeled aIF1 fluctuated over time in absence (0-5 min) and presence of 30S subunits (5-10 min) (Fluorolog3® spectrofluorometer, Horiba). FP fluctuations (red) were calculated as mean ± standard deviation.

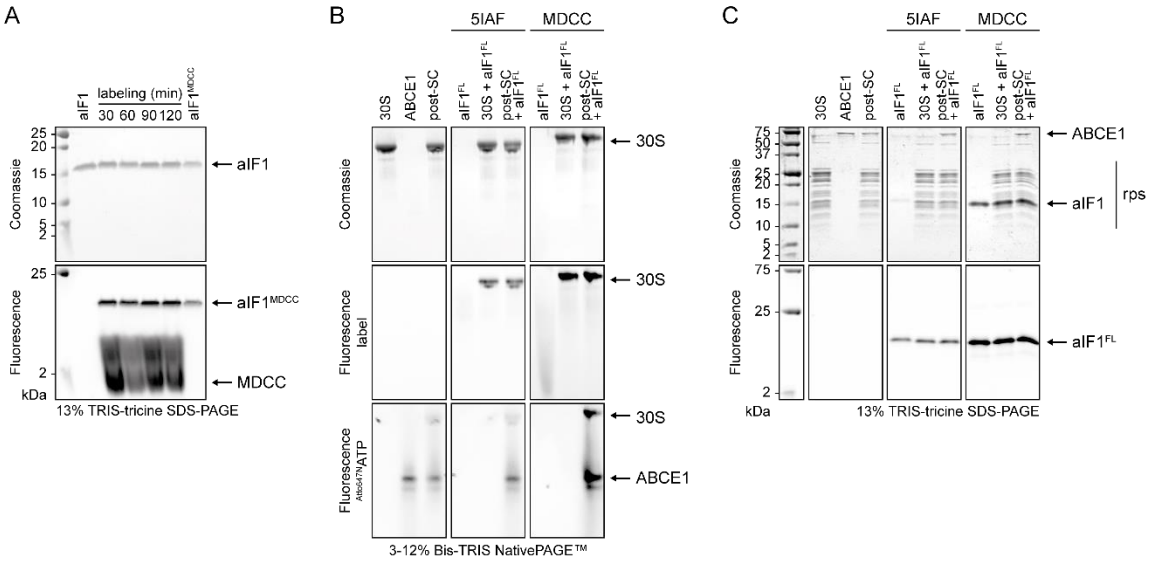

Figure S7: 5IAF- and MDCC-labeled aIF1 bind to 30S subunits and the post-SC. A) Time-dependent in-solution labeling of aIF1^{N45C} with MDCC is similar to 5IAF labeling (Figure 21). MDCC in-gel fluorescence was recorded at $\lambda_{ex/em}$ 440/480 nm. **B)** 5IAF and MDCC labeled aIF1^{FL} bound to 30S subunits and the post-SC in native PAGE. ABCE1 and the post-SC were visualized by ^{Atto647N}ATP occlusion of ABCE1. In-gel fluorescence of aIF1^{5IAF}, aIF1^{MDCC}, and ^{Atto647N}ATP was recorded at $\lambda_{ex/em}$ 480/535 nm, 440/480 nm, and 640/710 nm, respectively. **C)** Composition of native PAGE samples (B) was analyzed by TRIS-tricine SDS-PAGE. In-gel fluorescence as described in (B).

6.5 Functional characterization of MutS2

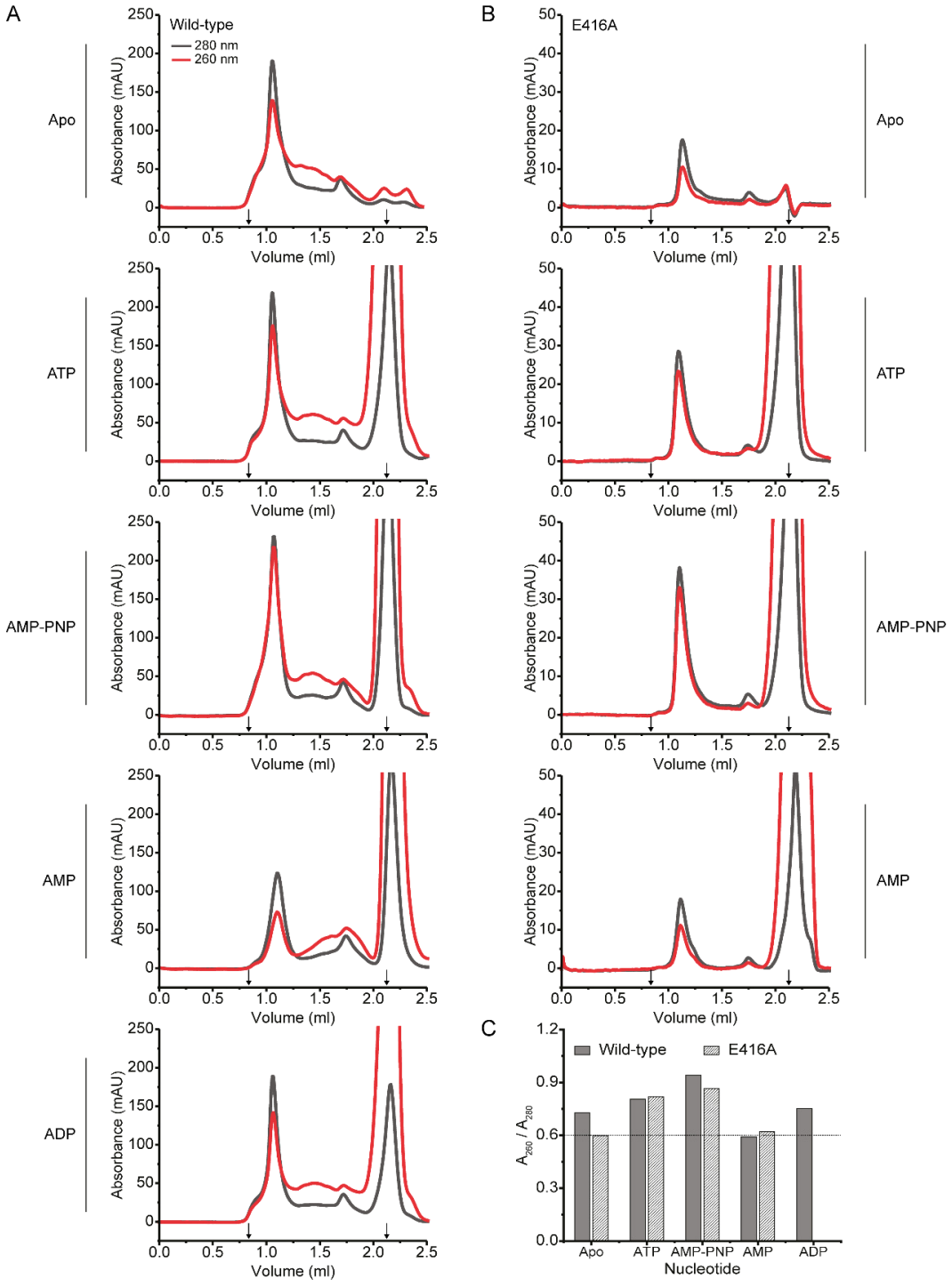

Figure S8: MutS2 bound ATP and AMPPNP but not ADP or AMP. A-B) 1.5 nmol MutS2 wild-type (A) and 250 pmol MutS2 E416A (B) were incubated for 2 min at 35 °C with 10- and 14-fold molar excess nucleotides, respectively (Superdex® 200 Increase 3.2/300 GL, Cytiva). For all conditions, MutS2 eluted at $V_e \approx 1.1$ ml. Void ($V_0 \approx 0.8$ ml) and total column volume ($V_t \approx 2.15$ ml) are marked by arrows. Excess nucleotides eluted at V_t. **C)** Increased A_{260}/A_{280} for ATP and AMP-PNP indicated binding by MutS2. The A_{260}/A_{280} ratio of each nucleotide condition was calculated using the peak maxima at $V_e \approx 1.1$ ml.

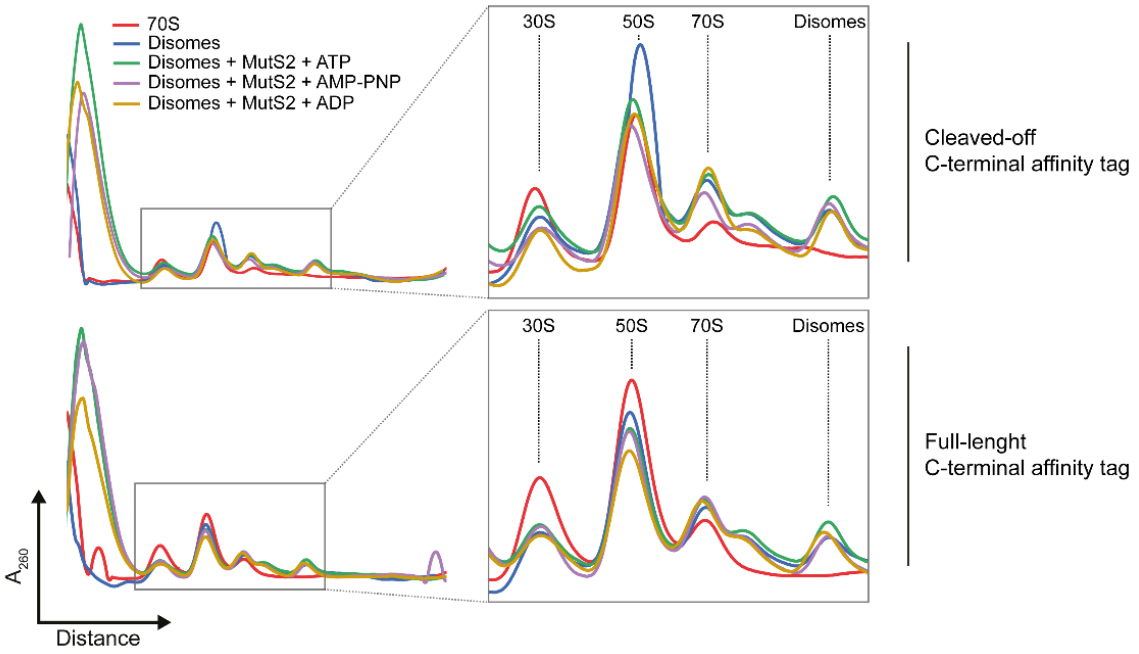

Figure S9: Neither different nucleotides nor length of the C-terminus resulted in a functional effect of MutS2 on ribosome populations. The Disome population did not change in presence of MutS2^{WT} with full-length or cleaved-off C-terminal affinity tag and under all nucleotide conditions in sucrose density gradient centrifugation analysis.

Publications

Nürenberg-Goloub E‡, Kratzat H‡, Heinemann H‡, Heuer A, Kötter P, Berninghausen O, Becker T, Tampé R* & Beckmann R* (2020) Molecular analysis of the ribosome recycling factor ABCE1 bound to the 30S post-splitting complex. *EMBO J* 39: e103788

Gouridis G‡, Hetzert B‡, Kiosze-Becker K‡, de Boer M‡, Heinemann H, Nürenberg-Goloub E, Cordes T* & Tampé R* (2019) ABCE1 controls ribosome recycling by an asymmetric dynamic conformational equilibrium. *Cell Rep* 28: 723-34.e6

Nürenberg-Goloub E‡, Heinemann H, Gerovac M & Tampé R* (2018) Ribosome recycling is coordinated by processive events in two asymmetric ATP sites of ABCE1. *Life Sci Alliance* 1: e201800095

‡ First author / equal contributions

* Corresponding author

Abbreviations

5IAF	5-Iodoacetamidofluorescein
5'-UTR	5'-untranslated region
5-FOA	5-fluoroorotic acid
a	archaeal
ABC	ATB binding cassette
ABCE1	ABC subfamily E protein 1
ABCE1^{IIEA}	ABCE1 E238/485A
AIEX	Anion exchange chromatography
aIF1^{FL}	Fluorescently labeled archaeal mRNA translation initiation factor 1
APS	Ammonium persulfate
^{Atto647N}ATP	N^6-(6-Aminohexyl)-ATP-ATTO647N
B	Beads (IP)
B. subtilis	*Bacillus subtilis*
Bs	*Bacillus subtilis*
cam	Chloramphenicol
carb	Carbenicillin
CAT	C-terminal alanine and threonine
cryo	Cryogenic
^{Cy3}ATP	N^6-(6-Aminohexyl)-ATP-Cy3
dd	Distilled, deionized
DDM	n-Dodecyl-beta-maltoside
DMSO	Dimethyl sulfoxide
DTT	Dithiothreitol
E	Eluate (IP)
e	eukaryotic
E. coli	*Escherichia coli*
ECL	Enhanced chemiluminescence
EF	mRNA translation elongation factor
EM	Electron microscopy
FeS	Iron-sulfur cluster
FeSD	Iron-sulfur cluster domain
FPLC	Fast-protein liquid chromatography
FRET	Förster resonance energy transfer
FSC	Fourier shell correlation
HLH	Helix-loop-helix
IC	mRNA translation initiation complex
IF	mRNA translation initiation factor
IMAC	Immobilized metal ion affinity chromatography

IP	Immunoprecipitation
IPTG	Isopropyl-β-D-galactopyranoside
kan	Kanamycin
L	Load (IP)
LB	Lysogeny broth
$LP_{red.}$	SDS-PAGE loading buffer, reducing
LSU	Large ribosomal subunit
MetRS	Methionine-tRNA synthetase
$^{Met}tRNA_i^{Met}$	Methionylated initiator tRNA
MS	Mass spectrometry
NBD	Nucleotide-binding domain
NBS	Nucleotide-binding site
NEMF	Nuclear export mediator factor
NGD	No-go decay
NMD	Nonsense-mediated decay
NSD	No-stop decay
nt	Nucleotide
ORF	Open reading frame
PABP	Poly-A binding protein
PAGE	Polyacrylamide gel electrophoresis
P_i	Inorganic phosphate
poly-A	Poly adenosine
post-SC	Post-splitting complex
post-TC	Post-termination complex
pre-SC	Pre-splitting complex
PTC	Peptidyl transferase center
RF	Release factor
Rli 1	RNase L inhibitor 1
rpm	Rotations per minute
rps	Ribosomal proteins
RQC	Ribosome-associated quality control
RRF	Bacterial ribosome recycling factor
rRNA	Ribosomal RNA
S. acidocaldarius	*Sulfolobus acidocaldarius*
S. cerevisiae	*Saccharomyces cerevisiae*
S. solfataricus	*Saccharolobus solfataricus*
Sa	*Sulfolobus acidocaldarius*
Sc	*Saccharomyces cerevisiae*
SD	Standard deviation
SDG	Sucrose density gradient
SDS	Sodium dodecyl sulfate

SEC	Size exclusion chromatography
SN	Supernatant (IP)
SOB	Super optimal broth
SOC	Super optimal broth with catabolite repression
SRL	Sarcin ricin loop
Ss	*Saccharolobus solfataricus*
SSU	Small ribosomal subunit
T. celer	*Thermococcus celer*
TB	Terrific broth
Tc	*Thermococcus celer*
TCEP	TRIS(2-carboxyethyl)phosphine
TEMED	Tetramethylethylenediamine
TMD	Transmembrane domain
tmRNA	Transfer-messenger RNA
TRIS	Tris(hydroxymethyl)aminomethane
$tRNA_i^{fMet}$	Formyl-methionyl initiator tRNA
v/v	Volume per volume
V_0	Void volume
V_e	Elution volume
V_t	Total volume (SEC)
V_{tot}	Total sample volume
w/v	Weight (mass) per volume
WT	Wild-type